Realia et naturalia

DISSERTATIONES
CHIMICAE
UNIVERSITATIS
TARTUENSIS
128

IVAR KRUUSENBERG

Electroreduction of oxygen on carbon nanomaterial-based catalysts

TARTU ÜLIKOOL
1632
UNIVERSITAS TARTUENSIS

DISSERTATIONES CHIMICAE UNIVERSITATIS TARTUENSIS
128

DISSERTATIONES CHIMICAE UNIVERSITATIS TARTUENSIS
128

IVAR KRUUSENBERG

Electroreduction of oxygen on carbon nanomaterial-based catalysts

UNIVERSITY OF TARTU
PRESS
1632

Institute of Chemistry, University of Tartu, Estonia

Dissertation in Colloid and Environmental Chemistry

Dissertation is accepted for the commencement of the degree of Doctor of Philosophy in Chemistry on June 11, 2013 by the Doctoral Committee of the Institute of Chemistry, University of Tartu.

Doctoral advisor: Dr. Kaido Tammeveski,
University of Tartu, Institute of Chemistry

Opponent: Prof. Michael Bron,
Institut für Chemie, Martin-Luther-Universität Halle

Commencement: August 27, 2013 at 13:00 in Tartu, Ravila 14A, room 1021

Publication of this dissertation is granted by FMTDK

ISSN 1406–0299
ISBN 978–9949–32–335–7 (print)
ISBN 978–9949–32–336–4 (pdf)

University of Tartu Press
www.tyk.ee
Order No. 267

TABLE OF CONTENTS

1. LIST OF ORIGINAL PUBLICATIONS

This thesis consists of nine original articles listed below and a review. The articles are referred in the text by Roman numerals I–IX.

I **I. Kruusenberg**, N. Alexeyeva, K. Tammeveski, J. Kozlova, L. Matisen, V. Sammelselg, J. Solla-Gullón, J.M. Feliu, Effect of purification of carbon nanotubes on their electrocatalytic properties for oxygen reduction in acid solution, Carbon 49 (2011) 4031–4039.

II **I. Kruusenberg**, M. Marandi, V. Sammelselg, K. Tammeveski, Hydrodynamic deposition of carbon nanotubes onto HOPG: The reduction of oxygen on CNT/HOPG electrodes in alkaline solution, Electrochemical and Solid-State Letters 12 (2009) F31–F34.

III **I. Kruusenberg**, L. Matisen, H. Jiang, M. Huuppola, K. Kontturi, K. Tammeveski, Electrochemical reduction of oxygen on double-walled carbon nanotube modified glassy carbon electrodes in acid and alkaline solutions, Electrochemistry Communications 12 (2010) 920–923.

IV **I. Kruusenberg**, N. Alexeyeva, K. Tammeveski, The pH-dependence of oxygen reduction on multi-walled carbon nanotube modified glassy carbon electrodes, Carbon 47 (2009) 651–658.

V **I. Kruusenberg**, J. Leis, M. Arulepp, K. Tammeveski, Oxygen reduction on carbon nanomaterial modified glassy carbon electrodes in alkaline solution, Journal of Solid State Electrochemistry 14 (2010) 1269–1277.

VI **I. Kruusenberg**, L. Matisen, K. Tammeveski, Oxygen electroreduction on multi-walled carbon nanotube supported metal phthalocyanines and porphyrins in acid media, International Journal of Electrochemical Science 8 (2013) 1057–1066.

VII **I. Kruusenberg**, L. Matisen, K. Tammeveski, Oxygen electroreduction on multi-walled carbon nanotube supported metal phthalocyanines and porphyrins in alkaline media, Journal of Nanoscience and Nanotechnology 13 (2013) 621–627.

VIII **I. Kruusenberg**, L. Matisen, Q. Shah, A.M. Kannan, K. Tammeveski, Non-platinum cathode catalysts for alkaline membrane fuel cells, International Journal of Hydrogen Energy 37 (2012) 4406–4412.

IX **I. Kruusenberg**, J. Mondal, L. Matisen, V. Sammelselg, K. Tammeveski, Oxygen reduction on graphene-supported MN_4 macrocycles in alkaline media, Electrochemistry Communications 33 (2013) 18–22.

Author's contribution

Paper I: The author has performed all electrochemical measurements and data analysis. The author is responsible for the interpretations of electrochemical testing results and writing the paper.

Paper II: The author has performed all electrochemical measurements and data analysis. The author is responsible for the interpretations of electrochemical testing results and writing the paper.

Paper III: The author has performed all electrochemical measurements and data analysis. The author is responsible for the interpretations of electrochemical testing results and writing the paper.

Paper IV: The author has performed all electrochemical measurements and data analysis. The author is responsible for the interpretations of electrochemical testing results and writing the paper.

Paper V: The author has performed all electrochemical measurements and data analysis. The author is responsible for the interpretations of electrochemical testing results and writing the paper.

Paper VI: The author has performed all electrochemical measurements and data analysis. The author is responsible for the interpretations of electrochemical testing results and writing the paper.

Paper VII: The author has performed all electrochemical measurements and data analysis. The author is responsible for the interpretations of electrochemical testing results and writing the paper.

Paper VIII: The author has performed all electrochemical measurements and data analysis. The author is responsible for the interpretations of electrochemical testing results and writing the paper.

Paper IX: The author has performed all electrochemical measurements and data analysis. The author is responsible for the interpretations of electrochemical testing results and writing the paper.

2. ABBREVIATIONS AND SYMBOLS

A	geometric surface area of an electrode
AEM	anion exchange membrane
AEMFC	anion-exchange membrane fuel cell
AFM	atomic force microscopy
BDD	boron-doped diamond
CDC	carbide-derived carbon
CNFs	carbon nanofibers
CNTs	carbon nanotubes
CoPc	cobalt(II)phthalocyanine
CoPh	5,10,15,20-tetrakis(4-methoxyphenyl)-21H,23H-porphine cobalt(II)
CTAB	cetyltrimethylammonium bromide
CVD	chemical vapour deposition
$c_{O_2}^{b}$	concentration of oxygen in the bulk solution
CV	cyclic voltammetry
D_{O_2}	diffusion coefficient of oxygen
DHP	dihexadecyl hydrogen phosphate
DWCNTs	double-walled carbon nanotubes
E	electrode potential
E^0	standard potential
$E_{1/2}$	half-wave potential
EC	electrochemical-chemical
EDS	energy dispersive X-ray spectroscopy
F	Faraday constant
FePc	iron(II)phthalocyanine
FePh	5,10,15,20-tetrakis(4-methoxyphenyl)-21H,23H-porphine iron(II)
GC	glassy carbon
GO	graphene oxide
HOPG	highly oriented pyrolytic graphite
HR-SEM	high-resolution scanning electron microscopy
HR-TEM	high-resolution transmission electron microscopy
I	current
I_d	diffusion-limited current
I_D	disc current
I_k	kinetic current
I_R	ring current
J	current density
j_d	diffusion-limited current density
j_k	kinetic current density
k	heterogeneous electron transfer rate constant

k^0	the apparent electrochemical rate constant for O_2 reduction
K-L	Koutecky-Levich
MEA	membrane-electrode assembly
MWCNTs	multi-walled carbon nanotubes
n	number of electrons transferred per O_2 molecule
N	collection efficiency
NG	nitrogen-doped graphene
OCV	open circuit voltage
ORR	oxygen reduction reaction
PEMFC	proton-exchange membrane fuel cell
PG	pyrolytic graphite
Pt/C	carbon-supported Pt catalyst
PTFE	polytetrafluoroethylene
Q	quinone
RDE	rotating disk electrode
rGO	reduced graphene oxide
RH	relative humidity
RHE	reversible hydrogen electrode
RRDE	rotating ring-disk electrode
rpm	revolutions per minute
RVC	reticulated vitreous carbon
S_A	specific surface area
SEM	scanning electron microscopy
SCE	saturated calomel electrode
SDS	sodium dodecyl sulphate
SHE	standard hydrogen electrode
SWCNTs	single-walled carbon nanotubes
T	temperature
TEM	transmission electron microscopy
V_p	total volume of pores
V_μ	volume of micropores
v	potential scan rate
XRD	X-ray powder diffraction
XPS	X-ray photoelectron spectroscopy
θ	electron take-off angle
ν	kinematic viscosity of the solution
Φ	percentage of peroxide formation on the disk
ω	electrode rotation rate

3. INTRODUCTION

Over the past few decades different carbon nanomaterials such as nanocrystals, nanowires, nanotubes, nanofibers, graphene and carbide-derived carbons have been extensively studied and they have found numerous promising applications in energy conversion and storage [1,2]. Nanomaterials can be defined as those whose characteristic length scale lies within the range between one and several hundreds of nanometers [3]. Carbon nanostructures can be classified by using terminology in terms of three allotropic modifications of carbon materials: 1) flat sp^2 hybridisation of carbon in graphite, 2) curved sp^2 hybridisation in fullerenes, nanotubes or nanofibers and 3) sp^3 hybridisation in diamond [4].

The real nano-boom of carbon nanomaterials started after discovery of carbon nanotubes in early 1990s [5]. Since then there has been immense interest in the research of carbon and its related nanomaterials [6]. Research of carbon nanomaterials has led to many new technical developments and applications and this is mainly due to their excellent chemical and physical properties. Recent electrochemical studies have demonstrated that carbon nanomaterials have the ability to promote electron-transfer reactions [7].

The electrochemical reduction of oxygen continues to be an attractive research area with different experimental and fundamental approaches focused on understanding the mechanism of its catalysis [8–11]. The oxygen reduction reaction (ORR) proceeds by either two-electron pathway, where the final product is hydrogen peroxide or by a direct four-electron pathway, which is a crucial reaction in fuel cells and produces water as the final product. The reduction of O_2 proceeds on the cathode side of a fuel cell and the efficiency of the cell depends directly on the kinetics of this reaction [12].

The aim of this PhD thesis was to study the effect of different carbon nanomaterial-based catalysts on the electrocatalysis of the ORR. The main attention was focused on the electrocatalytic activity of carbon nanotubes and carbon nanotube supported catalysts. In addition carbide-derived carbons and graphene-supported catalysts were investigated. The kinetic parameters of O_2 reduction on these catalysts were determined and anion-exchange membrane fuel cell studies were performed.

In the first part of this work, the electrocatalytic reduction of oxygen has been studied on single-walled and multi-walled carbon nanotube modified glassy carbon electrodes in acid solution and the effect of the acid treatment of carbon nanotubes was investigated [I].

In the main part of the thesis the electroreduction of oxygen has been studied on carbon nanotube-based electrodes [II,III] and both, the effect of surfactants and pH dependence have been investigated on these materials [IV]. Oxygen reduction on different carbon nanomaterials in alkaline media has been compared as well [V].

In the third part of the work the ORR on multi-walled carbon nanotube supported metal phthalocyanines and porphyrins was investigated, both in acid

[VI] and alkaline media [VII]. In addition, anion-exchange membrane fuel cell experiments with iron and cobalt phthalocyanine/multi-walled carbon nanotube cathode catalysts have been performed [VIII].

Finally metallophthalocyanines and metalloporphyrins supported on graphene nanosheets were studied as electrocatalysts for ORR in alkaline media [IX].

The surface structure, composition and morphology of carbon nanomaterials and nanocarbon supported catalysts has been examined by transmission electron microscopy, high-resolution scanning electron microscopy, X-ray photoelectron spectroscopy, Raman spectroscopy and X-ray powder diffraction analysis. Electrochemical experiments were carried out using cyclic voltammetry, the rotating disc electrode and the rotating ring-disc electrode methods.

4. LITERATURE OVERVIEW

4.1. The general scheme of oxygen electroreduction

The oxygen reduction reaction (ORR) is a multielectron reaction which in aqueous solutions can proceed by two major pathways. The ORR proceeds by either two- or four-electron pathway yielding hydrogen peroxide or water as the final product.

In alkaline solutions these reactions are:

$$O_2 + 2H_2O + 4e^- \rightarrow 4OH^- \qquad E^0 = 0.401 \text{ V vs. SHE} \qquad (1)$$

$$O_2 + H_2O + 2e^- \rightarrow HO_2^- + OH^- \qquad E^0 = -0.065 \text{ V}, \qquad (2)$$

hydrogen peroxide intermediate can be further reduced:

$$HO_2^- + H_2O + 2e^- \rightarrow 3OH^- \qquad E^0 = 0.867 \text{ V}, \qquad (3)$$

or catalytic decomposition (disproportion) takes place:

$$2HO_2^- \rightarrow 2OH^- + O_2. \qquad (4)$$

In acid solutions, the corresponding reactions are:

$$O_2 + 4H^+ + 4e^- \rightarrow 2H_2O \qquad E^0 = 1.229 \text{ V}, \qquad (5)$$

$$O_2 + 2H^+ + 2e^- \rightarrow H_2O_2 \qquad E^0 = 0.67 \text{ V}, \qquad (6)$$

peroxide can be further reduced:

$$H_2O_2 + 2H^+ + 2e^- \rightarrow 2H_2O \qquad E^0 = 1.77 \text{ V}, \qquad (7)$$

or catalytically decomposed (disproportionated):

$$2H_2O_2 \rightarrow 2H_2O + O_2 \qquad (8)$$

[13–16].

The simplified reaction pathway is shown in Scheme 1 [16].

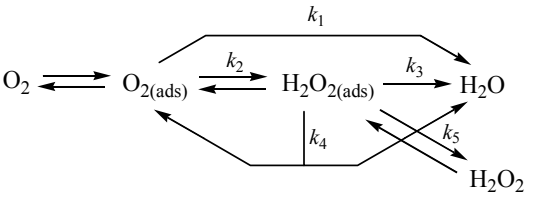

Scheme 1. Simplified mechanism of oxygen reduction in acid solutions. The rate constants for different steps are indicated in the scheme (k_i). (ads) denotes the species in their adsorbed state.

In spite of apparent simplicity, these overall reactions represent a complex electrocatalytic network and involve many elementary steps. The dominating pathway depends on different factors, like solution pH, electrode material and electrode potential [15,16].

4.2. Oxygen reduction on bulk carbon electrodes

The electrochemical reduction of oxygen on carbon-based electrodes has received a long-standing interest and has been extensively studied [17]. It has been recognised that different types of carbons have different electrocatalytic properties for ORR. Oxygen reduction on carbon materials, such as pyrolytic graphite (PG), highly oriented pyrolytic graphite (HOPG), glassy carbon (GC), boron-doped diamond (BDD), reticulated vitreous carbon (RVC) and other carbon materials has been reviewed by Tryk et al. [18]. Oxygen reduction on carbon electrodes has been mainly investigated in alkaline solution, because most of the carbon materials have catalytically active properties for ORR at higher pHs [19–24]. The only exceptions are basal plane HOPG and BDD, which strongly inhibit this reaction [25]. The ORR on bulk carbon electrodes has been also examined in acid media [26–29]. Even though the process of ORR on different carbon materials has been extensively studied, the mechanism of this reaction is still not entirely clear. It is generally considered that both in acid and alkaline media oxygen reduction on carbon electrodes comprises the formation of hydrogen peroxide.

The early work on the ORR on carbon materials was made by Davies et al. [30], who proved that the ORR on carbon electrodes occurs without the rupture of the O-O bond. In the further research Yeager et al. [31] demonstrated on the basis of the results obtained with pyrolytic carbon and porous carbon that the rate-determining step of O_2 reduction in alkaline media is the first electron transfer to form hydroperoxyl radical ($HO_2^{\bullet}$) or superoxide anion (O_2^{-}) and speculated about the role of surface functional groups in the electrocatalysis of the ORR. In the following studies, Morcos and Yeager demonstrated the inhibiting effect of the basal plane HOPG on the electroreduction of oxygen. They compared the electrocatalytic properties of edge plane and basal plane and

speculated again about the possible involvement of the native oxygen-containing groups of carbon in the ORR [19].

Sabirov and Tarasevich investigated the kinetics of the ORR on PG and GC electrodes [32]. They showed that the ORR on PG and GC in alkaline solution and on PG in acid solution proceeds via intermediate peroxide formation. At $E > -0.2$ V vs. RHE in 0.5 M H_2SO_4 peroxide is a stable product of reaction results. The same group of researchers studied the pH-dependence of the oxygen electroreduction on PG electrodes and concluded that in the pH range between 1 and 4 the rate of O_2 reduction is independent of pH [33].

Inspired by the previous studies and ideas about the possible role of the oxygen-containing functional groups in the process of the ORR, Yeager and co-workers finally proved this fact in 1989 [21]. They demonstrated that quinones adsorbed on the basal plane of HOPG act as effective electrocatalysts for ORR in alkaline media. They suggested that the mechanism involves a redox mediation process with the one-electron reduced quinone (radical anion), which is followed by the further reduction of the radical anion to dianion at more negative potentials. After their leading work, many studies have been made to examine the ORR on quinone-modified electrodes [22,34–40]. To confirm the theory of the surface functional groups, Yano et al. prepared as-deposited CVD diamond surface similar to HOPG material and tested it as the ORR catalyst. BDD was even less active than HOPG because of the absence of surface functional groups [41]. These studies made new insights into the role of surface functional groups of carbon materials as catalyst centres for oxygen reduction.

As mentioned above, the mechanism of O_2 reduction is influenced by the solution pH [18]. The pH effect on the kinetics of O_2 reduction has a considerable practical importance. Tarasevich et al. claimed that the half-wave potential ($E_{1/2}$) of O_2 reduction on PG is almost constant in the pH range from 1.5 to 14 [42]. A similar effect was also observed by Tryk et al. on BDD and HOPG [18]. However, more recent studies have indicated that O_2 reduction on carbon materials is still dependent on pH. Yang and McCreery found that for pH 12–14 the reduction of O_2 appears to be independent of pH but as pH decreases, O_2 reduction turns to be dependent on pH [28]. Taylor and Humffray stated that the product of oxygen electroreduction is also dependent on pH [43]. It has been proposed that the pH dependence at higher pHs is caused by quinone functionalities of carbon materials [21]. It is considered that the semiquinone radical anion ($Q^{\bullet -}$) is responsible for the electrocatalysis of oxygen reduction [22,25]. In this case the reduction of O_2 follows an electrochemical-chemical (EC) mechanism according to:

$$Q_{(\sigma)} + e^- \longrightarrow Q^{\bullet -}_{(\sigma)} \tag{9}$$

$$Q^{\bullet -}_{(\sigma)} + O_2(\mathrm{aq}) \xrightarrow{k_i} Q\text{-}O^{\bullet -}_{2(\sigma)} \tag{10}$$

The superoxide intermediate is represented as $Q–O_{2(\sigma)}^{\bullet -}$. The intermediate reacts with a second electron and protons from water, thus producing hydrogen peroxide (Reaction (11)).

$$Q\text{-}O_{2(\sigma)}^{\bullet -} + 2H^+ + e^- \xrightarrow{i} Q_{(\sigma)} + H_2O_2 \qquad (11)$$

At pH > 12 hydroperoxide anions (HO_2^-) are the main products of this reaction. As supposed by Wass et al. [44] reactions (9–11) correspond to the reduction of O_2 in solutions with pH > pK_a of the semiquinol present as a radical anion, however, at pH < pK_a the semiquinol formed by Reaction (12) undergoes Reaction (13), in which case the superoxo intermediate is protonated ($Q\text{-}HO_{2(\sigma)}^{\bullet}$, Reaction (13)). This species reacts with a second electron and a proton producing hydrogen peroxide (Reaction (14)).

$$Q_{(\sigma)}^{\bullet -} + H^+ \longrightarrow HQ_{(\sigma)}^{\bullet} \qquad (12)$$

$$HQ^{\bullet} + O_2(aq) \xrightarrow{k_i} Q\text{-}HO_{2(\sigma)}^{\bullet} \qquad (13)$$

$$Q\text{-}HO_{2(\sigma)}^{\bullet} + H^+ + e^- \xrightarrow{i} Q_{(\sigma)} + H_2O_2 \qquad (14)$$

The kinetics of O_2 reduction on quinone-modified electrodes has been thoroughly studied by our group and the results obtained are summarised in the PhD thesis by A. Sarapuu [45] and M. Kullapere [46]. The pH-dependence of O_2 reduction on bare GC electrodes has been studied by Jürmann et al. [47]. The rate constant for O_2 reduction on GC electrodes increases with increasing solution pH. It was found that the O_2 reduction activity was higher in the solutions of high pH. At lower pH, the nature of active sites on GC changes and as a result, the value of $E_{1/2}$ for O_2 reduction is almost independent of pH. All this is also confirmed by Tryk et al. [18] who compared the pH dependence of O_2 reduction on BDD and GC surfaces. It appears from their results that there is no pH dependence of O_2 reduction on the BDD electrode which has no quinone-type functionalities on the surface. At the same time, the reduction on the bare GC electrode which has a variety of different quinones on the surface, is sensitive to pH. Thereby it is a well proven fact that the pH dependence is caused primarily by the surface oxygen functionalities like quinone-type groups, not the carbon material itself.

4.3. Oxygen reduction on carbon nanomaterials

There have been numerous recent efforts to characterise different carbon nanomaterials as possible electrocatalyst supports as reviewed by Sharma and Pollet [48]. A number of carbon materials, such as activated carbons, carbon nanotubes and other types of carbon along with a large variety of precursors and synthesis conditions have rendered long and systematic research [49]. Carbon materials used in these studies range from conventional carbon powders such as Vulcan XC72, Ketjen Black, Black Pearls BP2000, Shawinigan carbon black and activated carbons, to fewer known carbon fibers, hard carbon spherules and carbide-derived carbons. Along with the scientific breakthrough of synthesis of nanostructured carbon materials, several new forms of nanocarbons have been synthesised like carbon nanocapsules and different forms of carbon nanotubes [49,50]. For many years micro- and mesoporous carbon materials and the optimisation of the pore size of these materials have been in the special focus of scientific research [49].

4.3.1. Oxygen reduction on CNTs and carbon nanofibers

Carbon nanotubes are long cylinders of 3-coordinated carbon, slightly pyramidalised by curvature from the pure sp^2 hybridisation of graphene, towards the diamond-like sp^3 [1,51]. Carbon nanotubes were discovered by Iijima in 1991 as a minor by-product of fullerene synthesis [5]. Since then a remarkable progress has been made in the field of carbon nanotube research including the discovery of three different structures of CNTs (single-walled, double-walled and multi-walled carbon nanotubes). Out of these different forms of CNTs, multi-walled carbon nanotubes (MWCNTs) have been most frequently employed in research and in different practical applications, this is mainly because of the ease of production of this material. Carbon nanotubes have unique structural, mechanical, electronic and chemical properties including exceptional strength, stiffness and high thermal and electric conductivity [1]. The closed topology and tubular structure make them unique compared with other forms of carbon [52–54]. Great steps and numerous studies have been taken in their synthesis, purification and elucidation of fundamental physical and chemical properties. Besides all the other investigations, immense work has been made to clarify the electrochemical properties of carbon nanotubes, including the electrocatalysis of oxygen reduction in both acid [29,55–57] and alkaline media [58–64].

CNT-modified electrodes are active electrocatalysts for O_2 reduction in alkaline solution [61,64], whereas in acid media their activity is much lower [29,65]. Therefore in acid media, carbon nanotubes have been mostly employed as catalyst supports [66,67]. Ajayan´s group has reported that some of the reasons for the improved activation behaviour for ORR are heptagon-heptagon defect pairs in the lattice pentagons at CNT tips and curvature of CNT [52].

Different carbon-oxygen functionalities on the surface of CNTs are related to the electrocatalytic activity for ORR in alkaline media whereas in acid media the effect and role of the oxygen functionalities formed on the edge plane-like defects at the open ends of the MWCNTs and at the hole defects on the tube walls are not yet clear and identified. Matsubara and Waki demonstrated that the onset potential of oxygen reduction on oxidised MWCNTs shifts positive approximately 60 mV compared with the untreated MWCNTs [68]. This positive shift demonstrates the possibility that oxygen functionalities introduced by acid treatment have considerable effect on the ORR in acid media. Similar performance has been observed for other carbon materials as well [27,69]. Strelko et al. attributed the improved electrocatalytic activity of MWCNTs in acid media to the oxygen heteroatoms incorporated in groups of carbonyl and furan types [70].

Even though carbon-oxygen functionalities can change the ORR activity of MWCNTs in acid media, the ORR still follows the $2e^-$ pathway in the potential range between –0.4 and –0.15 V vs. SCE and thereby H_2O_2 is the final product of the electroreduction of O_2 [29]. It has been proposed that this reaction pathway of the ORR is affected and the further reduction of H_2O_2 is limited by the larger amount of oxygen functionalities on MWCNTs. This theory is based on the presumption that the presence of oxygen functionalities can inhibit the ability of releasing electrons and the reductive adsorption of oxygen [68]. O-functionalised CNTs have been thought to act similar to graphite oxide/ graphene oxide (GO) because functionalisation by corrosive acids turns CNTs into CNT-oxides which should theoretically perform similar to GO [58]. As observed for GO, defecting nature and reduced electric conductivity will impair the outstanding properties of CNT material [58,71].

It has been proposed that in many cases the catalyst impurities remaining in CNTs during their fabrication by chemical vapour deposition (CVD) are responsible for their electrocatalytic activity in various reactions. The role of the metal impurities in the improvement of the ORR kinetics has been discussed recently [29]. Banks et al. reported that metal impurities in CNTs are partially overcoated with graphite shells [72,73] and thereby it is extremely difficult to purify the CNTs from catalyst impurities, which are left behind in the CVD method of preparation of carbon nanotubes. Even acid washing of the as-prepared CNTs does not help to completely get rid of iron impurities existing in the nanotubes [I]. Because of this, one of the most fundamental challenges in carbon nanotube science is the development of efficient and simple but not harsh purification methods for cleaning the CNTs from the significant amount of embedded secondary phases, such as graphitic particles, amorphous carbon and residual metal catalyst impurities (typically Fe, Co, Mo or Ni) used in their growth [74–79]. When the content of amorphous carbon and metal nanoparticles is high, it is essential that the impurities are removed if one wishes to work with a specific carbon material and not a composite. For that reason there has been an extensive research interest in using various methods of

removing impurities from CNTs. Several highly effective purification techniques have been established, including microfiltration, chromatography and centrifugation, although these are rarely used. A far-spread method has been the use of oxidative treatments, usually employing strong oxidising acids [76]. Acid treatment typically involves refluxing CNTs in HNO_3, H_2SO_4, HCl or mixtures of these acids [78,80,81]. In some cases CNTs have been purified even in more oxidative and extreme conditions like using piranha solution for this purpose [82], but the problem in this case is that the shortening of CNTs takes place during acid treatment of the nanotube material in such harsh conditions [83,84].

Mixtures of concentrated HNO_3 and H_2SO_4 are most effective in removing amorphous carbon, while the HCl treatment, in conjunction with sonication, is considered to assist the removal of catalytic metal nanoparticles [85]. Different groups advocate slightly different acidic treatment conditions based on variations in duration, concentration, use of sonication and repeated cycles. An important consideration in choosing the suitable purification method is the secondary effect of the acid purification process, which typically results in the "cutting" effect of CNTs, i.e. opens the ends of CNTs, cuts CNTs, damages surface structure, damages oxidatively the sidewall and introduces oxygenated functional groups on CNTs ends and side holes [86]. The ends and defects formed in the CNT sp^2 structure are functionalised with oxygen-containing groups, such as hydroxylic, carboxylic and ketone groups. While oxygen-containing surface species can aid certain electrochemical reactions, the presence of sidewall defects causes significant changes in the CNT electronic states near the Fermi level. It has also been shown that the increase of graphitic defects and thereby also oxygen-containing groups created during the acid oxidation process can cause a slight improvement in the oxygen reduction activity [87]. At the same time it has been reported that for many electro-chemical reactions, the oxygen-containing species formed as a result of acid washing of CNTs are not considered electrocatalytically active sites because they do not considerably influence the kinetics of heterogeneous charge-transfer processes, as demonstrated by Banks et al. [88].

Although the exact electrocatalytic role of the surface functionalities attached by the acid treatment is not yet clear and proven, the influence of these oxygen-containing groups on the surface modification of CNTs is well studied and confirmed. Acid treatment is important from the catalyst support point of view because to support an active electrocatalyst on their surface, CNTs should have some functional groups to hook up or to anchor the active entities on the functional groups [65]. Unfortunately the CVD synthesised CNTs are hydrophobic and therefore the modification of CNTs with other catalysts is complicated and introducing a suitable functionality requires special methods [89,90]. Treatment with oxidising agents such as acids is one of the most common methods to form these carbon-oxygen functionalities. Another possibility is to use electrochemical oxidation methods to get CNTs wetted and

immersed in the solution for electrochemical applications involving aqueous electrolytes [91].

For alkaline media, some research groups have proposed that the enhanced O_2 reduction current at pre-wave potentials is caused by quinone-type functionalities [22,92]. Surface-confined quinones were employed as electro-catalysts for the quantitative reduction of O_2 to hydrogen peroxide [22,25,36]. It is considered that the semiquinone radical anion ($Q^{\bullet -}$) is responsible for the electrocatalysis of oxygen reduction [21,22]. The reduction of oxygen follows an electrochemical-chemical (EC) mechanism according to the Reactions (9–11) [22]. Reaction (10) is considered to be the rate-determining step in the overall reduction of oxygen. Besides the carbon nanotubes, carbon nanofibers (CNFs) have been extensively studied as a possible catalyst and catalyst support material [93,94]. Carbon nanofibers could be defined as sp^2-based linear filaments with diameter of ca. 100 nm that are characterised by flexibility and their high aspect ratio (above 100) [95]. Carbon materials in the form of fiber are of great practical and scientific importance. CNFs can be used for a variety of promising applications such as functional and structural composites and catalyst support in fuel cells because of their long cycle life, high electrical conductivity and low price compared to similar nanostructures like carbon nanotubes [96]. Moreover, the ratio of edge to basal plane atoms is controllable, providing a means to adjust the interaction of metal with the support [97]. The main advantage of CNFs over many other carbon nanomaterials is that their unique microstructure and texture are tunable. Such parameters as diameter, the ratio of the edge atoms to basal atoms and graphite plane angle to the fiber axes are changeable, which makes it possible to modify the catalytic properties of CNFs and alter the deposition methods of various catalysts. Generally, CNFs can be divided into three different forms according to the different arrangement of graphene layers – platelet CNF, tubular CNF and fish-bone CNF [98]. Similarly to CNTs, common method for CNF synthesis is thermal CVD where the carbon source is decomposed on metal catalysts. Even though the synthesis process is very similar to the growth condition of carbon nanotubes, their geometry is different from concentric carbon nanotubes containing an entire hollow core, because they can be visualised as regularly stacked truncated conical or planar layers along the filament length [99,100]. In common to the CNT production, the metal catalyst residues will remain in the as-grown CNFs after the process of synthesis and therefore CNF material needs to be purified from metal nanoparticles before usage as a catalyst support [101]. Otherwise the impurities and metal catalyst will alter the electrochemical properties of CNFs [102]. CNFs are also considered as the potential candidate for ORR cathode catalyst for alkaline fuel cells because of their high chemical and thermal stability and high surface area [103]. It has been shown that the electrocatalyst supported on CNF exhibits a higher electrochemical surface area and more positive onset potential for ORR than that supported on activated carbon [104]. The ORR activity of CNFs is not only dependent on the microstructure and

surface area but is also significantly determined by surface functional groups [105]. Similar to CNTs, these surface functional groups can be attached to the CNF material during the acid treatment [106].

4.3.2. Oxygen reduction on carbide-derived carbons

One of the promising classes of carbon materials with optimisable pore size and structure can be synthesised by the selective extraction of metal atoms out of metal carbides [107,108]. This extraordinary material produced by the extraction of metals from carbides is called carbide-derived carbon (CDC). These CDC materials offer variable pore diameters as well pore volumes and high specific surface area up to 2000 $m^2 g^{-1}$ [109]. CDCs are produced at temperatures from 200 to 1200 °C as a powder with or without mesopores. These materials can find application in gas storage, catalysts, adsorbents, battery electrodes, supercapacitors, water/air filters and medical devices [110]. Different CDCs have been investigated and different pore sizes have been achieved by the selection of metal carbide and optimising chlorination temperatures [110]. Gogotsi et al. have reported major efforts towards the control of the size, shape and uniformity of the pores as well demonstrated the possibility of tuning porosity of carbide-derived carbons with subångström accuracy in a wide range by controlling the chlorination temperature [110].

From the electrochemistry and oxygen reduction electrocatalysis point of view, one of the most important aspects concerning the electrocatalytic properties of CDCs is related to their catalytically effective pore size. It appears that micropores are hard to be reached by reacting species in electrochemical conditions [111] and for this reason, the process of O_2 reduction proceeds basically on the surface of carbon particles and in mesopores. Therefore, for the optimisation of synthesis of CDC materials it is important to achieve catalyst material with maximum amount of mesopores which thereafter would give a higher oxygen reduction activity for these materials. It has been found that similarly to other carbon materials, the CDC-modified electrodes are active electrocatalysts for O_2 reduction in alkaline solution [V]. Up to now only a few studies have been made to investigate the electrocatalytic properties of CDCs for oxygen reduction [112–114]. Most of these studies of ORR have been made with CDC supported precious-metal materials because CDCs afford perfect porosity for metal nanoparticle modification and encapsulation [115,116]. The electrocatalytic properties of CDCs for O_2 reduction are of great fundamental and practical importance, because of the possibility of using CDC as support material for various catalysts in fuel cell applications [117].

4.3.3. Oxygen reduction on graphene

Graphene is a flexible and expandable two-dimensional carbon nanostructure consisting of sp^2 carbon atoms. Graphene is densely packed into honeycomb lattice and is the base of graphitic materials such as fullerenes, carbon nanotubes and graphite [118,119]. It has promising applications thanks to several features: the mechanical strength inherent in the strong covalent bond between adjoining carbon atoms in a basal plane, the unique chemistry of the edges of a graphene sheet, large theoretical surface area, high electrical conductivity and high thermal and chemical stability [120,121]. Graphene has attracted a great interest in different electrochemical applications especially because of its high specific surface area and good electrical conductivity [122,123] and therefore has found usage in various applications, such as batteries, supercapacitors and fuel cells [124,125]. Besides other applications, graphene nanosheets have been successfully used as electrocatalysts for ORR [126–130].

The most practical and efficient procedure to generate individual graphene sheets in bulk quantities is thermal or chemical reduction of graphene oxide (GO) [92]. The preparation of GO itself proceeds to large scale introduction of abundant oxygen-containing functional groups on to the vacancy defects to the basal and edge plane of the exfoliated GO [132]. All of this will afford a large number of reactive sites for various chemical modifications, such as doping with nitrogen atoms. Doping or modification is usually needed because graphene nanosheets themselves have low intrinsic capacitance and poor electron donor or acceptor properties [125].

Modifying with organic compounds or doping with heteroatoms is a common strategy to design electrocatalytically active graphene-based catalysts for ORR [133]. Generation of C-N is one of the methods for the formation of catalytic sites for ORR. To this end, it is possible that nitrogen-doped graphenes (NG) derived from GO can have relatively high surface density of ORR catalytic sites [125]. Several groups have recently reported that NG possessed extraordinary catalytic activity towards the ORR in alkaline medium [134,135].

While doping with heteroatoms is quite a common strategy to design electrocatalytically active graphene-based catalysts for ORR [130] then recently different MN_4 macrocycles, such as metal phthalocyanines and porphyrins, have been employed as promising materials to prepare electrocatalysts with graphene for ORR in alkaline media [IX]. Even though graphene has been considered as a good catalyst support for ORR, there are only a few works dealing with MN_4 macrocycle modified graphene [136–138,IX].

4.4. Oxygen reduction on carbon-supported metallophthalocyanines and metalloporphyrins

When O_2 reacts on the cathode side of a fuel cell, it is crucial to reduce O_2 via direct four-electron pathway to water. In reality, most of catalyst materials only promote the two-electron pathway or the pathway, where the intermediate product is H_2O_2. This is because of the relatively high dissociation energy of the O-O bond. Platinum catalyses O_2 reduction almost entirely via four-electron pathway both in acid and alkaline conditions [14] but a limiting aspect in using platinum in widespread fuel cell industry as an oxygen reduction catalyst is the high cost of this metal. This, in turn, has led to an immense research activity to search for less expensive alternative materials including non-noble metal catalysts. MN_4 macrocycles as one of the most promising non-noble metal catalysts have been investigated intensively since the pioneering work of Jasinski [139]. Since then several review articles about O_2 reduction on MN_4 macrocyles have been published [14,140–143].

The ability of MN_4 macrocycles to reduce O_2 has led to an enormous research activity of these materials in the field of oxygen reduction electrocatalysis both in alkaline and acid media [144–158]. Several authors have shown, that the mechanism of the ORR depends on the nature of the metal center in these complexes. For iron phthalocyanine it has been found that at low overpotentials a four-electron reduction is favourable while many other (Ni, Co and Cu) MN_4-macrocycles promote oxygen reduction mostly via two-electron pathway. There are, of course, always exceptions like vitamin B_{12} which resembles the structure of cobalt porphyrin and also promotes the four-electron electroreduction of oxygen [159]. Similar electrocatalytic activity has in some cases been reported for Co phthalocyanine. It has been shown to have the ability to promote the $4e^-$ oxygen reduction to water without the formation of peroxide intermediates [160]. Besides the other factors, the $2e^-$ or $4e^-$ pathway of the ORR on MN_4-macrocycles depends highly on solution pH [161].

The catalytic activity of MN_4-macrocycles is often related to the redox potential of M(III)/(II) complexes. The more positive the redox potential of the M(III)/(II) couple, the higher the catalytic activity of the metallomacrocycle. The prevailing interactions between O_2 molecule and central metal atom will weaken the O-O bond and premise the breaking of this bond. The metal in the complex should be in the M(II) state for that reaction. If the central metal atom is in the M(III) state, then reduction of this atom to M(II) is required.

In alkaline solutions the following reactions will take a place [162]:

$$\text{M(III)-OH} + e^- \leftrightarrows \text{M(II)} + OH^- \tag{15}$$

$$\text{M(II)} + O_2 \rightarrow \text{M(III)} - O_2^- \text{ or M(II)} - O_2 \tag{16}$$

which undergoes as follows:

$$M(III) - O_2^- + e^- \rightarrow M(II) + \text{intermediates} \quad (17)$$

The scheme is valid for Fe and Mn. For Co the process could involve the M(II)-O_2 instead of M(III)-O_2^-. In the case of Co-N_4 macrocycles Co(III) is not formed in the reaction with O_2 but Reaction (15) is still crucial because of the active site of Co(II) [140]. In acid solutions the whole reaction follows a similar pathway but the process will involve proton.

The onset potential of the ORR follows the redox potential of M(II/III) and also the pH dependence is in most cases the same as that of the M(II/III) couple in the absence of O_2 [156]. The only requirement for this assessment is that the M(II/III) redox potential should be measured in exactly the same conditions (same electrolyte with same pH) in which the ORR is investigated, because the M(II/III) redox couples are pH dependent [163–166].

As the support material has its own impact on the electrocatalytic process, it is essential to measure the redox potential of the M(II/III) couple on the same support material as used for MN_4-macrocycles, because of the possible redox potential differences in the aqueous media vs. support adsorbed state. It has been shown that for the Fe and Co tetrakis(4-N-methylpyridyl)porphyrin) differences of +0.3 V and +0.41 V respectively were found between the edge plane of pyrolytic graphite adsorbed and solution-based material [167,168].

Despite all that, it is still not entirely clear why these materials catalyse the ORR. Some authors have proposed that the splitting of the O-O bond takes place because of the formation of peroxo dimer on the two metal active sites (dual-site mechanism) [162]. Other authors suggest that MN_4 macrocycles will catalyse the ORR via dual-site mechanism where oxygen will coordinate to the metal active center and to N-atom on the macrocyclic ligand [169]. There is a general agreement in the literature, that besides the transition metal the nitrogen ligands in MN_4 macrocycle catalysts play an important role in their stability and activity, even if the constituents of the final active sites are uncertain [170,171].

It is worth mentioning that support material can also act as an axial ligand, therefore the properties of the complexes on the adsorbed state could be different [162]. Catalyst supports including carbon nanotubes, carbon nano-fibers, graphene, Ketjen Black and Vulcan carbon have been employed for FePc and CoPc complexes in numerous studies in the field of oxygen reduction electrocatalysis [94,133,143,172–181]. Functionalising CNTs with phthalo-cyanines was reported to improve the electrocatalytic properties of these complexes [180–182]. Phthalocyanines adsorb strongly on CNTs via non-covalent π–π interactions and form “molecular phthalocyanine electrodes” [142,143].

Another aspect that influences the electrocatalytic activity of a catalyst material is the amount of the MN_4 catalysts on the surface of the support material. It has been found that the O_2 reduction currents are directly related to the thickness of catalyst layer on the support material. Scherson et al. have reported that only 30% of the catalyst deposited on the porous support material

is active for ORR [183]. It has also been found, that only the outmost layer of the catalyst is accessible to oxygen molecules and therefore active for O_2 reduction. Too thick layer of the catalyst starts to affect the electrical conductivity and thereby decrease the O_2 reduction current [184].

Long-term stability is a major problem of MN_4 macrocycles. The formation of hydroxyl radicals play a primary role in rapid degradation of MN_4 catalysts, not H_2O_2, as sometimes suggested [185]. It has been found that pyrolysis in an inert atmosphere increases both the catalytic activity and stability of catalyst materials [186,187]. Since the pioneer study of Jahnke et al. [188], who reported the effect of heat-treatment, numerous research efforts have been made to find and optimise the conditions of pyrolysis as well to clarify the exact structure of the catalytic center causing the electrocatalytic activity towards the ORR [189–192]. The choice of temperature for the heat-treatment depends on the specific MN_4-macrocycle. Temperatures used for the pyrolysis of MN_4-macrocycles in inert atmosphere vary usually from 500 to 1000 °C but it has been found that most macrocycles achieve the highest activity at temperatures from 500 to 600 °C. At higher temperatures the activity of catalyst material can decrease but at the same time stability increases. One of the first studies about improved stability at high temperatures has been reported by Bagotsky et al. [193] who heat-treated MN_4-macrocycle catalyst at various temperatures from 400 to 1000 °C. They observed stability change from 150 h (material pyrolysed at 400 °C) to 10000 h (catalyst heat-treated at 800 °C). The exact chemical processes taking place during the pyrolysis and resulting catalytically active chemical species are still under debate. There are several reviews published about this topic since the mid-1980s [164,194].

There are three main opinions about the mechanism occurring during the pyrolysis of the MN_4-macrocycles [195]:

1. Van Veen proposed that the best catalytic activity can be achieved at temperatures between 500 to 600 °C and it does not lead to the complete destruction of the macrocycles. Instead ligand modification takes place. Stability is achieved by the bounding of the ligands to the carbon support, which will eliminate the oxidative attack to the catalyst material.
2. Yeager disagreed with the results achieved by van Veen and concluded that the decomposition of the macrocycles starts already at 400 °C. At 800 °C all the macrocycles are decomposed and metal is not coordinated to the nitrogen ligand atoms anymore. Instead of that, metallic ions coordinate or adsorb to the carbon surface and involve nitrogen to the formed composition as-well. Yeager proposed that the resulting structure is catalytic site for ORR.
3. According to Wiesener, metal ions of the MN_4-macrocycles promote the decomposition of the chelate at higher themperatures and then formation of nitrogen-doped carbon takes place. In this case, metal residues of the decomposed MN_4-macrocycles have no remarkable role in the ORR and incorporation of nitrogen into carbon yields active group for oxygen reduction.

In the latter case it was found that the transition metal of the precursor is bonded via nitrogen to a graphite-like carbon matrix, which was formed by the pyrolysis reaction. It has been proposed that the inner core structure of the MN_4 macrocycle remains after the pyrolysis and acts as a catalytic centre towards the ORR [196].

Different research groups have reported achievements in enhancing the electrocatalytic activity as well as stability of CoPc supported on nanocarbon material by pyrolysis in inert atmosphere [197]. It has been found that after heat-treatment the cobalt complexes are more stable that the iron complexes [198]. Despite the numerous studies there is still a lot unclear in the reduction process and exact catalytic active sites are still unknown and under the debate [199]. On the one hand MN_4-centers are believed to be responsible for the improved catalytic effect, on the other hand, nitrogen heteroatoms are favoured as catalytic sites [194,200,201]. The important role of nitrogen in the MN_4 catalyst material has been proved by Lalande et al. [181]. Metal-N_4^- or metal-N_{2+2} are suggested as active sites also by Wiesener [194].

Some research groups have also suggested that quinone groups present on the surface of carbon materials could take part in the formation of active sites. Elbaz et al. presented evidence about the formation of stabilised MN_4 macrocycle-quinone complexes at carbon-based surfaces towards the design of non-noble metal catalysts for the ORR [202].

4.5. Principles of alkaline fuel cell

Traditionally fossil fuels such as coal, oil and gas, have been used to satisfy the world´s needs for energy. However, these resources are not endless and the topic of reducing CO_2 production has already been under debate for many years. Replacing fossil fuel by H_2 would be one of the alternatives and would help to reduce the production of greenhouse gases remarkably. Therefore the development and production of fuel cells is a worldwide priority. Fuel cell is a system that directly converts the chemical energy into electrical energy, heat and water by a redox reaction [203]. Fuel cells are classified according to the type of the electrolyte and the operating temperature used. Two main types of fuel cells are classified as low-temperature fuel cells with operating temperatures below 120 °C: proton-exchange membrane fuel cells (PEMFCs) and anion-exchange membrane fuel cells (AEMFCs). The working principle of the AEMFC is as follows: pure oxygen or air oxygen is reduced on the cathode, producing hydroxide ions. These ions are transferred through the electrolyte (formerly a liquid electrolyte, now a polyelectrolyte consisting of a polymer that bears cationic groups) to the anode, on which the oxidation of the hydrogen to water takes place. Anion exchange membranes (AEM) are usually solid polymer electrolyte membranes that contain positive ionic functional groups and the negatively charged anions (usually OH^-) will be transported through the

membranes [204]. Among all the types of fuel cells, the AEMFC is the most recent one [205], as early works on anion-exchange membranes for fuel cells were published in early 2000 [206]. However, a prototype was designed by Hunger in 1960 [207]. AEMFCs have several advantages over PEMFCs including the faster kinetics of the ORR in alkaline conditions and therefore providing lower activation losses than in acid conditions [208,209]. Another advantagew are that non-precious metal catalysts can be used [200] (because these materials are often more active and stable in alkaline media than in acid environment of PEMFCs) and investments for fuel cell components can be reduced due to less corrosive environment [210]. Another major issue of PEMFCs is water management, crossover and cathode flooding which for AEMFCs is solved by taking water and ion transport away from the cathode to the anode, justifying crossover and flooding issues [215].

Several research groups have been developing AEMFCs for many potential applications [200,211–215]. The increased interest in the research and development of AEMFCs in recent years has been caused mainly by of the development of new anion exchange membranes [204]. For almost half a century, the major barrier to the commercialisation of alkaline fuel cells has been the lack of a practical polymer electrolyte anion exchange membrane. However, within the past few years, Tokuyama Corporation has developed an AEM which has been demonstrated to give power densities competitive to Nafion in PEMFCs [VIII]. The alkaline environment is significantly less corrosive to the catalysts, which would permit the use of less noble catalysts which is one of the main advantages besides the ones mentioned above [216]. However, there are two main drawbacks in the usage of AEM as well. The main drawback of this fuel cell lies in its membrane which can either yield carbonation phenomena or generate leaks and this leads to thermal and chemical instability [217].

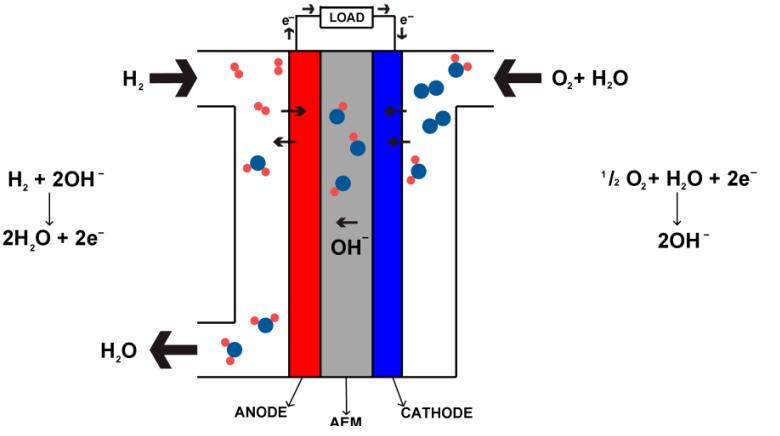

Scheme 2. Illustration of the H_2/O_2 AEMFC´s working principle.

5. EXPERIMENTAL

5.1. Chemicals and materials

The single-walled carbon nanotubes (SWCNTs, purity >90%, diameter 1–2 nm, length 5–30 μm) used were purchased from Nanostructured & Amorphous Materials, Inc. (Houston, TX, USA). The double-walled carbon nanotubes (DWCNTs, purity >95%, diameter 4±1 nm, length 5–20 μm) and the multi-walled carbon nanotubes (MWCNTs purity >95%, diameter 30±10 nm, length 5–20 μm) used were purchased from NanoLab, Inc. (Brighton, MA, USA). Commercial carbon powder Vulcan XC72R was purchased from Cabot Corp. 20 wt.% Pt commercial catalyst supported on Vulcan XC-72 was purchased from E-TEK, Inc. (Frimingham, MA, USA) and commercial 46.1 wt.% Pt catalyst supported on Ketjen Black was purchased from Tanaka Kikinzoku Kogyo K.K. (Japan). Several surfactants were used in the preparation of aqueous dispersions of MWCNTs. Dihexadecyl hydrogen phosphate (DHP) was a product of Fluka, cetyltrimethylammonium bromide (CTAB), sodium dodecyl sulfate (SDS) and Triton X-100 were purchased from Aldrich. Polytetrafluoroethylene (PTFE) (Sigma-Aldrich) aqueous dispersion (60 wt.%) was employed. A 0.5% Nafion solution used in this work was prepared by diluting the 5% Nafion solution (Aldrich) into ethanol. 5 wt.% OH^- ionomer solution (Tokuyama Corp.) was used in the preparation of catalyst ink in 2-propanol. The iron(II)phthalocyanine (FePc), cobalt(II)phthalocyanine (CoPc), 5,10,15,20-tetrakis(4 methoxyphenyl)-21H,23H-porphine cobalt (II) (CoPh) and 5,10,15,20-tetrakis(4methoxyphenyl)-21H,23H-porphine iron (II) chloride (FePh) were purchased from Sigma Aldrich.

The electrolyte solutions for studying O_2 reduction were prepared from 96% H_2SO_4 (Suprapur, Merck) and KOH pellets (AristaR, BDH) in Milli-Q water; these were saturated with O_2 (99.999%, AGA or 99.95%, AGA) or deaerated with Ar gas (99.999%, AGA). All other chemicals were analytical grade reagents and all the solutions were prepared with Milli-Q water (Millipore, Inc.).

Glassy carbon (GC) electrodes employed for RDE experiments were prepared by mounting the GC disk of geometric area of 0.2 cm^2 in a Teflon holder. GC disks were cut from rods (GC-20SS, Tokai Carbon). The GC electrode surface was polished to a mirror finish with 1 and 0.3 μm alumina slurries (Buehler). After alumina polishing the electrodes were sonicated in water for 5 min before use.

Highly oriented pyrolytic graphite (HOPG) disks of 0.2 cm^2 surface area (NII Graphite, Russia) were used for hydrodynamic experiments. The fresh surface of HOPG was prepared prior to each measurement by removing the top layers with adhesive tape.

For the rotating ring-disk electrode (RRDE) experiments the disk electrode with surface area of 0.2 cm^2 was employed. An interchangeable E6 series

RRDE tip of GC disk-Pt ring (Pine Research Instrumentation, Inc., Grove City, PA, USA) was used for the RRDE measurements. A collection efficiency (*N*) of 0.25 was determined from measurements of hexacyanoferrate(III) reduction. Both the GC disk and Pt ring electrodes were polished to a mirror finish with 1.0, 0.3 and 0.05 μm alumina slurries (Buehler) followed by sonication in water for 5 min. before use. Milli-Q water (Millipore, Inc.) was used throughout.

5.2. Acid-treatment of carbon nanotubes

For acid washing studies of SWCNTs or MWCNTs different acids (3 M HCl, 3 M HNO_3, concentrated H_2SO_4 and the mixture of HNO_3 and H_2SO_4) was used for carbon nanotube purification. As-received SWCNTs and MWCNTs were first treated by sonicating CNTs for 30 min in acid at room temperature and then stirring them in acid for 24 h. Finally the CNTs were washed with Milli-Q water and dried at 110 °C. For all the other studies carbon nanotubes were acid-treated by refluxing in a mixture of concentrated nitric and sulfuric acids (1:1, v/v) for 2 h at 55 ºC and then 3 h at 80 ºC. Afterward, the nanotubes were washed with Milli-Q water by centrifugation (3000 rpm, 10 min) for several times and the MWCNTs were resuspended in Milli-Q water. Finally, the MWCNTs were dried under vacuum for 15 h.

5.3. Synthesis of carbide-derived carbon

Aluminium carbide (Accumet, 325 mesh or Cerac, 1–5 μm average particle size) with or without graphitisation catalyst, was loaded in the horizontal quartz tube and was reacted with a flow of chlorine gas (99.999%) at a fixed temperature, which is indicated in Table 1. The byproduct, $AlCl_3$, was evacuated by the flow of the excess chlorine. During the heating and cooling the reactor was flushed with a slow stream of argon. After chlorination the product was additionally treated with hydrogen at 800 °C to deeply dechlorinate the sample.

Table 1. The physical parameters of Al_4C_3- derived carbons.

Notation of CDC material	Origin of Al_4C_3	Catalyst $NiCl_2/CoCl_2/FeCl_3$ [mg g^{-1} (carbide)]	T_{Cl} [°C]	S_A [m^2 g^{-1}]	V_p [cm^3 g^{-1}]	V_μ [cm^3 g^{-1}]
C824	Accumet	70 / 70 / 70	1100	177	0.12	~0
C1551	Cerac	3.5 / 3.5 / –	700	684	0.88	~0

5.4. Preparation of graphite oxide, graphene oxide and rGO

Graphite oxide was prepared from graphite powder by the modified Hummers method [218,219]. Briefly: 0.5 g of graphite powder was taken in a 500 mL flask, 0.25 g of $NaNO_3$ and 12 mL of H_2SO_4 were added and cooled in ice bath for 30 min. While maintaining vigorous shaking 1.5 g of $KMnO_4$ was added slowly to prevent the temperature of the suspension exceeding 10 ºC. Then ice bath was removed and the temperature of the suspension brought to room temperature (23±1 ºC), where it was maintained for 2–3 h for complete oxidation of graphite powder. Then 25 mL of deionised water was slowly added into the paste and stirred, suspension was kept for 30 min. The suspension was further diluted with 50 mL warm deionised water and to the diluted suspension 5 mL of 7% H_2O_2 was added to completely remove permanganate ions. The resulting suspension was filtered and washed several times with deionised water. Finally, the solid brownish filtered material was re-dispersed in deionised water containing molecular sieve to remove unwanted ions, then filtered and washed several times with deionised water. The final product was dried in air.

Graphene oxide (GO) was prepared from graphite oxide in water by 5 h ultrasonication (22 KHz). During ultrasonication the temperature of the suspension was controlled under 40 ºC by sufficient cooling of the system. The suspension was kept for 48 h to settle down larger particles. Then centrifugation was performed at 6000 rpm for 8 h. After centrifugation decantation was carried out by pipetting top part of the suspension.

Reduced graphene oxide (rGO) was prepared by chemical reduction of GO using reducing agents (Fe/HCl) at room temperature. In a typical experiment 1 g of Fe powder and 20 mL of 37% HCl were added into a beaker containing 100 mL of GO suspension. The mixture was stirred vigorously for 6 h to complete the reduction of GO. Then 15 mL of HCl was added into the solution to fully remove excess Fe powder. Finally, the resulting rGO nanosheets were collected by filtration, washed with deionised water and ethanol several times and were re-dispersed in deionised water.

5.5. Preparation of FePc/MWCNT, CoPc/MWCNT, FePh/MWCNT and CoPh/MWCNT catalysts

In order to adsorb the metal macrocyclic catalyst on the surface of MWCNTs, a mixture of 200 mg FePc, CoPc, FePh or CoPh and 200 mg MWCNTs in 40 mL isopropanol was prepared and sonicated for 30 min followed by magnetic stirring for 1 h. The homogeneous mass was placed in a ceramic boat, dried at 100 ºC and pyrolysed at 400 ºC or 800 ºC for 2 h in flowing argon atmosphere. The initial loading of FePc, CoPc, FePh or CoPh on the MWCNTs was 50 wt.% and the final loading was not ascertained.

5.6. Preparation of FePc/rGO and CoPh/rGO catalysts

For the physical adsorption of metal macrocyclic catalysts on the surface of rGO, a mixture of 50 mg FePc or CoPh and 50 mg rGO in 40 mL isopropanol was prepared and sonicated for 30 min followed by magnetic stirring for 24 h.

5.7. Preparation of SWCNT and MWCNT modified GC electrodes for studies of the effect of purification of carbon nanotubes

To obtain a uniform layer of SWCNTs and MWCNTs onto GC surface, the electrodes were modified with nanotubes using aqueous suspensions (1 mg mL^{-1}) containing 0.5% Nafion. All the suspensions were sonicated for 1 h. Then a 20 μL aliquot of SWCNTs or MWCNTs suspension was pipetted onto GC surface and the solvent was allowed to evaporate in air.

5.8. Preparation of MWCNT modified HOPG electrodes

The HOPG electrodes were modified with MWCNTs in 1 mg mL^{-1} suspension in isopropanol. Long-term sonication of the suspension is needed to enable the separation of individual MWCNTs from nanotube bundles. For MWCNTs deposition a hydrodynamic technique was applied. The HOPG electrodes were rotated in the MWCNTs suspension at 360 rpm for 10 min. After deposition, the electrodes were immediately rotated in clean isopropanol at 4600 rpm for 1 min and then were allowed to dry in air at room temperature.

5.9. Preparation of DWCNT modified GC electrodes

To obtain a uniform layer of DWCNTs onto GC surface, the electrodes were modified with nanotubes using aqueous suspensions (1 mg mL^{-1}) containing 0.3% Triton X-100 for measurements in alkaline media or 0.5% Nafion for acid conditions. All the suspensions were sonicated for 1 h. Then a 20 μL aliquot of a DWCNT suspension was pipetted onto GC surface and the solvent was allowed to evaporate in air.

5.10. Preparation of MWCNT modified GC electrodes for the pH-dependence studies

To obtain a uniform layer of MWCNTs onto GC surface, the electrodes were modified with nanotubes using aqueous suspensions (1 mg mL^{-1}) in the presence of surfactants: 1% SDS, 0.3% CTAB, 0.3% Triton X-100 and 0.1% DHP. These concentrations exceed the critical micelle concentration. All the suspensions were sonicated for 1 h. Ultrasonication is needed to provide a high local shear that enables the dispersion of individual nanotubes (or smaller aggregates) from the bundles of MWCNTs. Then a 10 μL aliquot of the MWCNT-surfactant suspension was pipetted onto GC surface and the solvent was allowed to evaporate in air.

5.11. Preparation of CDC modified GC electrodes

The GC disk electrodes were modified with carbon nanomaterials using aqueous suspensions of 4 mg cm^{-3} in the presence of 0.3% non-ionic surfactant Triton X-100 (Sigma-Aldrich) and 0.4 mg cm^{-3} polytetrafluoroethylene, PTFE (Sigma-Aldrich). The surfactant was used to make a uniform dispersion of nanocarbons. All the suspensions were sonicated for 1 h. Carbon nanomaterials were physically attached to the surface of electrodes by pipetting 10 μL aliquot of the suspension onto GC surface and allowing the solvent to evaporate in air. For the RDE measurements, the carbon nanomaterial modified GC electrodes were heated at 80 °C in an oven for 1 h before use. For the RRDE measurements the modified GC electrodes were heated at 350 °C for 0.5 h. At this temperature the surfactant used decomposes [220].

5.12. Preparation of MN_4 macrocycles/MWCNT and MN_4 macrocycles/rGO modified GC electrodes

To obtain a uniform layer of electrocatalyst onto GC surface, the electrodes were modified with different catalysts using aqueous suspensions (1 mg mL^{-1}) containing 0.5% Nafion for experiments in 0.5 M H_2SO_4 and 0.5% OH^- ionomer for measurements in 0.1 M KOH. All the suspensions were sonicated for 1 h. Then a 20 μL aliquot of the prepared catalyst suspension was pipetted onto GC surface and was allowed to dry in air for 24 h.

For the rGO supported catalyst studies the electrodes were modified with different catalysts using isopropanol suspensions (1 mg mL^{-1}) containing 0.5% OH^- ionomer. A 20 μL aliquot of the prepared catalyst suspension was pipetted onto GC surface and was allowed to dry in air for 24 h.

5.13. Electrode fabrication and performance evaluation for AEMFC

Membrane-electrode assemblies (MEAs) were fabricated with commercial carbon-supported Pt catalyst (Pt/C) as anode catalyst and FePc/MWCNT, CoPc/MWCNT and commercial catalyst (Pt/C) on cathode sides of the Tokuyama polymer membrane (A201 membrane, Tokuyama Corporation, Japan). Catalyst ink was prepared by adding Milli-Q water to catalyst material (2 mL for 100 mg of electrocatalyst). In order to extend the reaction zone of the catalyst layer, 5 wt.% ionomer (AS4 ionomer, Tokuyama Corporation, Japan) dispersion (0.8 mL for 100 mg of electrocatalyst) was added to the catalyst slurry. Catalyst layer was coated on the alkaline membrane with 5 cm^2 geometrically active area applying the catalyst ink by spraying method on both sides of the membrane and vacuum dried at 70 ºC for 15 min. The catalyst loadings were about 0.4 and 0.6 mg cm^{-2} on the anode and cathode sides, respectively. The MEA was assembled by sandwiching the catalyst coated membrane inside the test cell (Fuel Cell Technologies Inc, Albuquerque, NM, USA) with gas diffusion layers on both sides. Gas sealing was achieved using silicone coated fabric gasket (Product # CF1007, Saint-Gobain Performance Plastics, USA) and with a uniform torque of 0.45 kg m.

5.14. Instrumentation and measurements

An EDI101 rotator and a CTV101 speed control unit (Radiometer, Copenhagen) were used for the rotating disk electrode (RDE) experiments. The electrode rotation rate was varied between 360 and 4600 rpm. A saturated calomel electrode (SCE) was employed as the reference electrode. The counter electrode compartment of the three-electrode cell was separated from the main cell compartment by a glass frit and Pt wire served as a counter electrode. The potential was applied with an Autolab potentiostat PGSTAT10 or PGSTAT30 (Eco Chemie B.V., The Netherlands) and the experiments were controlled with General Purpose Electrochemical System (GPES) software. All experiments were carried out at room temperature (23±1°C).

For all RDE measurements the adhesion of the composite electrocatalysts to the GC disk was excellent and no loss of the catalyst occurred during the measurements as evidenced by an unchanged and stable cyclic voltammogram before and after the ORR testing.

Transmission electron microscopy (TEM) experiments were performed with a JEOL, JEM-2010 microscope working at 200 kV, with Tecnai instrument operated at a 120 kV accelerating voltage and with JEOL JEM 3010 instrument operated at 300 kV. The sample for TEM analysis was obtained by placing a droplet of a CNT suspension onto a formvar/carbon coated copper grid and waiting until the complete evaporation of the solvent in air at room temperature.

High-resolution scanning electron microscope experiments were performed with HR-SEM, Helios 600, FEI).

Atomic force microscope studies (AFM) were performed with AutoProbe CP II, Veeco machinery in intermittent contact mode using NSG11S (NT-MDT) cantilevers. For the AFM imaging a 2 mm-thick HOPG substrate (1×1 cm^2, SPI-2, West Chester, PA, USA) was employed.

The X-ray photoelectron spectroscopy (XPS) experiments were carried out with a SCIENTA SES-100 spectrometer by using a non-monochromatised Mg Kα and Al Kα X-ray source (incident energy = 1253.6 eV for Mg Kα and 1486.6 eV for Al Kα), electron take-off angle θ = 90 ° and a source power of 300 W. The pressure in the analysis chamber was below 10^{-9} Torr. While collecting the survey scan, the following parameters were used: energy range = 950–0 eV, pass energy = 200 eV, step size = 0.5 eV and for the high resolution scan in the: energy range = 540–525 eV for the O1s region; energy range = 420 to 395 eV for the N1s region; energy range = 740 to 700 and 800 to 775 eV for the Fe2p and Co2p regions, respectively. Pass energy = 200 eV and step size = 0.1 eV for the high resolution scans. The composition of SWCNT and MWCNT materials was analysed using INCA Energy 350 (Oxford Instruments) energy dispersive X-ray spectrometer (EDS) equipped with X-Max 50 mm^2 detector from the same company, connected to scanning dual beam microscope Helios^{TM} NanoLab 600 (FEI). The Microanalysis Suite version 4.13 program was used for the evaluation of sample composition.

Complete conversion of carbide into carbon was confirmed by the X-ray powder diffraction (XRD) measurements using CuKα radiation (λ = 1.54 Å).

The low-temperature N_2 sorption experiments were performed at –196 °C. The specific surface area (S_A) was calculated according to the Brunauer–Emmett–Teller theory up to the nitrogen relative pressure (P/P_0) of 0.2. The total volume of pores (V_p) was calculated at relative pressure (P/P_0) of 0.95 and the volume of micropores (V_μ) from *t*-plot, using Harkins-Jura thickness values between 5 Å and 90 Å.

The single cell fuel cell performance was evaluated with humidified (100% RH) H_2 and O_2 gases at 45 °C using Greenlight Test Station (G50 Fuel cell system, Hydrogenics, Vancouver, Canada). The flow rates were fixed at 200 and 400 SCCM for H_2 and O_2, respectively.

6. RESULTS AND DISCUSSION

6.1. Effect of purification of carbon nanotubes on their electrocatalytic properties for oxygen reduction

In this section a detailed study of the effect of acid treatment of carbon nanotubes on the oxygen reduction reaction is presented [I], because it has been shown that iron impurities are responsible for the electrocatalytic properties of CNTs in several reactions [221,222]. We compare four different acid-treatment methods (treating CNTs in 3 M HCl, 3 M HNO_3, concentrated H_2SO_4 and in the mixture of HNO_3 and H_2SO_4) and their efficiency for carbon nanotube purification from metal residues. A systematic study was carried out to clarify the catalytic role of the metal catalyst impurities of CNTs in the ORR on the CNT modified GC electrodes. The concentration of metal catalysts in the CNT materials was determined by EDS and the surface morphology of the carbon nanotube samples was examined by TEM. The acid-treated MWCNTs were also characterised by Raman and X-ray photoelectron spectroscopies. We also compare the electrocatalytic properties of SWCNTs and MWCNTs for oxygen reduction before and after acid treatment. The oxygen reduction reaction has been investigated on acid-treated SWCNT and MWCNT modified GC electrodes in acid media using the RDE method.

6.1.1. Physical characterisation of acid-treated CNTs

The presence of catalytic metal impurities, amorphous carbon, defects and the structure of SWCNTs and MWCNTs were investigated with transmission electron microscopy. Figures 1a and 1b present TEM images of as-received and 3 M HNO_3 treated MWCNTs, respectively, deposited on a formvar/carbon coated copper grid. The MWCNT material consists of a notable amount of metal nanoparticles as well different types of carbons in various sizes, different shapes and the molecular organisations: free MWCNTs, carbon nanotubes trapped in amorphous carbon and some carbon lamellas. The lamellar carbons can form at any carbon surface where carbon free radicals exist which nucleate and subsequently add parallel carbon layers [223]. Figure 1b reveals substantial removal of catalyst impurities by acid treatment. Figures 1c and 1d present TEM images of as-received and acid-treated SWCNTs, respectively. The as-received SWCNTs seem to be much cleaner of metal catalyst and amorphous carbon as compared to the MWCNTs. After purification in 3 M HNO_3 most of the metal catalyst is removed. Figure 1d shows the clean-cut structure of SWCNTs, having no observable defects on the surface of the nanotubes.

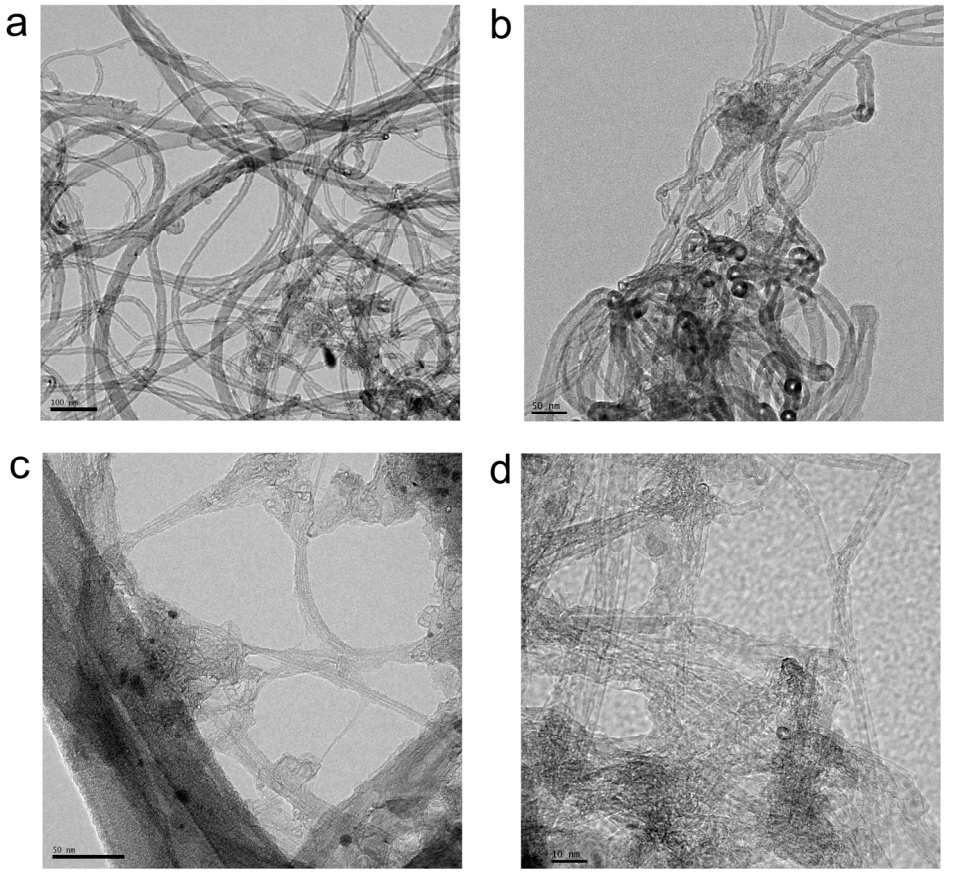

Figure 1. TEM images of CNT materials deposited on formvar/carbon coated copper grids: as-received MWCNTs (a), 3 M HNO_3 purified MWCNTs (b), as-received SWCNTs (c) and 3 M HNO_3 purified SWCNTs (d).

According to the EDS analysis the concentration of iron in MWCNTs was as follows: as-received material 1.2 wt.%, 3 M HCl purified 0.95 wt.%, concentrated H_2SO_4 purified 1.0 wt.% and 3 M HNO_3 purified 0.4 wt.%. The concentration of cobalt in SWCNTs was as follows: as-received material 1.0 wt.%, 3 M HCl purified 0.8 wt.%, concentrated H_2SO_4 purified 0.67 wt.% and 3 M HNO_3 purified 0.75 wt.%. In addition, in the as-received SWCNTs the sulphur content was as high as 0.9 wt.% and the concentrations of iron were lower than the detection limit of the method (< 0.1 wt.%).

Figure 2a and 2b presents the XPS survey spectra of HNO_3 and acid mixture purified MWCNT samples. Four XPS peaks were observed for both samples, which correspond to emission from C1s (284.4 eV), satellite peak of the C1s spectrum, O1s and N1s levels. In addition, there was a small S2p XPS peak of the acid mixture treated MWCNTs. The O1s peak is caused by various carbon-oxygen functionalities on the surface of CNTs. Detection of different functional

groups from the O1s peak is not straightforward because of similar binding energies. However, more detailed investigations have shown that carboxyl and quinone groups are present on the surface of carbon nanotubes [224,225]. The XPS core-level spectrum in the N1s region of HNO_3-treated MWCNT shows two peaks. The N1s peak at higher binding energy (405.8 eV) corresponds to nitro groups and the one at 399.8 eV could be assigned to N introduced into the graphene layer. It should be noted that metal catalyst impurities were not detected in the acid-treated MWCNT samples by XPS.

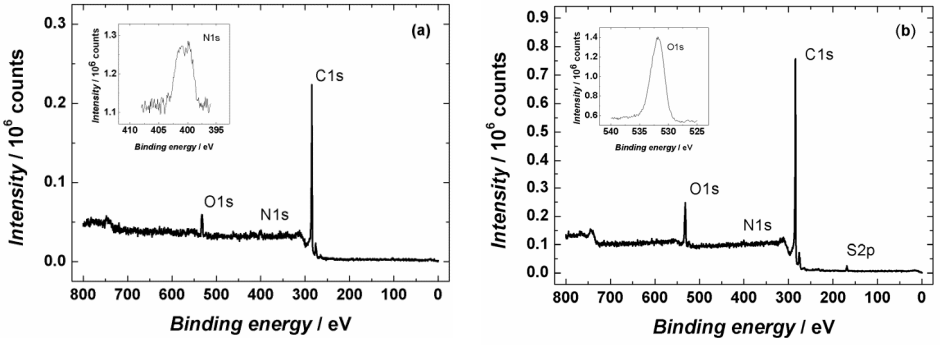

Figure 2. XPS spectra of HNO_3 (a) and $HNO_3 + H_2SO_4$ (b) purified MWCNTs.

In order to examine the defects induced by acid treatment and study the crystalline structure of MWCNTs the characterisation of MWCNTs was carried out by Raman spectroscopy. The main features in the Raman spectrum of carbon materials are the group of peaks called "D-band" around 1340 cm^{-1} and the peaks called "G-band" in the range of 1550–1600 cm^{-1}. The ratio of intensities of G and D band is often used to characterise quantity of defects in MWCNTs and graphitic materials [81]. The D-band is a disorder induced characteristic and assigned to the amorphous carbon and disordered graphitic material presented in the CNT material [226]. The structural disorders in CNT material are usually nanosized graphitic planes and other structures of carbon, such as rings along with defects on the nanotube walls, vacancies, heptagon-pentagon pairs, heteroatoms and kinks [82]. The G-peak at 1582 cm^{-1} corresponds to the tangential vibrations of the carbon atoms in the graphite [227]. Figure 3 presents Raman spectra of the acid-treated and as-received MWCNTs. When comparing the D and G peaks for the as-received and nitric acid treated nanotubes, one can see a decrease in the D-band intensity for 3 M HNO_3 treated MWCNTs, which indicates the reduction of disordered carbon and demonstrates the effectiveness of mild nitric acid treatment in diminution of amorphous carbon in the MWCNT material. Raman spectra of H_2SO_4 and acid mixture purified MWCNTs show an increase of D-band as compared to 3 M HNO_3 treated MWCNTs, which might be caused by defects and damages introduced to MWCNTs by more aggressive oxidation by acids.

The ratio of intensities between G and D band were as follows: as-received MWCNT material 1.3, 3 M HNO_3 purified MWCNTs 3.1, concentrated H_2SO_4 purified MWCNTs 1.6, and HNO_3 + H_2SO_4 purified MWCNTs 1.2. As the ratio of intensities of G and D band can be used as a measure of the graphitic structure of the carbon nanotubes, it can be concluded that using 3 M HNO_3 solution for the treatment of MWCNTs improves the structural order and purity of 3 M HNO_3 purified MWCNTs.

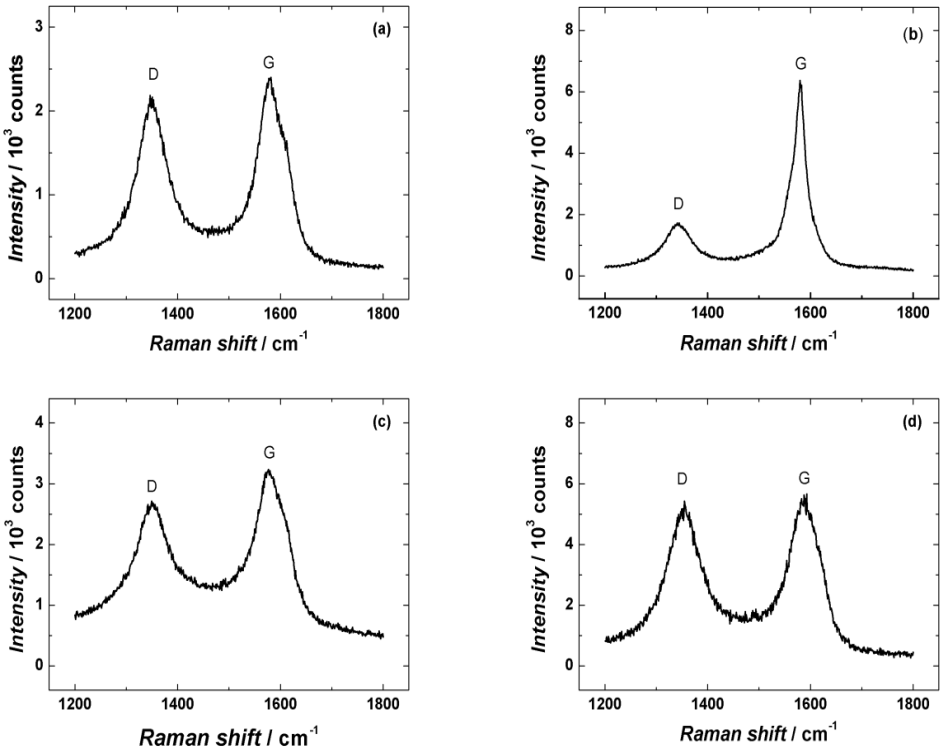

Figure 3. Raman spectra of as-received (a) and HNO_3 (b), H_2SO_4 (c) and HNO_3 + H_2SO_4 (d) purified MWCNTs

6.1.2. Cyclic voltammetry of CNT modified electrodes

Cyclic voltammetric (CV) experiments were performed to investigate the effect of carbon nanotubes microstructure on their electrochemical properties. The CVs were recorded in Ar-saturated 0.5 M H_2SO_4 at a scan rate of 100 mV s^{-1}. Figures 4a and 4b present typical CV responses of the differently purified carbon nanotube modified GC electrodes recorded between 0.8 and –0.4 V. For the SWCNT and MWCNT-modified GC electrodes purified in 3 M HNO_3, a clear pair of reduction and oxidation peaks is observed at approxi-

mately 0.4 V. These peaks can be designated to carbon-oxygen functionalities on the surface of the CNTs, most probably to quinone-type species [228]. It can be suggested that the high background current for 3 M HNO_3 purified SWCNT and MWCNT-modified GC electrodes is caused by minor defects on the CNTs walls and the opening of the ends of CNTs or more hydrophilic properties of oxidised CNTs [65,229]. This presumption is also in agreement with the research made by Britto et al. [52] who compared the ORR activities of CNT and graphite, and concluded that the CNTs activity is higher than that of graphite because of the graphitic defects of CNTs, e.g. pentagon and heptagon derived defects at the CNT tips. By contrast, the CV curves for the H_2SO_4 treated MWCNTs and SWCNTs are almost featureless and the current is rather low, which could be due to the less oxidative properties of sulphuric acid at room temperature, causing therefore smaller number of defects at the surface of CNTs.

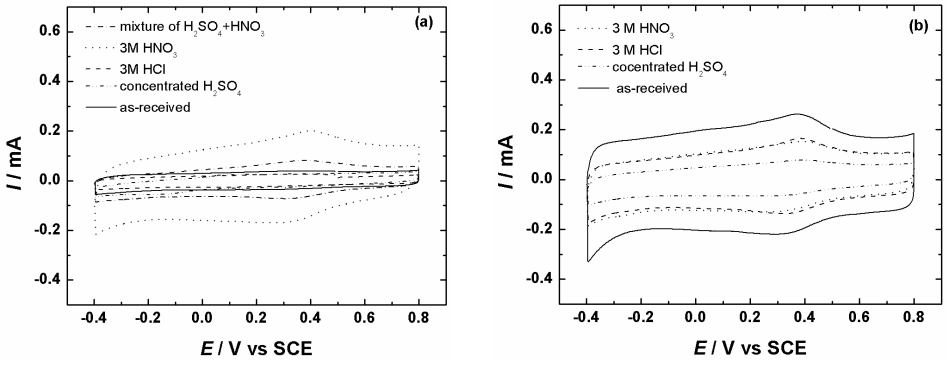

Figure 4. Comparison of cyclic voltammograms of acid-treated and as-received MWCNT (a) and SWCNT (b) modified GC electrodes in Ar-saturated 0.5 M H_2SO_4. $v = 100$ mV s^{-1}.

6.1.3. O_2 reduction on SWCNT/GC and MWCNT/GC electrodes

Acid treatment of CNTs has a considerable effect on the ORR. It is well-known that carbon material itself is rather inactive in acid media and mostly the metal nanoparticles remained on the walls and inside the CNTs catalyse the ORR. Figure 5a presents the polarisation curves for oxygen reduction in O_2 saturated 0.5 M H_2SO_4 on the acid-treated MWCNT-modified GC electrodes recorded between 0.8 and –0.4 V. One can see that the O_2 reduction results depend on the purification procedure used.

The onset potential of the as-received MWCNT-modified GC electrode is at 0.4 V while the reduction of oxygen on the acid purified MWCNT/GC electrodes commences at 0.3 V. The only exception are the results obtained with HNO_3 purified MWCNT/GC electrodes where the reduction current starts

to increase at 0.1 V, which indicates that this method of nanotube purification appears to be the most effective for the removal of metal impurities from MWCNT material. This was confirmed also by the EDS analysis, which showed a decrease in Fe content in the HNO_3 treated MWCNT material by a factor of three.

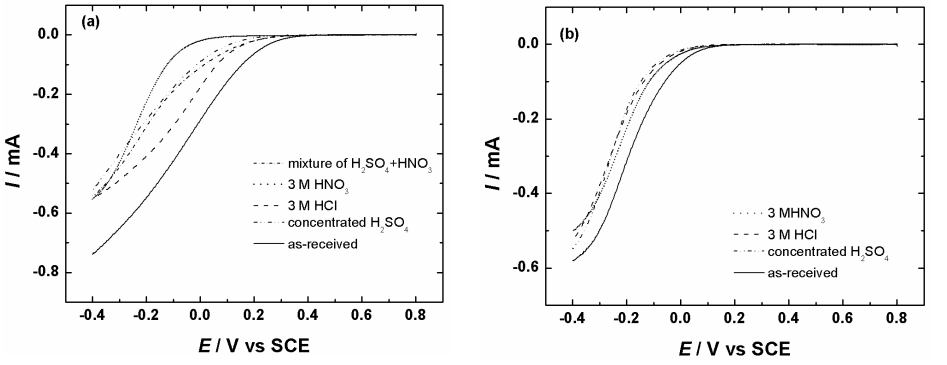

Figure 5. Comparison of RDE voltammetry curves for oxygen reduction on acid-treated and as-received MWCNT (a) and SWCNT (b) modified GC electrodes in O_2 saturated 0.5 M H_2SO_4. $\nu = 10$ mV s^{-1}. $\omega = 1900$ rpm.

The reduction current increases gradually with increasing cathodic potential and no current plateau is formed for any of the acid-treated MWCNT/GC electrodes indicating that not a considerable amount of metal catalyst remained on the surface of the MWCNT material. Slightly different electrocatalytic behaviour was observed for MWCNTs purified in 3 M HCl. This could be elucidated by a larger amount of metal nanoparticles remained on the MWCNTs and between the graphene sheets of MWCNTs. It is also important to mention hereby that even very small amounts of impurities in CNTs in random array coverage can dominate the electrochemistry of CNT materials [230]. The value of half-wave potential for O_2 reduction on the acid-treated MWCNT/GC electrodes shifted negative by almost 0.2 V compared with the untreated MWCNT modified electrodes. This is a notable effect, which shows that the metal catalyst impurities in CNT material can drastically shift the reduction wave to more positive potentials. We may also consider that minor electrocatalytic activity difference between the MWCNTs of various pre-treatment could be caused by the differences of the amount of metal residues which were not removed by acid washing.

It is important to bring forth the fact that besides the removal of metal residues the oxidative pre-treatment of carbon materials can also form different oxygen-containing functional groups, such as quinone, carboxylic acid, carbonyl, carboxylic anhydride, ether, lactone, phenol and pyrone-type groups [231,232]. Matsubara and Waki have shown that the amount of O-functionalities on the MWCNT surface can be increased noticeably by the oxidative treatment. Oxygen content in the pre-treated nanotube material rose more than

ten times [68]. Despite the rise of oxygen content, Biddinger and Ozkan demonstrated that the acid oxidation of carbon nanofiber does not lead to a significant improvement of the electrocatalytic properties of oxygen reduction in acid media [87]. The results obtained in the present research are in good agreement with the observations made by Alexeyeva [233].

The minor effect on the electrocatalytic activity for ORR could be caused also by Nafion. It has been reported that the kinetic current at Nafion–coated GC electrodes was smaller than that of bare GC [69]. Possible reason for the observed current decrease at Nafion-coated electrodes are the effect of pH change. As Nafion is a superacid and the H^+ concentration in the Nafion film is higher than in 0.5 M H_2SO_4, then the activity of Nafion-coated electrodes can be lower than that of bare GC [234]. The activity for O_2 reduction on carbon electrodes decreases as the pH decreases according to the results of early work by Tarasevich et al. [42]. Another reason for the current decrease could be the blocking effects of Nafion polymer side chains in the ionic cluster region [69].

Figure 5b shows the RDE voltammetry curves for oxygen reduction in O_2 saturated 0.5 M H_2SO_4 on SWCNT-modified GC electrodes recorded between 0.8 and –0.4 V. It can be seen from Figure 5b that the onset potential of oxygen reduction on the as-received SWCNT-modified GC electrode is 0.1 V while the reduction of oxygen on the acid purified SWCNT-modified electrodes starts at 0.0 V. The small difference of the onset potential could be explained by the lower amount of metallic impurities in the as-received SWCNT material as compared to as-received MWCNTs.

A set of RDE data on oxygen reduction recorded at rotation rates from 360 to 4600 rpm on 3 M HNO_3 purified MWCNT and SWCNT modified GC electrodes are presented in Figures 6a and 6b, respectively.

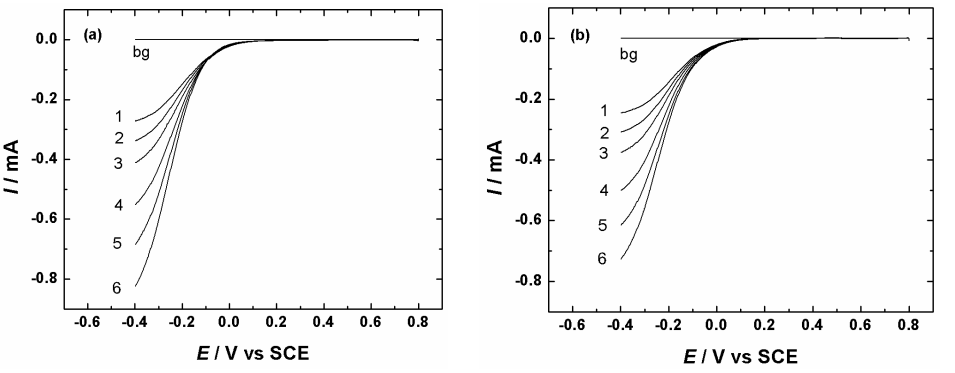

Figure 6. RDE voltammetry curves for oxygen reduction on HNO_3 treated MWCNT (a) and SWCNT (b) modified GC electrode in O_2 saturated 0.5 M H_2SO_4. v = 10 mV s^{-1}. ω: (1) 360, (2) 610, (3) 960, (4) 1900, (5) 3100 and (6) 4600 rpm. Curves bg correspond to the background current for CNT modified GC electrodes in Ar-saturated 0.5 M H_2SO_4.

The RDE results were analysed by the Koutecky-Levich method. The extrapolated K-L lines in Figure 7 shows non-zero intercepts, indicating that the process of O_2 reduction is under the mixed kinetic-diffusion control in a large range of potentials. The slope of K-L lines is directly related to the number of electrons involved in the reaction, the higher the slope the lower the number of electrons transferred.

The number of electrons transferred per O_2 molecule (n) was calculated from the Koutecky-Levich (K-L) equation [235]:

$$\frac{1}{I} = \frac{1}{I_k} + \frac{1}{I_d} = -\frac{1}{n\mathrm{F}\mathrm{A}kC_{O_2}^b} - \frac{1}{0.62n\mathrm{F}AD_{O_2}^{2/3}\nu^{-1/6}C_{O_2}^b\omega^{1/2}} \qquad (18)$$

where I is the measured current, I_k and I_d are the kinetic and diffusion limited currents, respectively; k is the electrochemical rate constant for O_2 reduction, D_{O_2} is the diffusion coefficient of oxygen ($D_{O_2} = 1.8\times10^{-5}$ cm^2 s^{-1} [236]), $c_{O_2}^b$ is its concentration in the bulk ($c_{O_2}^b = 1.13\times10^{-6}$ mol cm^{-3} [236] and ν is the kinematic viscosity of the solution (0.01 cm^2 s^{-1}).

The values of n at different potentials are shown as insets in Figure 7a and 7b for MWCNTs and SWCNTs, respectively.

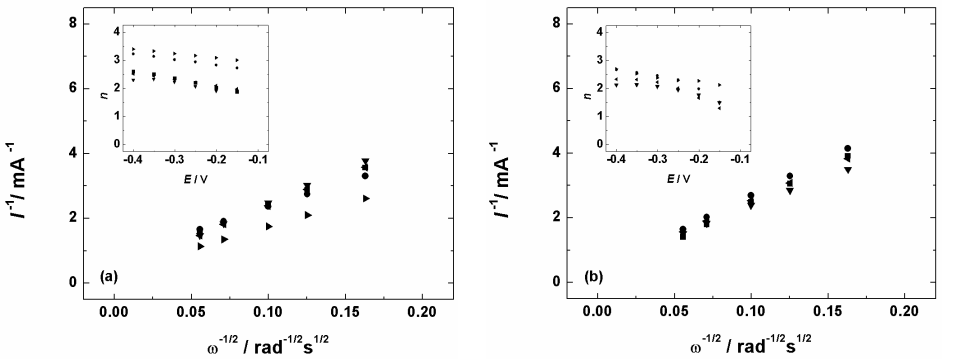

Figure 7. Koutecky-Levich plots for oxygen reduction on acid-treated and untreated MWCNT (a) and SWCNT (b) modified GC electrodes at –0.4 V. (■) $HNO_3 + H_2SO_4$ purified, (▼) HNO_3 purified, (◄) HCl purified, (●) H_2SO_4 purified and (►) as-received CNTs. The inset shows the potential dependence of n.

The results indicate that the reduction of oxygen produces H_2O_2 for acid-treated SWCNT, acid-treated MWCNT and as-received SWCNT modified GC electrodes, which is the final product in this case. For the as-received MWCNT modified electrodes the H_2O_2 produced on the disk reduces further at more negative potentials. The further reduction of peroxide on the as-received MWCNT-modified electrodes at more negative potentials is in agreement with previous observations [29].

The importance of pre-treatment of CNTs for the ORR is clear and the acid treatment of the CNTs should be considered for electroanalytical and electrocatalytic applications of CNT-modified electrodes, especially when the CNTs are used as a support material. The significance of metal-free carbon nanomaterials as catalysts for oxygen reduction has been highlighted recently [237].

6.2. Oxygen reduction on MWCNT modified electrodes

In this part of research a hydrodynamic deposition method was used to cover the surface of HOPG electrode with multi-walled carbon nanotubes. The electrochemical reduction of oxygen on these electrodes was studied in order to determine the catalytic effect of oxidatively pretreated MWCNTs in alkaline media and to test the feasibility of the hydrodynamic deposition method [II].

6.2.1. Surface characterisation of MWCNT/HOPG samples

The distribution and density of MWCNTs on the surface of the modified HOPG electrodes were investigated with the AFM technique. Figures 8a and 8b presents typical AFM micrographs of the bare HOPG and MWCNT/HOPG samples respectively. The AFM images revealed that the distribution of CNTs on the substrate surface was rather uniform and no large-scale agglomeration was evident. It was essential from the point of view of electrochemical measurements that there were no large uncovered areas on the surface (the size of the uncovered areas should be smaller than one-tenth of the diffusion layer thickness). The main advantage of the hydrodynamic deposition method used in this study, is that larger aggregates of MWCNTs are swept away and mainly individual nanotubes attach to the substrate surface. It is considered that only van der Waals forces occur between MWCNTs and the HOPG surface. The length of the nanotubes varies from submicrometer to several micrometers and only a small agglomeration is recognisable. The average length of MWCNTs is significantly smaller than that of the as-received nanotubes which is due to the acid treatment of the MWCNTs.

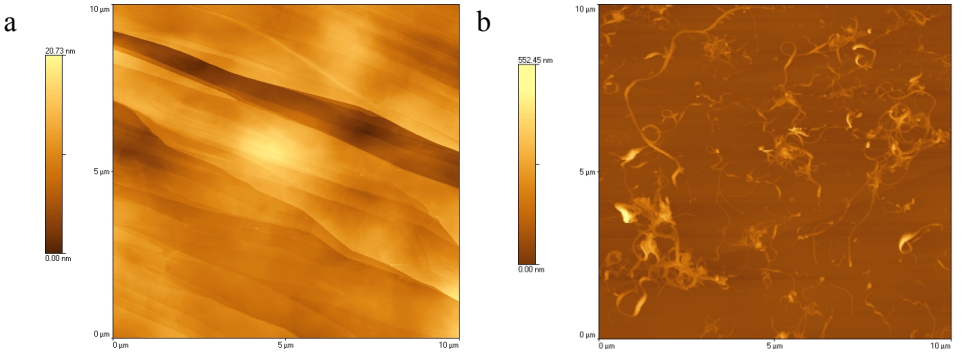

Figure 8. AFM images of the bare HOPG (a) and MWCNT modified HOPG (b).

6.2.2. O_2 reduction on MWCNT modified HOPG electrodes

In order to study the electrocatalytic properties of the MWCNTs at higher pH values, the ORR experiments were carried out on the MWCNT modified HOPG electrodes. HOPG as the support material has been chosen because of the inactive surface of the HOPG in alkaline media [25]. Figure 9 shows the experimental RDE results of O_2 reduction in 0.1 M KOH solution at different rotation rates. For the polarisation curves recorded by a linear scan from 0 to –1.2 V, the limiting current increases when the rotation rate increases and there is a clear prewave present at a potential of about –0.5 V. The second reduction wave is caused by the oxygen functionalities of the MWCNTs material and starts at approximately –0.7 V. As the O_2 reduction current on HOPG itself at these potentials in alkaline solutions is very low (Figure 9, curve a) [25] such a strong electrocatalytic effect could be only due to the electrocatalysis by quinone functionalities on the surface of MWCNTs. The coverage of oxygen-containing groups (including quinone-type sites) increases during the acid treatment of MWCNTs.

We consider that the electrocatalytic reduction of oxygen on the MWCNT surface may proceed according to the Reaction (9–14), the quinone-type functionalities of MWCNTs should be the reactive species of the overall O_2 reduction reaction. Analogous electrocatalytic behaviour presented for MWCNTs towards O_2 reduction has also been observed for polished GC electrodes [22]. The number of electrons transferred per O_2 molecule (n) at different potentials for MWCNT/HOPG electrode was calculated from the K-L equation (18), using the values of O_2 solubility (1.2×10^{-6} mol cm^{-3}) and diffusion coefficient (1.9×10^{-5} cm^2 s^{-1}) in 0.1 M KOH solution [238].

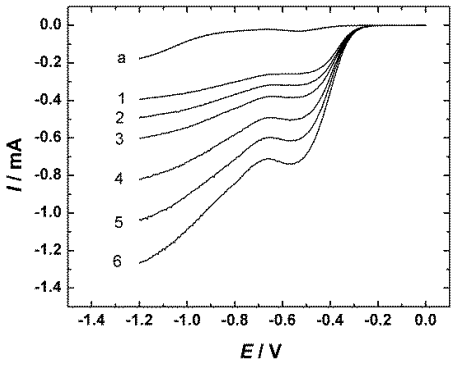

Figure 9. RDE voltammetry curves for oxygen reduction on a MWCNT modified HOPG electrode in O_2 saturated 0.1 M KOH at a sweep rate of 20 mV s^{-1}. ω: (1) 360, (2) 610, (3) 960, (4) 1900, (5) 3100 and (6) 4600 rpm. (a) RDE voltammetry curve for O_2 reduction on a bare HOPG electrode at 360 rpm.

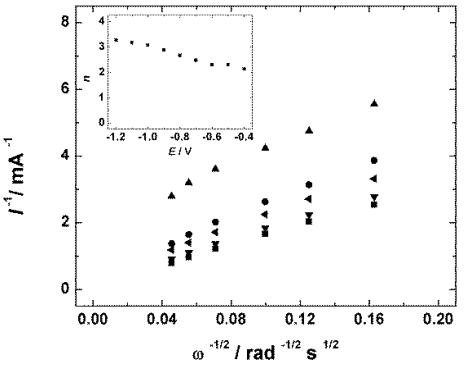

Figure 10. Koutecky-Levich plots for oxygen reduction on a MWCNT modified HOPG electrode in 0.1 M KOH at various potentials: –0.4 V (▲), –0.6 V (●), –0.8 V (◀), –1.0 V (▼), and –1.2 V (■). The inset shows the potential dependence of the number of electrons transferred per O_2 molecule. Data derived from Figure 9.

Figure 10 shows the Koutecky-Levich plots obtained from the RDE data on oxygen reduction at several rotation rates. The extrapolated K-L lines showed non-zero intercepts, indicating that the process of O_2 reduction is under the mixed kinetic-diffusion control. The inset to Figure 10 shows that at low overpotentials ($E > -0.6$ V) the value of n is close to two and the ORR produces HO_2^- which is the final product in this case. At more negative potentials the n value gradually increases ($n > 3$ at –1.2 V), which shows that the peroxide formed reduces further to water in this potential range. The increase of n at more negative potentials is probably due to hydrogen peroxide reduction governed by surface sites other than quinone groups and then the reduction of oxygen proceeds by co-existing two-electron and four-electron pathways. The further reduction of peroxide on MWCNT-modified electrodes at high overpotentials is in agreement with previous observations [63].

For comparison purposes the reduction of O_2 was studied also in the solution of higher pH. Figure 11 presents the RDE polarisation curves of oxygen reduction recorded in 1 M KOH. As expected, the reduction currents are lower in this solution as compared to that shown in Figure 9 at the same rotation rate.

The K-L analysis of the RDE data was made also for 1 M KOH and the results obtained are shown in Figure 12. The values of oxygen solubility (0.84×10^{-6} mol cm^{-3}) [238] and diffusion coefficient (1.65×10^{-5} cm^2 s^{-1}) [238] were used for these calculations. The potential dependence of n followed a similar trend as that observed for 0.1 M KOH (see inset to Figure 12).

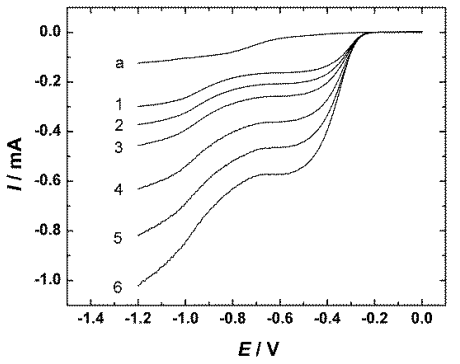

Figure 11. RDE voltammetry curves for oxygen reduction on a MWCNT modified HOPG electrode in O_2 saturated 1 M KOH at a sweep rate of 20 mV s^{-1}. ω: (1) 360, (2) 610, (3) 960, (4) 1900, (5) 3100 and (6) 4600 rpm. (a) RDE voltammetry curve for O_2 reduction on a bare HOPG electrode at 360 rpm.

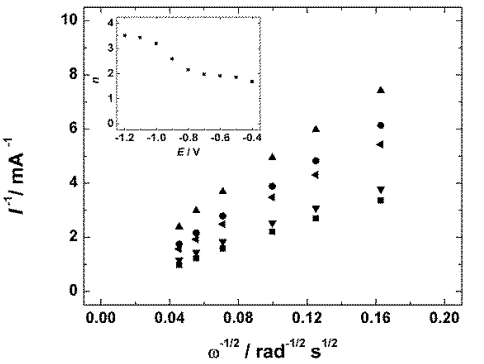

Figure 12. Koutecky-Levich plots for oxygen reduction on a MWCNT modified HOPG electrode in 1 M KOH at various potentials: –0.4 V (▲), –0.6 V (●), –0.8 V (◀), –1.0 V (▼), and –1.2 V (■). The inset shows the potential dependence of the number of electrons transferred per O_2 molecule. Data derived from Figure 11.

6.3. Oxygen reduction on DWCNT modified electrodes

The oxygen reduction reaction has been investigated on double-walled carbon nanotube modified glassy carbon electrodes in acid and alkaline media to test the electrocatalytic properties of these extraordinary type of carbon nanotubes [III].

6.3.1. Surface characterisation of DWCNT samples

The distribution and density of DWCNTs on the surface of the modified electrodes were investigated with transmission electron microscopy. Figures 13a and 13b present typical TEM images of DWCNTs deposited on a thin holey carbon supporting film. Figure 13a shows the clean-cut structure of nanotubes and also that there is no metallic catalyst left in the DWCNT material. Figure 13b reveals that the distribution of DWCNTs on the substrate surface was rather uniform.

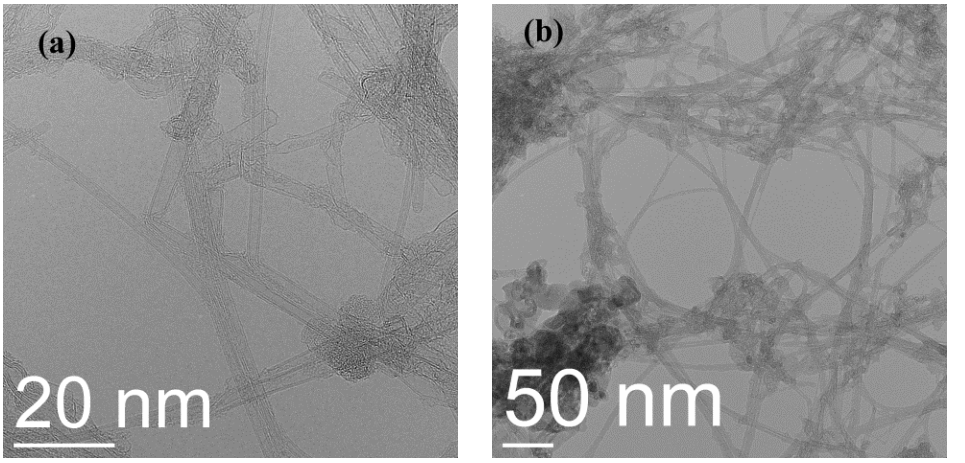

Figure 13. TEM images (a,b) for DWCNT samples. Scale bar: a) 20 nm and b) 50 nm.

The composition of the DWCNT material was investigated by the XPS method. Figure 14 presents the XPS survey spectrum of DWCNT modified GC surface. Four XPS peaks were observed corresponding to emission from C1s (284.4 eV), satellite peak of the C1s spectrum, O1s (532.8 eV) and Mo3d (232.2 and 235.5 eV) levels. The O1s peak is caused by various carbon-oxygen functionalities on the surface of DWCNTs. Detection of different functional groups from the O1s peak is not straightforward because of similar binding energies. However, more detailed investigations have shown that carboxyl and quinone groups are present on the surface of carbon nanotubes [224,225].

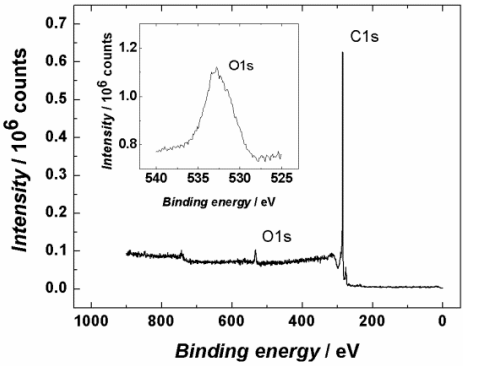

Figure 14. The XPS spectra for DWCNT sample. The inset to Fig. 14 shows the core-level spectrum in the O1s region.

6.3.2. O_2 reduction on DWCNT modified GC electrodes

For experiments made in alkaline media the GC electrodes were modified with DWCNTs in the presence of non-ionic surfactant Triton X-100. For the oxygen reduction studies in acid media DWCNTs were coated within a Nafion film. The RDE measurements were carried out in order to test the electrocatalytic behaviour of DWCNT/GC electrodes towards oxygen reduction. The electro-reduction of oxygen was first studied on DWCNT-surfactant modified GC electrodes in alkaline solution. Figure 15a shows the experimental RDE data of O_2 reduction in 0.1 M KOH. There is a clear pre-wave present at a potential of ca –0.5 V which is similar to the results obtained with undoped MWCNT modified HOPG electrodes in alkaline media [63,64] The half-wave potential of oxygen reduction ($E_{1/2}$) for a DWCNT/GC electrode is –0.38 V at 960 rpm. This value of $E_{1/2}$ is very close to that observed for MWCNT/GC electrodes in identical conditions ($E_{1/2}$ = –0.37 V) [IV]

The second reduction wave on these materials starts at approximately –0.7 V. It has been suggested that the improved O_2 reduction current at the potential range corresponding to the pre-wave could be caused by oxygen-containing groups on the surface of carbon materials. Similar electrocatalytic behaviour of DWCNTs towards O_2 reduction has also been observed for polished GC electrodes and it has been proposed that such a strong electro-catalytic effect could be caused by quinone-type functionalities on the surface of GC [22]. We consider that the electrocatalytic reduction of O_2 on DWCNT modified electrodes at low overpotentials may also be caused by the native quinone-type functionalities on the surface of DWCNTs and the ORR may proceed in an analogous manner to the reaction scheme proposed in Ref. [22].

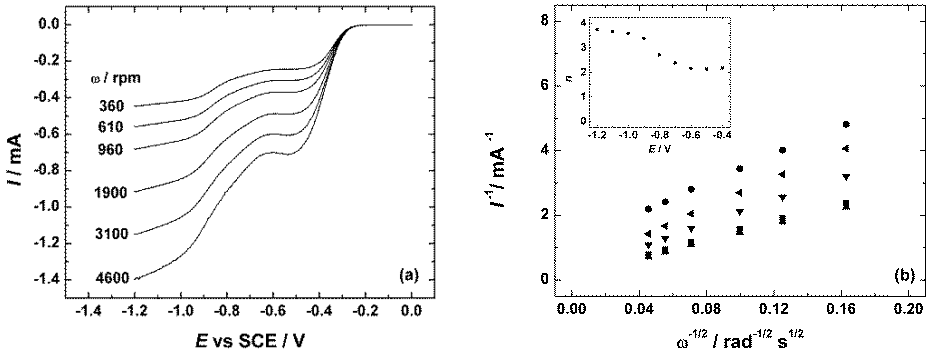

Figure 15. a) RDE voltammetry curves for oxygen reduction on a DWCNT modified GC electrode in O_2 saturated 0.1 M KOH at 10 mV s^{-1}. b) Koutecky-Levich plots for oxygen reduction on a DWCNT/GC electrode in 0.1 M KOH at various potentials: (●) –0.4, (◀) –0.6, (▼) –0.8, (■) –1.0 and (▲) –1.2 V. The inset shows the potential dependence of *n*.

Figure 15b presents the K-L plots obtained from the RDE data. The extrapolated K-L lines showed non-zero intercepts, indicating that the O_2 reduction process is under the mixed kinetic-diffusion control in a large range of potentials. The inset to Figure 15b shows that at low overpotentials ($E > -0.6$ V) the value of n is close to two and the reduction of O_2 produces HO_2^- which is the final product in this case. At more negative potentials the n value gradually increases ($n > 3$ at –1.2 V), which indicates that the peroxide formed reduces further to water in this potential range. The further reduction of peroxide on DWCNT-modified electrodes at high overpotentials is similar to the processes observed for MWCNT/GC electrodes [IV].

The RDE voltammetry curves for O_2 reduction shown in Figure 16 were recorded in O_2–saturated 0.5 M H_2SO_4 between 0.8 and –0.4 V. The reduction current increases gradually with increasing cathodic potentials and no current plateau is formed. The oxygen reduction wave commences at a rather negative potential (approximately 0 V). These results indicate that there is no considerable amount of metal catalyst impurities remained in and on DWCNTs and the DWCNT/GC electrodes studied possess rather low electrocatalytic activity for O_2 reduction. Because the iron impurities left in CNTs are responsible for the improved kinetics of the ORR and carbon material itself has relatively low catalytic activity in acid media as has been discussed previously [29]. As can be seen in Figure 14, the acid-treated DWCNTs are almost free of iron impurities and as a result the electrocatalytic activity of DWCNTs for O_2 reduction in acid media is rather low. Inset to Figure 16 presents the results of the K-L analysis of the RDE data on O_2 reduction in acid media. In acid media the DWCNTs are inactive for oxygen reduction in a large region of potentials and for this reason DWCNTs could be used as a support material to study the electrocatalytic properties of various catalysts deposited on their surface.

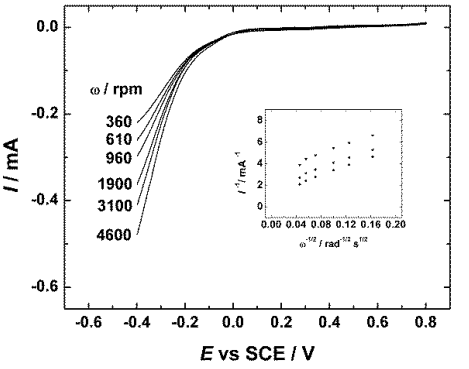

Figure 16. RDE voltammetry curves for oxygen reduction on a DWCNT modified GC electrode in O_2 saturated 0.5 M H_2SO_4 at 10 mV s^{-1}. The inset shows the Koutecky-Levich plots for oxygen reduction at various potentials: (▼) –0.3, (◀) –0.35 and (●) –0.4 V.

6.4. The pH-dependence of O_2 reduction and effect of surfactants on MWCNT/GC electrodes

The purpose of this part of work was to study systematically the pH-dependence of O_2 reduction on multi-walled carbon nanotube modified glassy carbon electrodes and to investigate the effect of different type of surfactants for oxygen electroreduction [IV].

6.4.1. The pH-dependence of the oxygen electroreduction on MWCNT/GC electrodes

To study the pH dependence the electrochemical experiments were carried out in 0.5 M H_2SO_4 solution, acetate buffer (pH 5), phosphate buffers (pH 6, 7 and 8), borate buffer (pH 10), 0.01 M KOH, 0.1 M KOH and in 1 M KOH solution, using the RDE method. The oxygen reduction behaviour of MWCNT modified GC electrodes at different pHs was compared.

The reduction of oxygen was first studied on MWCNT-SDS modified GC electrodes. Figure 17 shows the RDE results at different rotation rates for pH 5–14. On the basis of the experimental data the polarisation curves of O_2 reduction can be divided into three groups. For the first group of polarisation curves a reduction pre-wave is observed at a potential of about – 0.5 V for the solutions of high pH (pH 12–14). It can be proposed that this feature is due to the electrocatalysis by oxygen-containing groups on the surface of MWCNTs. Analogous electrocatalytic behaviour towards O_2 reduction has been observed for GC electrodes [92]. The second group of polarisation curves was obtained at pH 8–10 where only a small hump can be seen and a characteristic feature of these voltammograms is the absence of the reduction pre-wave. The third group is formed by *I-E* curves recorded at lower pH values (pH < 8), where the reduction pre-wave is totally absent. The electrochemical reduction of oxygen is strongly inhibited in acid media (data not shown). The O_2 reduction behaviour of MWCNT-SDS in 0.5 M H_2SO_4 is similar to that of the MWCNT-Nafion modified GC electrode [29].

Comparing with previous studies of the pH effect on the kinetics of oxygen reduction on various carbon materials [18,28] we obtained the same tendency for the pH-dependence of O_2 reduction in the present work. Namely at higher pH values the process of O_2 reduction on MWCNT modified GC electrodes is more dependent on pH than at lower pHs. Obviously it is caused by the reactivity of quinone-type functionalities on the surface of MWCNTs which is significantly lower in acid media than in alkaline electrolytes. It is reasonable to consider that the pH effect observed in the present work is caused by the similar types of quinones that have been found on the GC surface [239].

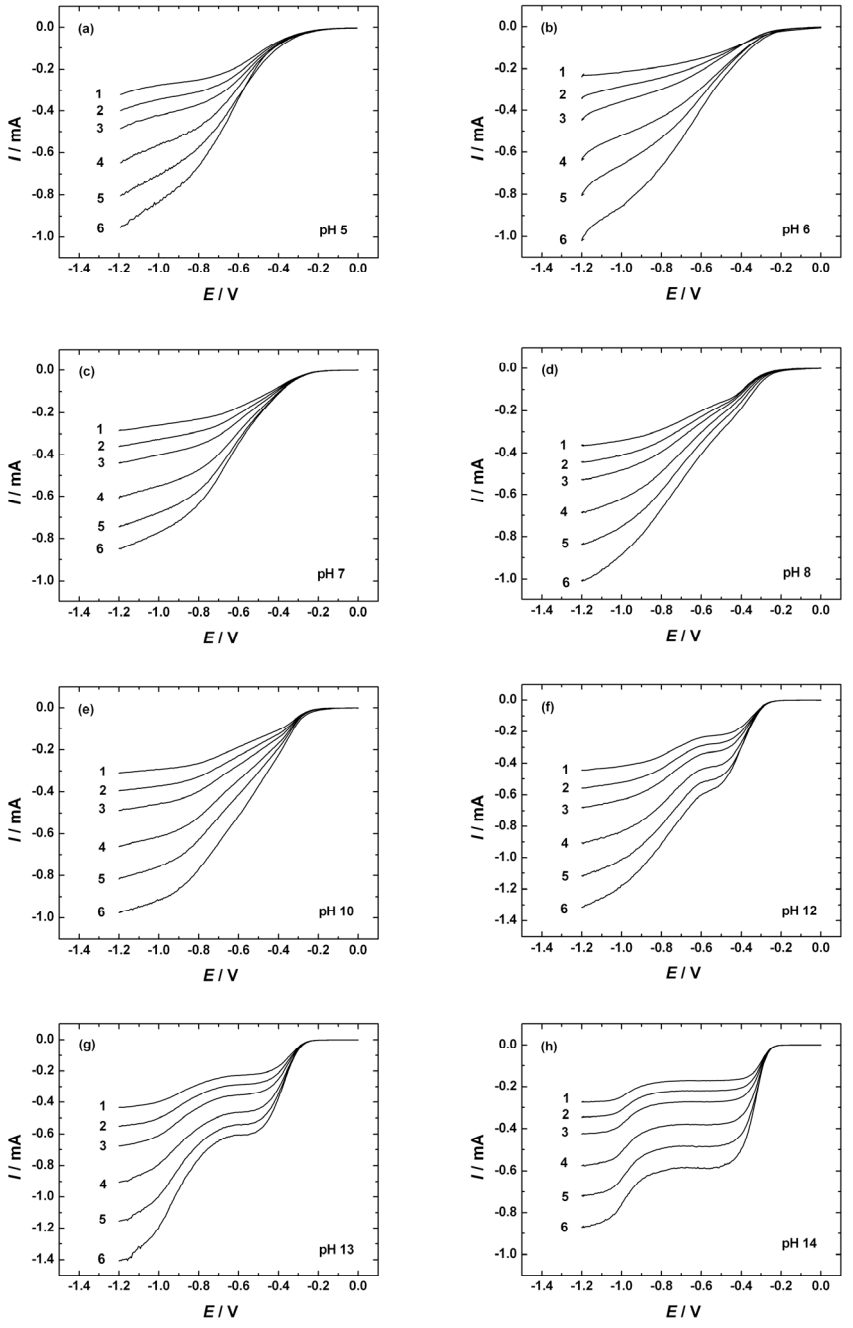

Figure 17. RDE voltammetry curves for O_2 reduction on MWCNT-SDS modified GC electrodes in O_2-saturated solutions of various pH: (a) 5, (b) 6, (c) 7, (d) 8, (e) 10, (f) 12, (g) 13 and (h) 14. v = 20 mV s^{-1}. ω: (1) 360, (2) 610, (3) 960, (4) 1900, (5) 3100 and (6) 4600 rpm.

6.4.2. The effect of surfactants on the electroreduction of oxygen on MWCNT/GC electrodes

There is an intriguing question about the fate of surfactant after the exposure of the MWCNT-surfactant film to surfactant-free aqueous solutions. Obviously, the surfactant remained on the surface of MWCNTs may affect their electrocatalytic properties. The effect of surfactants on the electrochemical response of MWCNT-modified electrodes and its pH dependence has not been thoroughly studied and there is not much information about that in the respective literature. Therefore comparative studies have been made using different types of surfactants. The RDE measurements of O_2 reduction were carried out with the GC electrodes modified in the presence of different surfactants (SDS, CTAB, DHP, Triton X-100). The RDE results were rather similar for all the MWCNT-modified electrodes studied. Representative sets of voltammetry curves of ORR recorded at a single rotation rate (ω = 960 rpm) are presented in Figure 18. These Figures summarise the observed pH-dependence of O_2 reduction showing that the electrocatalytic activity of MWCNTs is strongly dependent on pH and is the highest in more alkaline solutions.

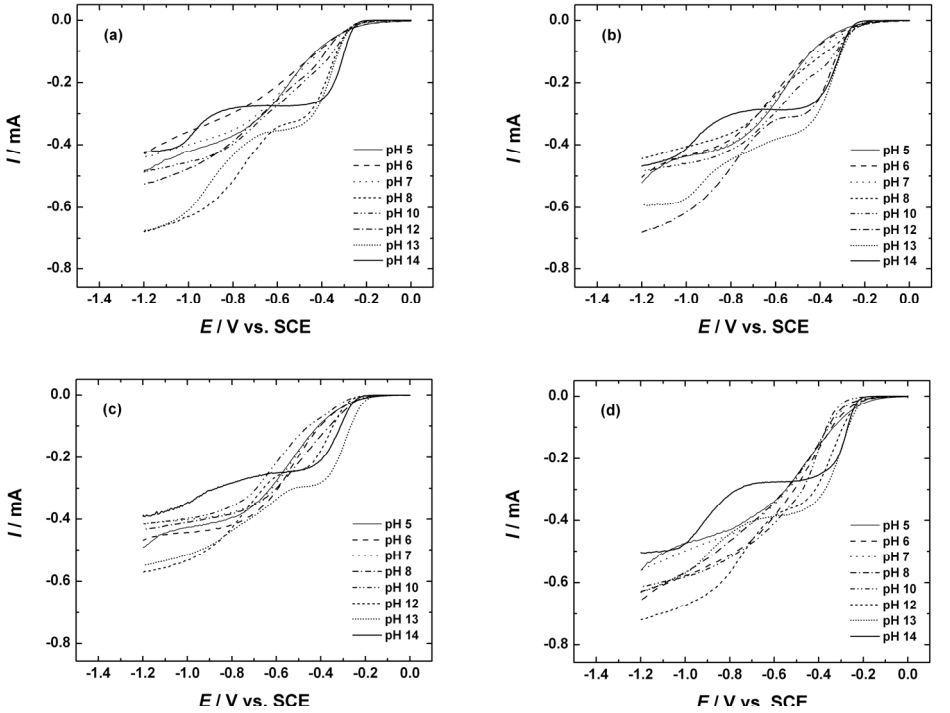

Figure 18. Comparison of the RDE data of oxygen reduction on MWCNT-surfactant modified GC electrodes at different pHs. Surfactants used: (a) SDS, (b) Triton X-100, (c) CTAB and (d) DHP. ω = 960 rpm. v = 20 mV s^{-1}.

At lower pHs, the nature of active sites on MWCNTs changes and as a result, the half-wave potential of O_2 reduction is almost independent of pH.

Figure 19 shows the Koutecky-Levich plots obtained from the RDE data on oxygen reduction at –1.2 V for all the MWCNT-modified GC electrodes at different pHs. At this potential the K-L lines are not parallel, indicating that the value of *n* is dependent on pH. The intercepts of the extrapolated K-L lines were close to zero, which shows that the process of O_2 reduction is almost entirely under diffusion control at high negative potentials.

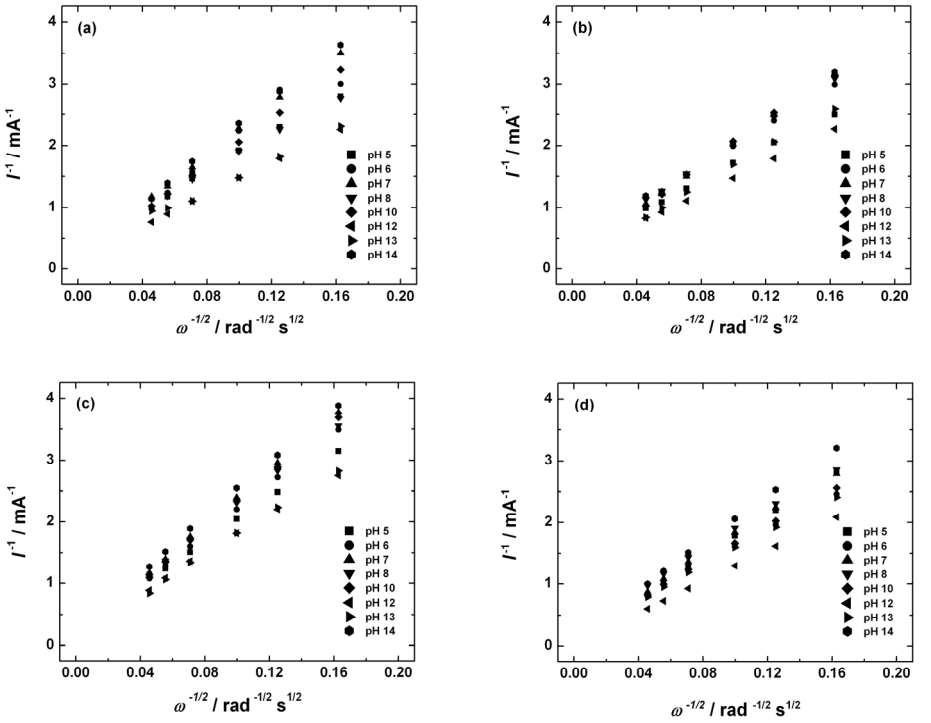

Figure 19. Koutecky-Levich plots for O_2 reduction on MWCNT-surfactant modified GC electrodes at different pHs (E = –1.2 V). Surfactants used: (a) SDS, (b) Triton X-100, (c) CTAB and (d) DHP.

Figure 20 compares the *n* values at various potentials. It is evident that at low overpotentials (E > –0.6 V) *n* was close to two and the reduction of O_2 produces H_2O_2 which is the final product in this case. At more negative potentials the *n* value gradually increases, which indicates that the peroxide formed reduces further in this potential range. The further reduction of peroxide at high overpotentials is in agreement with previous observations and as a consequence the value of *n* is higher than two [63]. At higher pHs (pH 12–14) the *n* value approaches four, however there are some differences depending on the surfactant used as a dispersing agent. For instance, the electrodes modified in

the presence of CTAB show anomalously low reduction current at high overpotentials in the solutions of high pH and n is approximately 3.

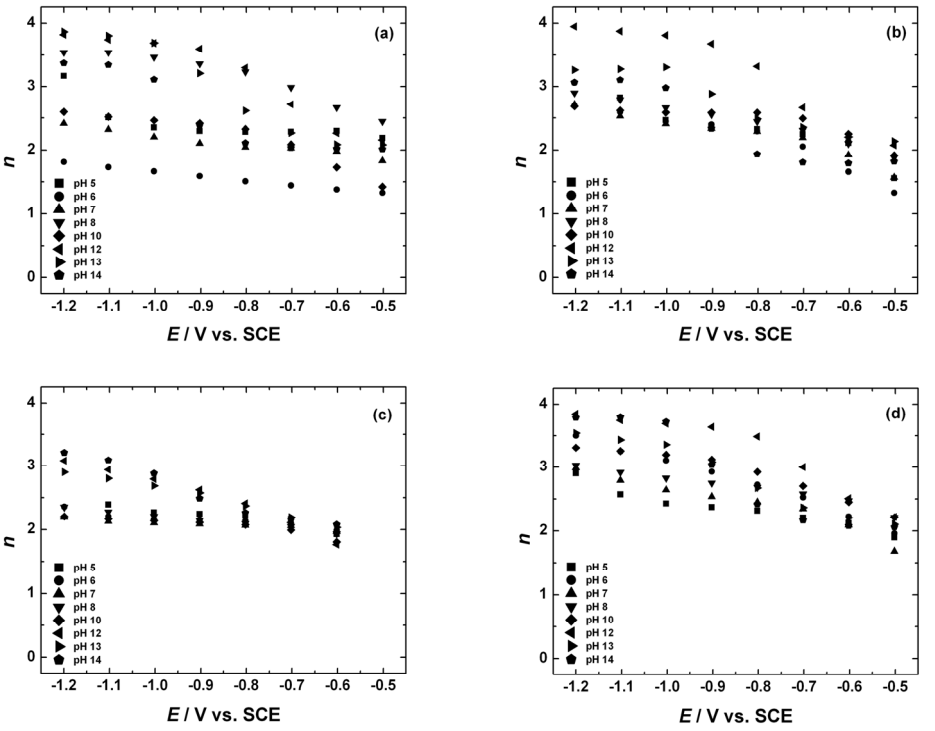

Figure 20. Potential dependence of n for O_2 reduction on MWCNT-surfactant modified GC electrodes at different pHs. Surfactants used: (a) SDS, (b) Triton X-100, (c) CTAB and (d) DHP.

Figure 21 shows the dependence of the half-wave potential for O_2 reduction on solution pH. At higher pHs the $E_{1/2}$ values are higher, but as the solution pH decreases the nature of active sites on MWCNTs changes and as a result $E_{1/2}$ becomes almost independent of pH. There is some scatter in the data, nevertheless, the results shown in Figure 21 represent the main tendencies observed. It is important to note that the overpotential of O_2 reduction is the lowest in the solutions of high pH. This is an essential aspect considering the application of the MWCNT-modified electrodes in practical electrocatalysis.

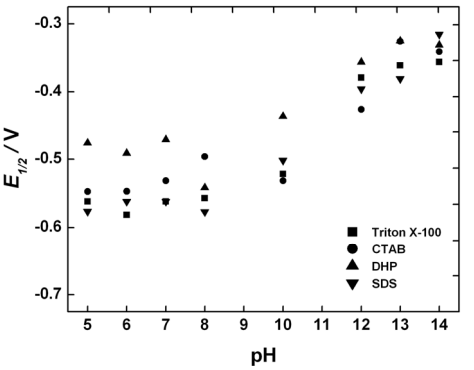

Figure 21. Dependence of the half-wave potential for O_2 reduction on MWCNT-surfactant modified GC electrodes on solution pH. ω = 960 rpm.

Baring in mind rather high concentrations of surfactants in the MWCNT suspensions used in the present work, one could expect a high coverage of surfactants on the surface of MWCNTs. It appears that there is an optimum amount of surfactant adsorbed on nanotubes for various applications (for example, for SDS [240]). If the amount adsorbed is too high then the surfactant layer may affect charge transport within the MWCNTs network, which is detrimental for electronic applications [228]. On the basis of the literature data and the results obtained in the present work we can conclude that there is only a little effect of surfactants used in the preparation of the MWCNT-modified electrodes on the electrocatalytic properties of these electrodes.

6.5. Oxygen reduction on CDC modified electrodes

Electroreduction of O_2 on glassy carbon electrodes modified with various carbon nanomaterials in alkaline solution has been investigated. Electrocatalytic behaviour of carbide-derived carbon materials was of special interest for oxygen reduction reaction [V].

6.5.1. Physical characterisation of CDC materials

For convenience, the CDC materials studied are designated as C824 and C1551. The former material can be classified as "turbostratic" carbon, whereas the latter one forms nanobarrel-like structures. The example of XRD patterns of C1551, C824 and respective precursor material, Al_4C_3, is shown in Figure 22. Figure 22a shows a typical powder XRD profile of the partially graphitic carbide-derived carbon. For both CDC materials the 002 Bragg diffraction peak at 2Θ ~26° corresponds to parallel graphene layers although there is no graphite like regularity. The 10 diffraction peak at 2Θ ~43° characterises the 2D in-plane

symmetry along the graphene layers. The graphitisation for C1551 is much lower than for C824, therefore high ordered 004 and 11 graphite interlayer diffraction peaks are very weak. Also, the peak at 26° is much narrower for C824 (Figure 22a). The formation of Al_4C_3 derived carbons proceeds by net Reaction (18):

$$Al_4C_3 + 6Cl_2 = 3C + 4AlCl_3 \uparrow \qquad (19)$$

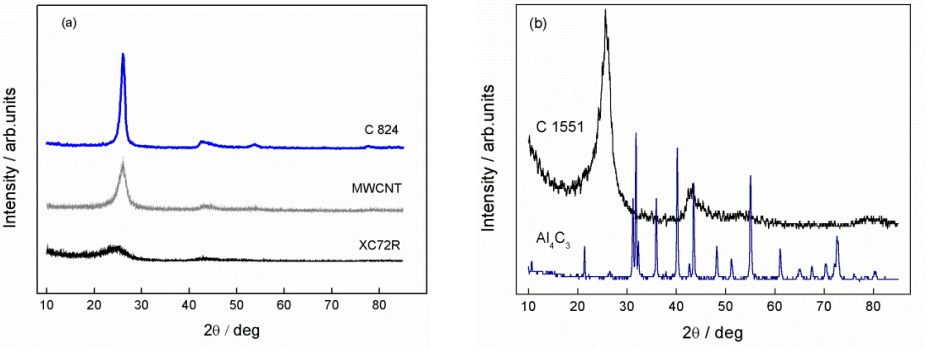

Figure 22. Characteristic XRD patterns for CDC sample C824, MWCNTs and Vulcan XC72R (a), C1551 (b) and the precursor material, Al_4C_3 (b).

The surface morphology of these materials was examined by high-resolution transmission electron microscopy (HR-TEM). Figure 23 shows a HR-TEM micrograph of a C1551 sample. One can see on the HR-TEM image a large number of nanobarrels and small flake-looking particles of a CDC. The HR-TEM image revealed that this sample consists of nanobarrels having sizes from 50 to 100 nm. However, there were also many particles that at a first view seemed to be amorphous, but at closer look were found to consist of small flakes which are actually nanobarrels sized about 10 nm. The thickness of the turbostratic carbon flakes varied from 2 to 15 graphene layers. The rest is mainly an intermediate between amorphous carbon and nanoparticles. Therefore, one may find several similarities between the XRD patterns from the nanocarbon-containing samples used in this study and those reported for MWCNTs.

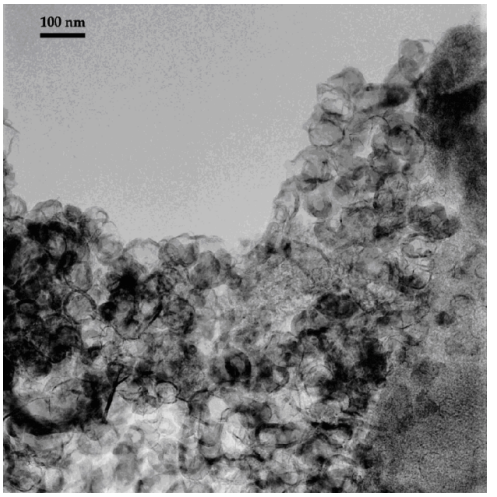

Figure 23. HR-TEM image of C1551 material deposited on an amorphous carbon film.

6.5.2. O_2 reduction on CDC modified GC electrodes

Figure 24 presents the RDE polarisation curves for oxygen reduction on CDC-PTFE (C824-PTFE and C1551-PTFE) modified GC electrodes in O_2 saturated 0.1 M KOH. For comparison, MWCNT-PTFE and Vulcan carbon-PTFE modified GC electodes were studied as-well. These electrodes were heated at 80 °C for 1 h before electrochemical testing. The RDE results were rather similar for all the modified electrodes studied. The limiting current increases when the rotation rate increases and there is a clear pre-wave present at low overpotentials. The second reduction wave on these materials starts at approximately –0.7 V.

For carbon nanomaterials C824 and C1551 a high reduction current was observed probably because of the high degree of graphitisation, which leads to a mesoporous structure of these carbons. Mesoporous materials potentially lead to faster charge transfer rate as observed previously [241,242], while the high surface area materials with a non-porous structure and fully accessible surface such as carbon onions were previously shown to have high response rates.

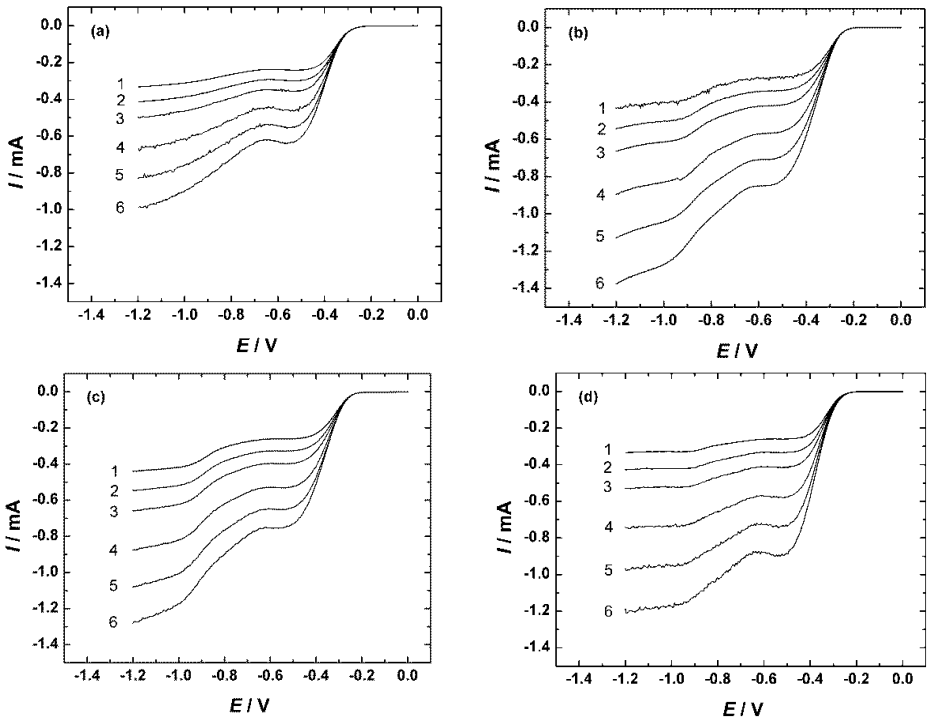

Figure 24. RDE voltammetry curves for oxygen reduction on carbon nanomaterial-PTFE modified GC electrodes in O_2-saturated 0.1 M KOH. Nanocarbons used: (a) MWCNT, (b) Vulcan XC72R, (c) C1551 and (d) C824. v = 10 mV s^{-1}. ω: (1) 360, (2) 610, (3) 960, (4) 1900, (5) 3100 and (6) 4600 rpm.

The number of electrons transferred per O_2 molecule was calculated from the Koutecky-Levich equation (18). Figure 25 shows the K-L plots obtained from the RDE data on oxygen reduction at –0.6 V for different carbon nanomaterial modified electrodes. At this potential the K-L lines are almost parallel, indicating that the reduction pathway is similar for different carbon materials studied. The intercepts of the extrapolated K-L lines were close to zero, which shows that the process of O_2 reduction is almost entirely under diffusion control. The inset of Figure 25 compares the n values calculated from the K-L equation at various potentials. For all carbon materials at low overpotentials (E > –0.6 V) the n value was close to two and the reduction of O_2 produces peroxide which is the final product in this case. At more negative potentials the value of n gradually increased up to four (the only exception was C824), which indicates that the peroxide formed reduces further in this potential range. For most carbon nanomaterials the n value approaches four, however, there are some subtle differences depending on the carbon nanomaterials used.

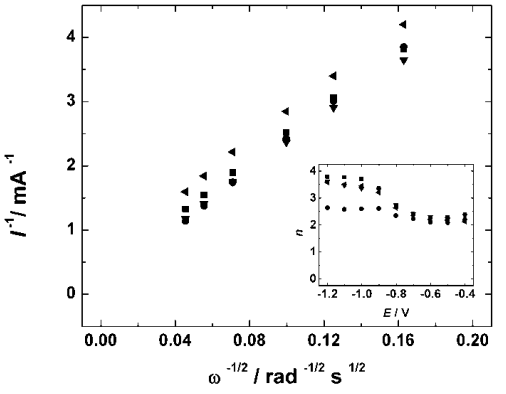

Figure 25. Koutecky-Levich plots for oxygen reduction on nanocarbon-PTFE modified GC electrodes at –0.6 V. Nanocarbon materials used: (■) C1551, (●) C824, (◀) MWCNT, (▼) Vulcan XC72R. Inset: Potential dependence of n for O_2 reduction on carbon nanomaterial-PTFE modified GC electrodes in 0.1 M KOH.

6.5.3. RRDE studies of O_2 reduction on CDC materials

Rotating ring-disk electrode was also used for the investigation of the electrochemical reduction of oxygen on carbon nanomaterials deposited on GC. In this case the nanocarbon-PTFE mixture was annealed at 350 °C for 0.5 h. This is a typical procedure for the preparation of commercial Pt/C catalysts using PTFE as a binder [243]. The PTFE content used (10 wt.%) was found to be suitable for the preparation of catalytically active and stable gas-diffusion electrodes [243,244]. The disk currents of oxygen reduction recorded on GC electrodes modified with different carbon nanomaterials are presented in Figure 26a. The corresponding ring currents are shown in Figure 26b. At the foot of the polarisation curves the C1551 material shows a higher reduction current than other nanocarbons studied and this is most probably related to its higher specific surface area (684 $m^2 g^{-1}$). At low overpotentials the reduction of oxygen yields primarily HO_2^-. This was confirmed by the K-L analysis of the disk current data. The $2e^-$ reduction pathway predominates at $E > -0.6$ V (see RRDE data analysis below). As can be seen in Figure 26a, an ill-defined current plateau forms at potentials between –0.6 and –0.4 V for all the nanocarbon modified electrodes studied. The disk currents at these potentials are close to the diffusion-limiting current for a $2e^-$ reduction of oxygen. In this potential range the production of peroxide is the highest, which is important from the point of view of the electrosynthesis of hydrogen peroxide [245]. At $E < -1$ V, the reduction current reaches a limiting value for all the carbon materials studied.

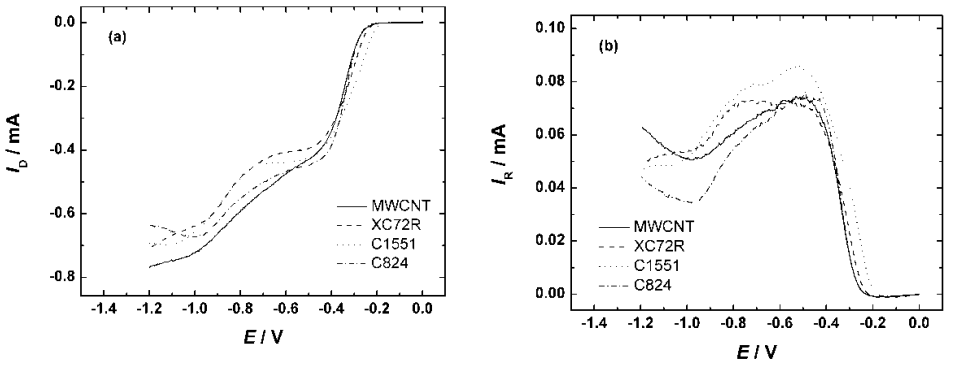

Figure 26. Ring and disk currents for oxygen reduction on carbon nanomaterial-PTFE modified GC electrodes in O_2-saturated 0.1 M KOH. v = 10 mV s^{-1}. ω = 960 rpm. (a) disk and (b) ring currents

The ring currents increase as the rotation rate increases and reach maximum value at *ca*. –0.5 V followed by a decrease of current at more negative potentials. This is a clear indication that the hydrogen peroxide starts to be reduced further on the disk electrode and as a consequence the contribution of the $4e^-$ pathway to the overall O_2 reduction reaction increases. The ring current decrease at $E < -0.5$ V depends somewhat on the carbon nanomaterial used. For instance, the I_R values for carbon black-PTFE modified electrode reach a plateau from –0.5 to –0.8 V, indicating that hydrogen peroxide is produced in similar quantities at these potentials. However, for MWCNT-PTFE, C824-PTFE and C1551-PTFE there is a tendency for a current decrease in the range of potentials from –0.5 to –1.0 V, which reveals that the production of peroxide also decreases.

The RRDE data of O_2 reduction were analysed using the ratio of disk to ring current [246]. The I_D/I_R vs. $\omega^{-1/2}$ plots were analysed at E = –0.6 V and the results for different nanocarbons are shown in Figure 27. These plots are very similar for all the carbon nanomaterials studied, which means that the I_D/I_R values are almost independent of the electrode rotation rate. Similar results were obtained in Ref. [247]. In all cases, the plots were rather parallel to the X-axis, indicating that the further reduction of peroxide is negligible at this potential. Some scatter in the data could occur because of the slightly non-quantitative detection of the peroxide on the Pt-ring. By extrapolating the NI_D/I_R vs. $\omega^{-1/2}$ lines to the infinite rotation rate, one can observe intercepts slightly higher than unity. This means that the predominant pathway is the two-electron reduction of oxygen to peroxide which is the final product in this case.

The percentage yield of peroxide formation (Φ) was calculated from [248]

$$\Phi = \frac{200 I_R/\mathrm{N}}{I_D + I_R/\mathrm{N}} \tag{20}$$

where I_D and I_R are the disk and ring currents, respectively, and N is the collection efficiency. The value of Φ was between 80 and 90% at low overpotentials and it decreased at potentials more negative than −0.7 V (Figure 28). At the potentials of the second reduction wave the yield of peroxide was dependent on rotation speed and increased at higher rotation rates. This shows that the number of surface sites at which HO_2^- undergoes electrochemical reduction is limited and as a consequence, the turnover rate at these sites is insufficient to provide the increased production rate of HO_2^- at high rotation rates, i.e., the reduction of HO_2^- ions becomes less favourable in comparison to the rate of desorption and diffusion into the bulk solution.

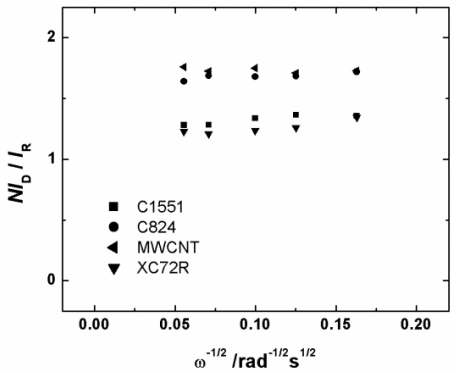

Figure 27. The dependence of NI_D/I_R on $\omega^{-1/2}$ at –0.6 V for oxygen reduction on carbon nanomaterial-PTFE modified GC electrodes in 0.1 M KOH.

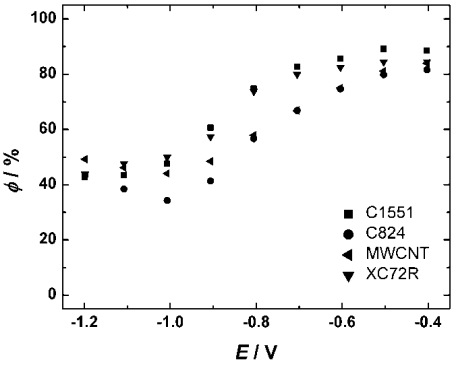

Figure 28. Dependence of the yield of peroxide formation (Φ) on potential for carbon nanomaterial-PTFE modified GC electrodes in 0.1 M KOH. Data derived from Figure 26.

Some research groups have proposed that the enhanced O_2 reduction current at pre-wave potentials in alkaline solutions is caused by quinone-type functionalities on carbon materials [92].

The practical relevance of this work is related to the electrochemical synthesis of hydrogen peroxide in alkaline solutions [245]. It has been found that peroxide will degrade the surface of carbon materials so it is highly challenging to find a carbon-based material, which shows a higher electrocatalytic activity for O_2 reduction to peroxide and at the same time improves corrosion resistance and chemical stability over commercial nanocarbon powders [249,250]. Up to now, hydrogen peroxide is produced by a chemical route [251]. The electrosynthesis of peroxide has several advantages over the chemical route and it is particularly attractive to carry out this process using a fuel cell technology [245].

6.6. Oxygen reduction on MN_4 macrocycle/MWCNT modified electrodes

Metal phthalocyanine and porphyrin functionalised multi-walled carbon nanotubes were used as non-precious electrocatalysts for the electroreduction of oxygen both in acid [VI] and alkaline media [VII]. The catalyst materials were heat-treated at different temperatures before electrochemical testing. The goal was to show difference of metalloporphyrins and metallophthalocyanines from ORR electrocatalysis point of view and to find optimum pyrolysing conditions in order to achieve a higher activity and stability of these catalysts.

6.6.1. Surface characterisation of MWCNT supported metal phthalocyanine and porphyrin samples

X-ray photoelectron spectroscopy was used to study the surface composition of the electrocatalysts and to determine the chemical states of metal and nitrogen species on the surface. Figure 29a and 29b presents the XPS survey spectra of heat-treated CoPh/MWCNT and CoPc/MWCNT samples, respectively. All the samples were heat-treated at 800 ºC. It is possible to separate five similar XPS peaks for both samples, which correspond to emission from C1s, satellite peak of the C1s spectrum, N1s, O1s, and Co2p levels. The XPS core-level spectrum in the N1s region of CoPc/MWCNT and CoPh/MWCNT samples shows two peaks. The N1s peak of higher binding energy at 400.2 eV corresponds to a new nitrogen species formed likely during the pyrolysis and the peak at 399.8 eV could be assigned to N introduced into the graphene layer but it is hard to define the exact chemical nature of these surface species and the identification of the species is still under debate. Two similar nitrogen peaks to CoPc/MWCNT and CoPh/MWCNT samples have been observed also for iron porphyrin on acetylene black and in this case they were assigned to C-N-Hx and C-N-M groups evolved from the decomposition of the MN_4 chelates [252].

The O1s peak is related to the MWCNT material and is caused by various carbon-oxygen functionalities on the surface of MWCNTs. Similarly to the N1s peak, it is hard to define the exact chemical nature of different surface species from O1s peak because of close binding energies and the topic is still under debate, but different investigations have shown that carboxyl and quinone groups are present on the surface of carbon nanotubes [220].

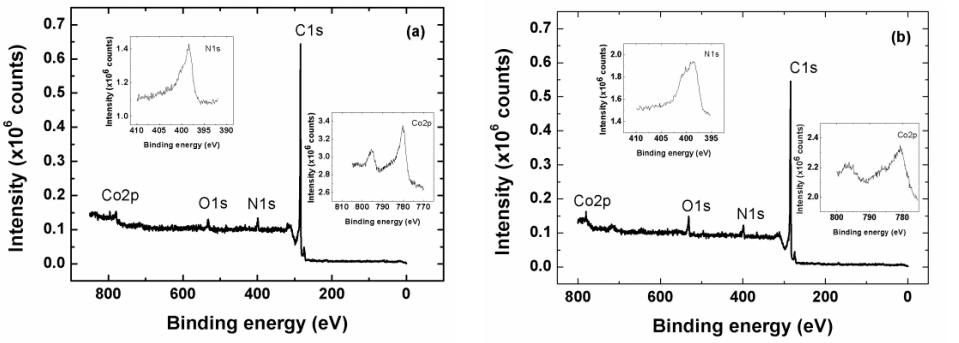

Figure 29. XPS spectra of the catalyst materials (a) CoPh/MWCNT and (b) CoPc/MWCNT with inset spectra of N1s and Co2p.

From the inset of Figures 29a and 29b one can observe XPS peaks at 795.8 eV which corresponding to $Co2p_{3/2}$ lower energy and 780.2 eV corresponding to $Co2p_{1/2}$ higher energy asymmetric bands originating from spin-orbital splitting. The peak at 780.2 eV belongs to Co^{2+} from all CoPc/MWCNT or CoPh/MWCNT, respectively. The XPS peak at 778.5 eV corresponds to metallic cobalt and peak at 781 eV corresponding to pure CoPc or CoPh respectively. It should be noted that nitrogen or metal catalyst impurities were not detected in the as-received MWCNT samples by XPS.

6.6.2. O_2 reduction on MWCNT supported metal phthalocyanines and porphyrins in acid media

Typical RDE polarisation curves obtained for different MN_4 macrocycle/ MWCNT modified GC electrodes towards the ORR in acid media is illustrated in Figure 30a and 30b. The Figures present the RDE results of oxygen electroreduction obtained with FePh/MWCNT and CoPh/MWCNT materials pyrolysed at 800 ºC. The experiments were performed at different rotation rates in O_2-saturated 0.5 M H_2SO_4 solution. An almost constant onset potential of the ORR on the same catalyst at different rotation rates shows that no catalyst material have left from the electrode and no changes are taking place with catalyst material during the experiment. As expected, the limiting currents in a hydrodynamic experiment increase with increasing rotation rate. It is possible to see from Figure 30 that the value of onset potential is similar for both materials but the difference in half-wave potential is almost 0.2 V. Also the current plateau is formed at a much more positive potential for the CoPh/MWCNT catalyst.

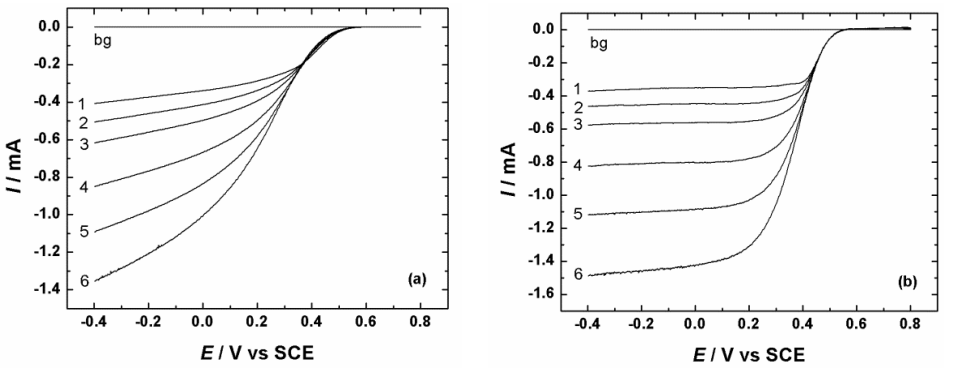

Figure 30. RDE voltammetry curves for oxygen reduction on (a) FePh/MWCNT and (b) CoPh/MWCNT modified GC electrodes in O_2 saturated 0.5 M H_2SO_4 solution. v = 10 mV s^{-1}. ω: (1) 360, (2) 610, (3) 960, (4) 1900, (5) 3100 and (6) 4600 rpm. The catalyst materials were heat-treated at 800 ºC.

Still both of the catalysts increase remarkably the ORR activity. For the heat-treated FePh/MWCNT and CoPh/MWCNT catalysts a high reduction current was observed probably because of the generation of electrocatalytically active species which usually form during the heat-treatment at temperatures higher than 650 ºC [154,253]. It has been proposed that the electrocatalytically active sites for ORR could be the central metal ion with N atoms [254]. Even if the metal nanoparticles on carbon supports are sometimes reported not to be related to the activity of the catalyst and nitrogen not being a part of the catalytically active site for ORR, these two species together can form highly active catalyst center for ORR [254].

The number of electrons transferred per O_2 molecule (n) was calculated from the Koutecky-Levich equation. Figure 31a and 31b presents the K-L plots obtained from the RDE data on oxygen reduction in 0.5 M H_2SO_4 for annealed (800 ºC) FePh/MWCNT and CoPh/MWCNT catalyst modified electrodes, respectively. The extrapolated K-L lines showed non-zero intercepts, indicating that the process of oxygen reduction is under the mixed kinetic-diffusion control in a large range of potentials. The values of n at different potentials are presented as insets in Figure 31a and 31b for FePh/MWCNT and CoPh/MWCNT, respectively.

For both the FePc/MWCNT and CoPh/MWCNT material the n value was close to 3 for all over the range of potential. This indicates that the mixed $2e^-$ and $4e^-$ process takes place and the reduction of O_2 produces both H_2O_2 and H_2O.

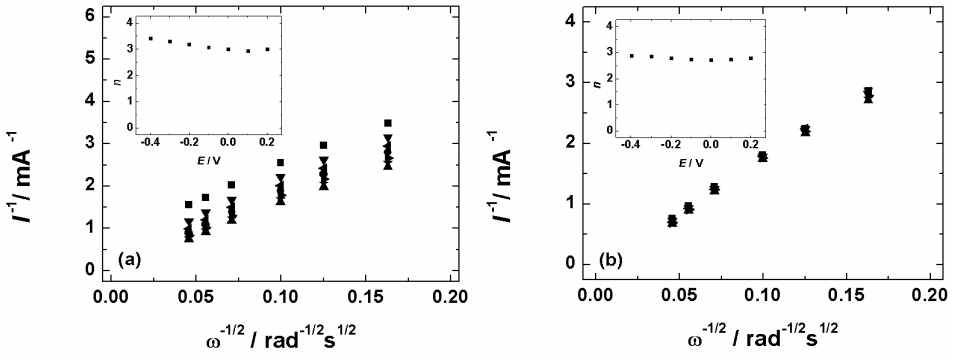

Figure 31. Koutecky-Levich plots for oxygen reduction on (a) FePh/MWCNT and (b) CoPh/MWCNT modified GC electrodes in O_2 saturated 0.5 M H_2SO_4 at various potentials: (■) 0.2, (▼) 0.1, (◄) 0, (●) –0.1, (►) –0.2, (★) –0.3 and (▲) –0.4 V. The inset shows the potential dependence of *n*.

Figure 32 presents the comparative RDE results of O_2 reduction obtained for GC electrodes modified with different MWCNT supported MN_4 macrocyclic catalyst materials annealed at different temperatures. For comparison purposes the RDE voltammetry curve of unmodified MWCNTs has been added. For each catalyst material the polarisation curves of oxygen reduction are presented for unannealed catalyst and materials pyrolysed at 400 ºC and 800 ºC. As presented in Figure 32, the electrocatalytic activity of metalloporphyrin/MWCNT modified electrodes for ORR was higher than that of the metallophthalocyanine/ MWCNT modified electrodes. Especially higher activity was observed for CoPh/MWCNT material for which the onset potential of O_2 reduction shifted positive for almost 0.1 V as compared to that of FePc/MWCNT, which was the catalyst with poorest ORR activity. As expected, the electrocatalytic activity of all metallophthalocyanine and metalloporphyrin modified MWCNT catalysts improved enormously compared with pristine MWCNTs. It is well-known that pure MWCNTs itself have rather low electocatalytic activity for O_2 reduction in acid media. One can see that the onset potential of O_2 reduction on unmodified MWCNTs is substantially more negative than that of metallophthalocyanine and metalloporphyrin modified MWCNTs. This indicates that the catalyst activity is entirely determined by the catalytically active sites formed by the attachment of MN_4 macrocycles to the surface of MWCNTs. We could expect similar performance for analogous catalysts to large conjugated organometallic molecules as phthalocyanines and porphyrins which easily adsorb on MWCNT support. However there are visible differences in catalytic activity between these materials, which could be explained by the existence of better π–π interactions between MN_4 macrocycle and MWCNTs and by small differences in the structure of the molecules [160, 173]. Given the results of the polarisation curves for different materials annealed at two different temperatures it can be

concluded that the samples heat-treated at 800 ºC showed the best electro-catalytic activity towards the ORR. It is proven that heat-treatment enhances the kinetic current of the catalyst materials and reduces the concentration of MN_4 macrocycles in the pyrolysis product. Gupta et al. stated that the presence of MN_4 macrocycles had only minor impact for the ORR activity in acid media without any annealing [255]. It has been proposed that pyridinic-type nitrogen, forming at temperatures as high as 800 ºC, could be responsible for the achieved catalytic activity [256].

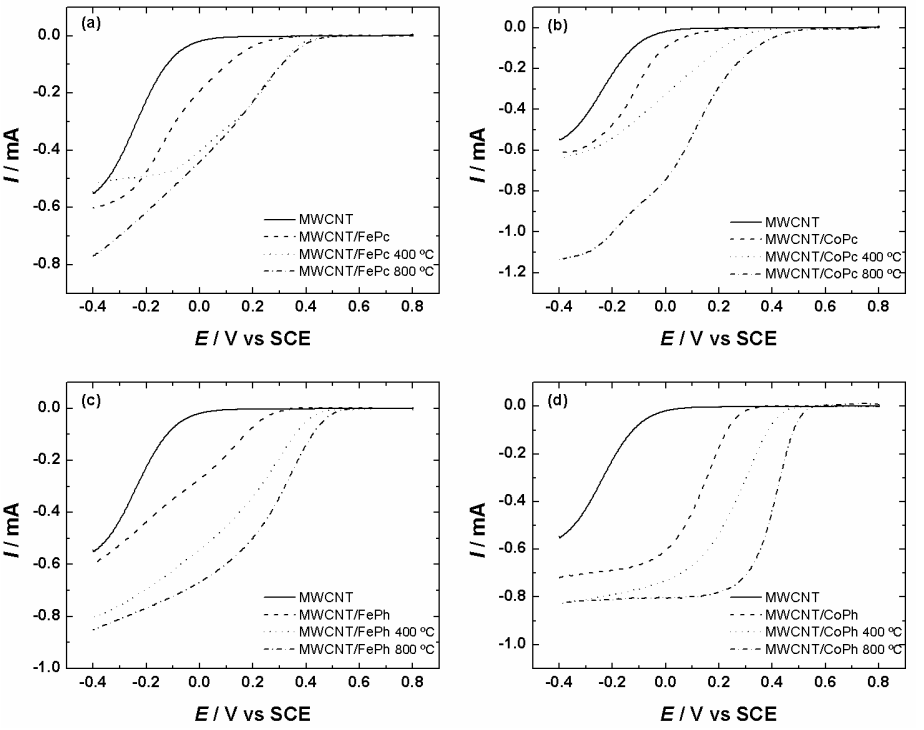

Figure 32. RDE voltammetry curves for oxygen reduction on (a) FePc/MWCNT, (b) CoPc/MWCNT, (c) FePh/MWCNT and (d) CoPh/MWCNT catalyst material modified GC electrodes in O_2-saturated 0.5 M H_2SO_4. v = 10 mV s^{-1}. ω = 1900 rpm.

6.6.3. O_2 reduction on MWCNT supported metal phthalocyanines and porphyrins in alkaline media

Figure 33a and 33b presents the RDE polarisation curves for oxygen reduction in alkaline media on GC electrodes modified with FePc/MWCNT and FePh/MWCNT material pyrolysed at 800 ºC. The experiments were performed in O_2 saturated 0.1 M KOH solution and at different rotating rates. As expected, the limiting currents in a hydrodynamic system increase with increasing rotation

rate. An almost constant onset potential of the ORR on the same catalyst at different rotation rates shows that no catalyst material have left from the electrode and no changes are taking place with catalyst material during the experiment. This phenomenon is observable for both materials and hence for the Figures 33a and 33b.

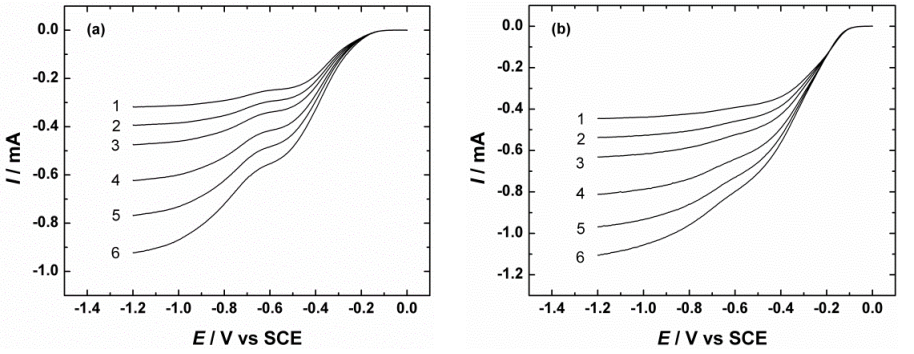

Figure 33. RDE voltammetry curves for oxygen reduction on (a) FePc/MWCNT and (b) FePh/MWCNT modified GC electrodes in O_2 saturated 0.1 M KOH. ν = 10 mV s^{-1}. ω = (1) 360, (2) 610, (3) 960, (4) 1900, (5) 3100 and (6) 4600 rpm. The catalyst materials were heat-treated at 800 ºC.

The onset potential of the ORR on the FePh/MWCNT is –0.05 V and shifts in the positive direction as compared to the FePc/MWCNT catalyst for which the onset potential is –0.1 V, which means that the FePh/MWCNT catalyst material is more active and with higher reduction current density than the FePc/ MWCNT. There is a visible pre-wave present at low overpotentials for both materials. The second reduction wave on FePc/MWCNT starts at approximately –0.7 V and on FePh/MWCNT at approximately –0.6 V. For the heat-treated FePc/MWCNT and FePh/MWCNT catalysts a high reduction current was observed probably because of the generation of electrocatalytically active species which usually form at temperatures from 700 to 950 ºC. Ladouceur et al. have reported that the electrocatalytic activity of CoPc/XC-72, which was annealed at 800 ºC, was twice as high as the activity of the non-pyrolysed CoPc/XC-72 [197]. It has been proposed that the electrocatalytically active sites for ORR could be the central metal ion with N atoms [197]. Even if the metal nanoparticles on carbon supports are sometimes reported not to be related to the activity of the catalyst [189] and nitrogen not being a part of the catalytically active site for ORR [246], these two species together can form highly active catalyst center for ORR.

Figure 34a and 34b shows the K-L plots obtained from the RDE data on oxygen reduction on FePc/MWCNT and FePh/MWCNT, respectively, and at several rotation rates in 0.1 M KOH. The linearity of the K-L plots is an indication that the reaction is first order with respect to molecular O_2. The

intercepts of the extrapolated K-L lines were close to zero, which shows also that the process of O_2 reduction is almost entirely under diffusion control at high negative potentials. The inset of Figures 34a and 34b shows the *n* values calculated from the K-L equation at various potentials. For the FePc/MWCNT material at low overpotentials ($E > -0.7$ V) the *n* value was close to 2.5 and at more negative potential *n* reaches 3, which means that the O_2 reduction reaction takes place as mixed $2e^-$ and $4e^-$ process and the reduction of O_2 produces both HO_2^- and OH^-. From the inset of Figure 34b corresponding to FePh/MWCNT, one can see that the value of *n* is close to 4 in a wide range of potentials. This indicates that the mixed $2e^-$ and $4e^-$ process takes place and the reduction of O_2 produces OH^- ions.

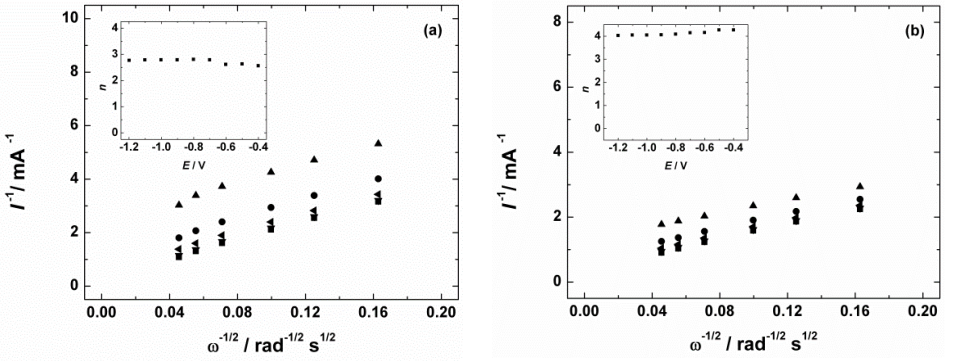

Figure 34. Koutecky-Levich plots for oxygen reduction on (a) FePc/MWCNT and (b) FePh/MWCNT modified GC electrodes in 0.1 M KOH at various potentials: (▲) –0.4, (●) –0.6, (◀) –0.8, (▼) –1.0 and (■) –1.2 V. The inset shows the potential dependence of *n*.

Figure 35 presents the comparative RDE results of O_2 reduction obtained for GC electrodes modified with different catalyst materials pyrolysed at different temperatures. The RDE voltammetry curve of pure MWCNTs has been added for comparison purposes. Figures 35a-d presents the RDE polarisation curves for oxygen reduction on GC electrodes modified with FePc/MWCNT, CoPc/MWCNT, FePh/MWCNT and CoPh/MWCNT respectively. The ORR polarisation curves are presented for unannealed material and catalysts heat-treated at 400 ºC and 800 ºC. As shown in Figure 35, the catalytic activity of metalloporphyrin/MWCNT modified GC electrodes was higher than for the metallophthalocyanine/MWCNT modified electrodes. Especially for CoPh/MWCNT material which onset potential were shifted positive for almost 0.1 V as compared to CoPc/MWCNT. As expected, the catalytic activity of all metal phthalocyanine and porphyrin modified MWCNT catalysts improves enormously compared with the unmodified MWCNTs.

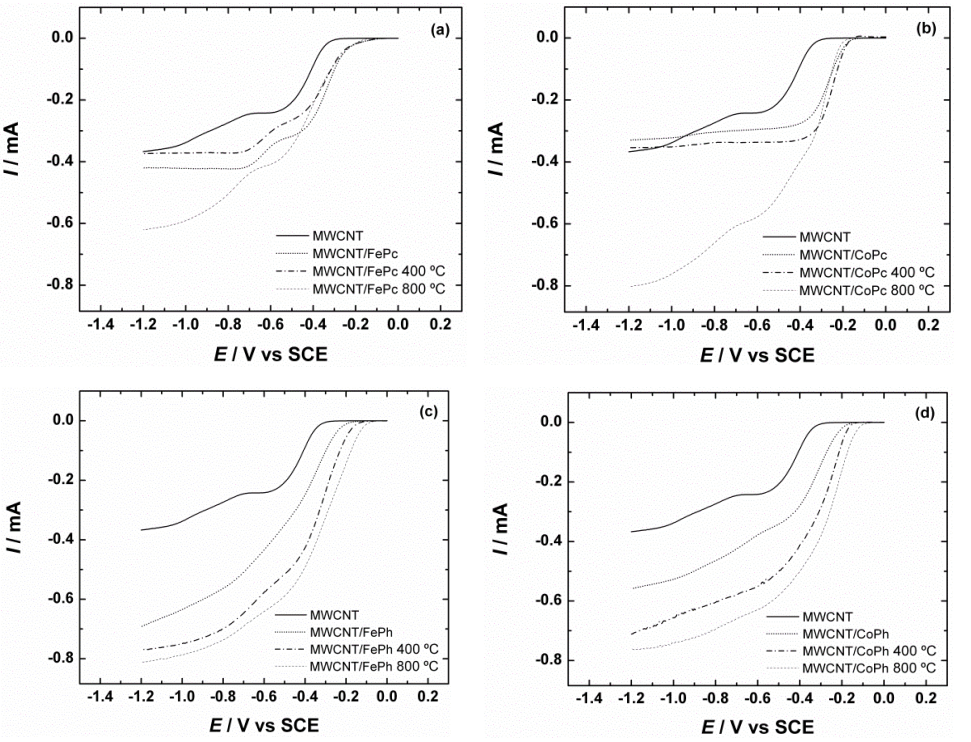

Figure 35. RDE voltammetry curves for oxygen reduction on (a) FePc/MWCNT, (b) CoPc/MWCNT, (c) FePh/MWCNT and (d) CoPh/MWCNT modified GC electrodes in O_2-saturated 0.1 M KOH. ν = 10 mV s^{-1}. ω = 1900 rpm.

One can see that the onset potential of O_2 reduction on unmodified MWCNTs is substantially more negative than that of metallophthalocyanine and metallo-porphyrin modified MWCNTs. This indicates that the catalyst activity is entirely determined by the catalytically active sites formed by the attachment of MN_4 macrocycles on the surface of MWCNTs.

There are also differences in the electrocatalytic activity of different metal phthalocyanines. These could be explained by the small differences in the structure of the molecule and existence of better π–π interactions between MN_4 macrocycle and MWCNTs [160,170]. As can be seen from Figure 35a and 35b the CoPc/MWCNT catalyst has much better electrocatalytic properties compared with FePc/MWCNT. This is in accord with previous studies of Arechederra et al. who found that cobalt doped Pc material requires less overpotential to achieve oxygen reduction than the iron doped material [178]. For the metal phthalocyanines the clear pre-wave is observed, whereas for the metaloporphyrins the pre-wave is almost absent.

Given the results of the polarisation curves for different materials annealed at different temperatures it can be concluded that the samples prepared at 800 ºC showed the best electrocatalytic activity towards the ORR. It has been

proposed that the achieved catalytic activity at this temperature could be assigned to the pyridinic-type nitrogen forming on these temperatures high as 800 ºC [256]. It is also proven that the catalytically active site for the cathodic ORR is not the Fe or Co in this case, because it a is well known fact that Fe and Co are playing minor role in the ORR in alkaline solutions and most of the metallic catalyst is encapsuled into the graphitic carbon materials at this temperature [257].

Metal phthalocyanine and porphyrin modified carbon nanomaterials may find application as cathode catalysts for fuel cells. It would be of utmost importance to replace the costly Pt or its alloys as a cathode material in low temperature fuel cells. The electrocatalysts studied in this work are particularly attractive as alternative cathodes for alkaline membrane fuel cell.

6.7. Fuel cell performance of MN_4 macrocycle/MWCNT catalyst

The purpose of this part of work was to evaluate H_2/O_2 fuel cells using an alkaline anion exchange membrane. Various non-platinum catalyst materials were investigated by fabricating membrane-electrode assemblies using Tokuyama membrane and compared with commercial Pt/C catalysts [VIII].

Before evaluating the catalyst materials in a fuel cell, the RDE measurements were performed. A comparison of the RDE data on oxygen reduction recorded on GC electrodes modified with different catalyst materials are presented in Figure 36. The commercial 46 wt.% Pt/C catalyst shows a higher reduction current than any other material compared and this is related to the high loading of platinum. At the foot of the polarisation curve the commercial 20 wt.% Pt/C catalyst also shows a higher reduction current than phthalocyanines but at more negative potentials the CoPc/MWCNT (heat-treated at 800 ºC) modified electrode becomes more active and its O_2 reduction current exceeds the current values of 20 wt.% Pt/C material. Annealed FePc/MWCNT also shows the extraordinary ORR performance in alkaline electrolyte but its current is not rising as high as that observed for the CoPc/MWCNT material. The RDE voltammetry curve of O_2 reduction on unmodified MWCNTs has been also added to Figure 36 for comparison purposes.

Figure 37 compares the fuel cell performance of MEAs with FePc/MWCNT and CoPc/MWCNT cathode electrocatalysts using humidified H_2 and O_2 gases at 45 ºC in a single cell fuel cell. In order to compare the performance of these non-noble metal catalysts, two commercial Pt/C catalysts (E-TEK and Tanaka) were also evaluated and the performance compared at identical operating conditions. As can be seen from the Figure 37, Tanaka Pt/C catalyst showed the highest performance (~120 mW cm^{-2}). CoPc/MWCNT material performed almost (power density ~100 mW cm^{-2}) similar to that of the E-TEK catalyst

based MEAs. However, the FePc/MWCNTs based MEA only showed about 60 mW cm^{-2} under similar conditions. MEAs with bare MWCNT based cathodes were also evaluated to see whether there was any ORR activity. Evidently, MWCNTs showed poor performance with lower OCV also. The fuel cell performance of the MEAs became fluctuating above 50 ºC, probably due to water balance issues in the cell. However, the reported power density with Tokuyma membrane was about 180 mW cm^{-2} using Co-Fe/C catalysts by Li et al [154]. Recent literature on the AFC using Pt catalyst ink with aminated tetramethyl polysulfone membrane showed much poorer performance even with 2 mgPt cm^{-2} under high operating pressure [258].

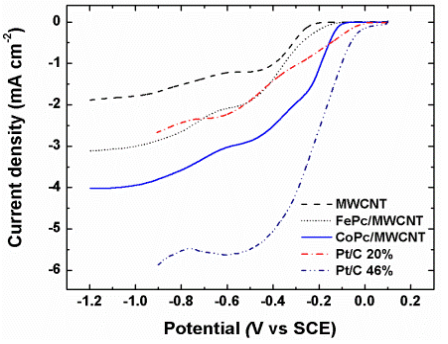

Figure 36. RDE voltammetry curves for oxygen reduction on different catalyst material modified GC electrodes in O_2-saturated 0.1 M KOH. v = 10 mV s^{-1}. ω: 1900 rpm.

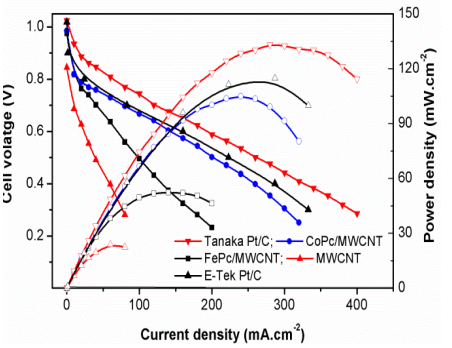

Figure 37. Fuel cell performance of MEAs with Co and Fe phthalocyanine modified MWCNTs along with E-TEK and Tanaka Pt/C catalysts based cathodes using Tokuyama's A201 series anion exchange membrane

6.8. Oxygen reduction on graphene-supported MN_4 macrocycles

Graphene was used as a support for MN_4 macrocycles and the electrocatalytic activity of these materials towards the ORR was studied in alkaline media using the rotating disc electrode method [IX].

6.8.1. Surface characterisation of rGO-supported metallophthalocyanine and metalloporphyrin samples

Figure 38a and 38b presents the XPS survey spectra of FePc/rGO and CoPh/rGO samples, respectively. Four similar XPS peaks were observed for both samples, which correspond to emission from C1s, satellite peak of the C1s

spectrum, O1s and N1s levels. In additon Fe2p and Co2p peaks were observed for FePc/rGO and CoPh/rGO samples, respectively. The O1s peak is related to the rGO material and is caused by various carbon-oxygen functionalities on the surface of rGO. It has been proved that some of the oxygen functionalities remain on the surface of rGO despite the reduction of the GO material [123].

The XPS core-level spectrum in the N1s region shows one peak at approximately 399 eV for both FePc/rGO and CoPh/rGO samples and could be assigned to pyridinic N and MNx. From the inset of Figure 38a one can observe XPS peaks in the Fe2p region. The peak at 709.2 eV corresponds to the $Fe2p_{3/2}$ emission. This is consistent with the iron in FePc macrocycle being mostly in the Fe(II) state. This means that no major change takes place in the chemical state of FePc without pyrolysis and these metallocomplexes are attached to the surface of rGO simply by physical adsorption. Inset to Figure 38b shows two XPS peaks of Co2p relating to similar metal species as for Fe.

Raman spectra of graphite, GO and rGO are presented in Figure 38c. The typical feature for carbon in Raman spectra is the G band around 1582 cm^{-1} and D band around 1350 cm^{-1}. G mode arises from the first order scattering of E_2g phonon of sp^2 carbon atoms and D mode arises from breathing mode of κ point phonons of A_1g symmetry. During Raman measurements the graphite G band is observed at around 1580 cm^{-1}, which is up shifted to 1588 cm^{-1} in case of GO and indicates the presence of isolated double bonds, which resonate at frequencies greater than that of G band of graphite. Upon reduction the G band for rGO is down shifted to 1583 cm^{-1}, attributed to the recovery of the hexagonal network of carbon atoms, re-gain of double bonds. The prominent D peak at ca. 1363 cm^{-1} is observed for GO, which is also observed for graphite (source material), clearly indicate the presence of structural imperfections. The intensity of 2D peak with respect to the D and G peak is smaller due to disorder. Non-planarity of GO sheet arises from the presence of sp^3 carbon atoms on GO sheet which causes wrinkle structure, which was observed during SEM surface morphology analysis of GO on silicon substrate. Upon reduction the GO sheets become flat, indicating re-gain of sp^2 structure of the surface, i.e. good graphitisation. SEM image of rGO is shown in Figure 38d.

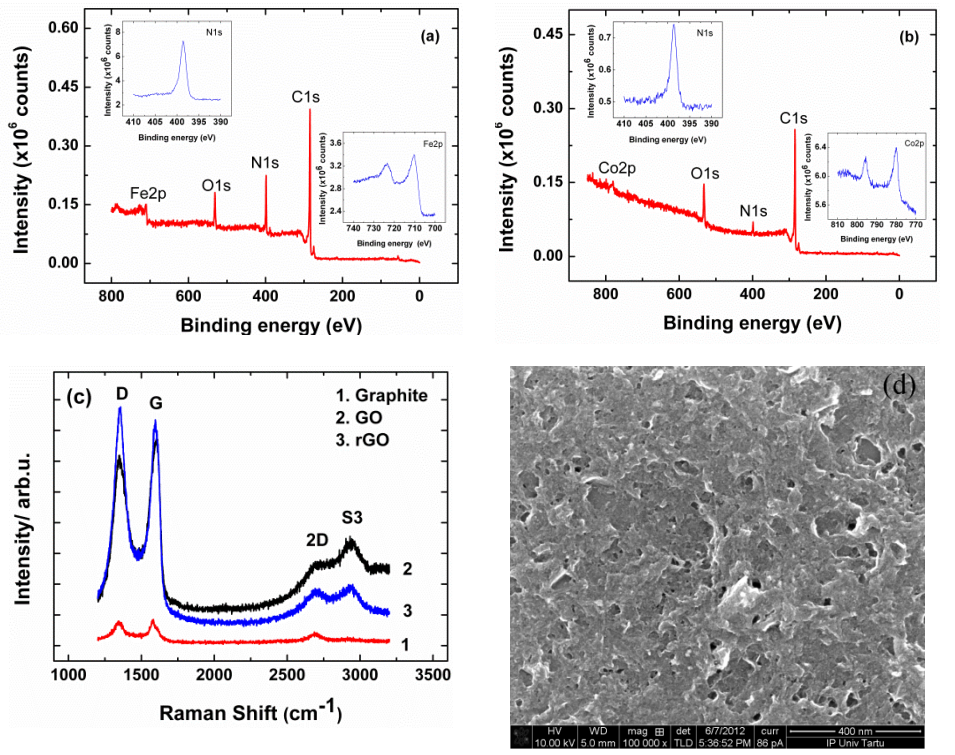

Figure 38. XPS spectra of (a) FePc/rGO and (b) CoPh/rGO samples with inset spectra of N1s, Fe2p and Co2p. (c) Raman spectra of graphite, GO and rGO. (d) SEM image of rGO.

6.8.2. O_2 reduction on rGO-supported metallophthalocyanine and metalloporphyrin modified electrodes

The ORR kinetics on GC electrodes modified with different catalyst materials was investigated using the RDE method. Figure 39a and 39b presents the RDE polarisation curves for O_2 reduction on GC electrodes modified with FePc/rGO and CoPh/rGO material, respectively. The experiments were performed in O_2-saturated 0.1 M KOH at different rotation rates. The onset potential of the ORR on FePc/rGO is –0.05 V and it shifts positive comparing to the CoPh/rGO catalyst for which the onset potential is –0.15 V. The ORR activity of catalyst materials could be attributed to the interaction between carbon atoms of the support material and the central metal atom in the metallocomplexes. For the CoPh/rGO catalyst a pre-wave is observed, whereas for the FePc/rGO material the pre-wave is absent and current plateau is reached at a rather positive potential. This could be explained by the small differences in the structure of the modifier molecules, difference in the central metal atom and existence of better π–π interactions between different MN_4 macrocycles [259].

Figures 39c and 39d present the K-L plots obtained from the RDE data on oxygen reduction on FePc/rGO and CoPh/rGO, respectively. The non-zero intercepts of the extrapolated K-L lines shows that the process of O_2 reduction is not entirely under the diffusion control even at high negative potentials. The inset to Figures 39c and 39d shows the *n* values calculated from the K-L plots at various potentials. For the CoPh/rGO material at low overpotentials ($E > -0.7$ V) the *n* value is close to 3 and at more negative potential *n* reaches 4, which means that O_2 reduction takes place as mixed $2e^-$ and $4e^-$ process and produces both HO_2^- and OH^-. From the inset to Figure 39c corresponding to FePc/rGO, one can see that the value of *n* is close to 4 in a wide range of potential.

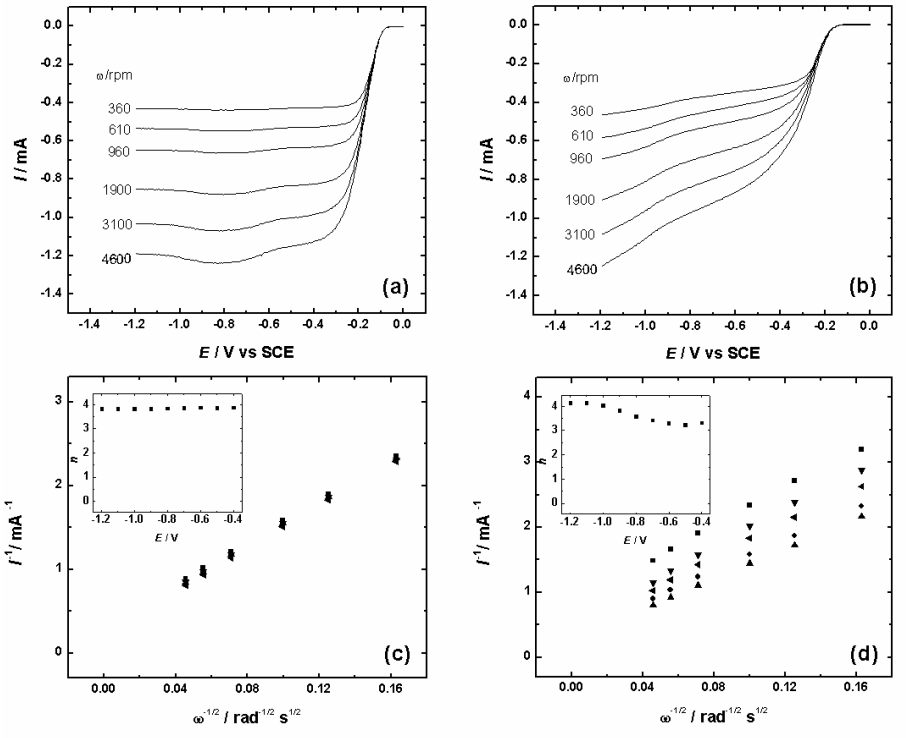

Figure 39. RDE voltammetry curves for ORR on (a) FePc/rGO and (b) CoPh/rGO modified GC electrodes in O_2–saturated 0.1 M KOH. v=10 mV s^{-1}. Koutecky-Levich plots for oxygen reduction on (c) FePc/rGO and (d) CoPh/rGO electrodes in 0.1 M KOH at various potentials: (■) –0.4, (▼) –0.6, (◄) –0.8, (●) –1.0 and (▲) –1.2 V. The inset shows the potential dependence of *n*.

Figure 40 presents the comparative RDE results of O_2 reduction obtained for GC electrodes modified with different catalyst materials. Pure GO and rGO are showing average electrocatalytic activity for ORR which is characteristic for most of carbon materials with high surface area. However the electrocatalytic

effect of GO and rGO is modest comparing to MN_4 macrocycle modified rGO catalysts. As one can see from Figure 40, the MN_4 macrocycles adsorbed on the surface of rGO significantly increase the ORR activity. These materials show a great promise as cathode catalysts for AEMFCs.

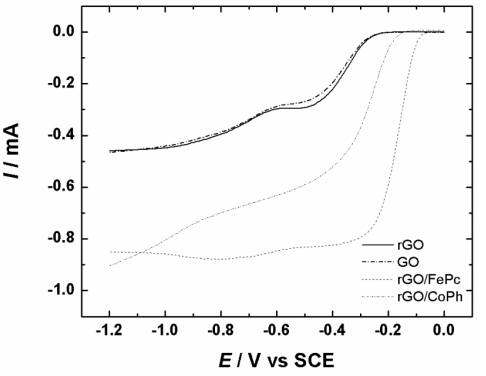

Figure 40. Comparison of RDE results for oxygen reduction on different catalysts in O_2–saturated 0.1 M KOH. v =10 mV s^{-1}. ω=1900 rpm.

The research carried out in the present work is one of the first efforts to study the ORR activity of graphene-supported MN_4 macrocycles. So far there have been only a few papers dealing with oxygen reduction on MN_4 macrocycle modified graphene catalysts [137,138,260].

7. SUMMARY

In this thesis the oxygen reduction reaction on different nanocarbons and nanocarbon supported metallophthalocyanines and metalloporphyrins has been studied. The electrochemical reduction of oxygen was explored on glassy carbon electrodes modified with carbon nanotubes purified in different acids (3 M HCl, 3 M HNO_3, concentrated H_2SO_4 and a mixture of HNO_3 and H_2SO_4). The half-wave potential of O_2 reduction shifted almost 0.2 V in the negative direction upon MWCNTs pre-treatment in acids. Thereby the RDE results obtained in this work showed that the acid treatment of MWCNTs has a strong effect on the electrocatalytic activity for oxygen reduction in acid solution and clearly demonstrated the effect of catalysts impurities remained in CNTs on the kinetics of the ORR. The untreated CNTs contain a high amount of metal impurities (mostly Fe, Co) which are used as catalysts for their preparation by CVD and can be largely removed by treatment in acids [I].

MWCNTs supported on HOPG electrodes and DWCNTs on GC electrodes were investigated as electrocatalysts for ORR in alkaline media. A hydrodynamic deposition method was employed to modify the HOPG electrodes with MWCNTs. The RDE results showed that MWCNTs possess the excellent electrocatalytic activity towards the ORR in alkaline solution. The AFM studies of MWCNT modified HOPG surface confirmed the effectiveness of the hydrodynamic modification method [II]. Similar electrocatalytic activity was achieved for DWCNT modified GC electrodes in alkaline media, whereas the measurements performed with DWCNT/GC electrodes in acid media showed that DWCNTs are rather inactive in a large range of potentials in these conditions and therefore could be used as an interesting support material for various catalysts [III].

The pH-dependence of the ORR and the effect of surfactants on this reaction was studied with MWCNT modified GC electrodes and carbon nanotubes were dispersed in the presence of various surfactants (SDS, CTAB, DHP, Triton X-100). The electrochemical reduction of oxygen was studied in aqueous solutions of different pH using the RDE method. The RDE results revealed that MWCNTs are active catalysts for O_2 reduction in the solutions of high pH. The overpotential for O_2 reduction increases with decreasing pH. The pH dependence of oxygen reduction on MWCNT-modified electrodes follows the same trend as that of the unmodified GC electrode. The effect of surfactants for ORR on MWCNT/GC electrodes was in evidence [IV].

The electrochemical reduction of oxygen has been studied on carbon nanomaterial modified GC electrodes employing the RDE and RRDE methods. Polytetrafluoroethylene was used as a binder material. The results obtained in this part of research indicate that these nanocarbon modified electrodes are highly active for the reduction of oxygen in alkaline solution and this activity might be caused by native quinone-type groups on their surface. Besides surface

functionalities, the differences in the structure and porosity of these materials may influence the process of oxygen reduction [V].

Co phthalocyanine, Fe phthalocyanine, Co porphyrin and Fe porphyrin were supported on MWCNTs with 50% loading through a simple adsorption method and studied as non-noble metal electrocatalysts for ORR in both acid [VI] and alkaline media [VII]. These catalyst materials were also heat-treated at two different temperatures. The XPS analysis of these catalysts showed decomposition of the phthalocyanine and porphyrin rings because of the pyrolysis and the formation of different electrocatalytically active metal and nitrogen surface groups. The ORR kinetics were investigated by RDE and it was found that metal porphyrin and phthalocyanine-based electrodes heat-treated at 800 °C yielded an extraordinary electrocatalytic activity.

Metallophthalocyanine/MWCNTcatalysts were also evaluated in anion exchange membrane fuel cell. Membrane electrode assemblies were fabricated using catalyst coated Tokuyama® membrane (# A201) and compared with E-TEK and Tanaka commercial Pt/C catalysts. The fuel cell performance of the MEAs with Co phthalocyanine was found to be only slightly inferior to Tanaka Pt/C cathode catalysts but similar to that of E-TEK catalysts using H_2 and O_2 gases. The fuel cell power densities of the MEAs with Co and Fe phthalocyanines and Tanaka Kikinzoku Kogyo Pt/C cathode catalysts were 100, 60 and 120 mW cm^{-2}, respectively, using H_2 and O_2 gases [VIII].

Finally the reduced graphene oxide nanosheets as advanced electrocatalyst support materials were prepared and thoroughly studied by various surface characterisation methods. The catalyst materials were prepared by functionalisation of rGO with metal porhyrin and metal phthalocyanine via physical adsorption. The resulting catalyst materials exhibited excellent electrocatalytic activity towards the ORR in alkaline media. This indicates an efficient electron transfer between metallocomplexes, rGO and GC electrode and therefore these types of materials are promising for wide-spread electrochemical applications in many fields [IX].

8. REFERENCES

[1] Y. Gogotsi, Nanomaterials Handbook. CRC Press, Broken Sound Parkway, Nevada, 2006.

[2] T. Akasaka, F. Wudl, S. Nagase, Chemistry of Nanocarbons, Wiley, West Sussex, 2010.

[3] L.M. Liz-Marzan, P.V. Kamat, Nanoscale Materials, Kluwer Academic Publishers, Norwell, Massachusetts, 2003.

[4] P. Serp, J.L. Figueiredo, Carbon Materials for Catalysis, Wiley, Hoboken, New Jersey, 2009.

[5] S. Iijima, Nature 354 (1991) 56.

[6] S.B. Yoon, B. Fang. M. Kim, J.H. Kim, J.-S. Yu, in: G. Wilde (Ed.), Nano-structured Materials, Elsevier, Oxford, 2009, pp. 173–231.

[7] R.L. McCreery, Chem. Rev. 108 (2008) 2646.

[8] M. Shao, Electrocatalysis in Fuel Cells, Springer-Verlag, London, 2013

[9] A. Rabis, P. Rodriguez, T.J. Schmidt, ACS Catal. 2 (2012) 864.

[10] Z. Chen, D. Higgins, A. Yu, L. Zhang, J. Zhang, Energy Environ. Sci. 4 (2011) 3167.

[11] F. Jaouen, E. Proietti, M. Lefevre, R. Chenitz, J.–P. Dodelet, G. Wu, H.T. Chung, C.M. Johnson, P. Zelenay, Energy Environ. Sci. 4 (2011) 114.

[12] J. Zhang, PEM Fuel Cell Electrocatalysts and Catalyst Layers, Springer, London, 2008.

[13] K. Kinoshita, Electrochemical Oxygen Technology, Wiley, New York, 1992.

[14] E. Yeager, Electrochim. Acta 29 (1984) 1527.

[15] R. Adzic, in: J. Lipkowski, P.N. Ross (Eds.), Frontiers in Electrochemistry, Vol. 5, Electrocatalysis, Wiley-VCH, New York, 1998, pp.197-242.

[16] M.R. Tarasevich, A. Sadkowski, E. Yeager, in: B.E. Conway, J.O'M. Bockris, E. Yeager, S.U.M. Khan, R.E. White (Eds.), Comprehensive Treatise of Electro-chemistry, vol. 7, Plenum Press, New York, 1983, pp. 301–398.

[17] B. Šljukic, C.E. Banks, R.G. Compton, J. Iran. Chem. Soc. 2 (2005) 1.

[18] D.A. Tryk, C.R. Cabrera, A. Fujishima, N. Spataru, in: J. Prakash, D. Chu, D. Scherson, M. Enayetullah, I. Tae Bae (Eds.), Fundamental Understanding of Electrode Processes in Memory of Professor Ernest B. Yeager, PV 2003–30, The Electrochemical Society Proceedings, Pennington, New Jersey, 2005, pp. 45–57.

[19] I. Morcos, E. Yeager, Electrochim. Acta 15 (1970) 953.

[20] R.J. Taylor, A.A. Humffray, J. Electroanal. Chem. 64 (1975) 85.

[21] M.S. Hossain, D.A. Tryk, E. Yeager, Electrochim. Acta 34 (1989) 1733.

[22] K. Tammeveski, K. Kontturi, R.J. Nichols, R.J. Potter, D.J. Schiffrin, J. Electroanal. Chem. 515 (2001) 101.

[23] J. Xu, W. Huang, R.L. McCreery, J. Electroanal. Chem. 410 (1996) 235.

[24] C. Paliteiro, A. Hamnett, J.B. Goodenough, J. Electroanal. Chem. 233 (1987) 147.

[25] A. Sarapuu, K. Helstein, D.J. Schiffrin, K. Tammeveski, Electrochem. Solid-State Lett. 8 (2005) E30.

[26] M.I. Awad, M.M. Saleh, T. Ohsaka, J. Solid State Electrochem. 12 (2008) 251.

[27] M.M. Saleh, M.I. Award, T. Okajima, K. Suga, T. Ohsaka, Electrochim. Acta 52 (2007) 3095.

[28] H.-H. Yang, R.L. McCreery, J. Electrochem. Soc. 147 (2000) 3420.
[29] N. Alexeyeva, K. Tammeveski, Electrochem. Solid-State Lett. 10 (2007) F18.
[30] M.O. Davies, M. Clark, E. Yeager, F. Hovorka, J. Electrochem. Soc. 106 (1959) 56.
[31] E. Yeager, P. Krouse, K.V. Rao, Electrochim. Acta 9 (1964) 1057.
[32] F.Z. Sabirov, M.R. Tarasevich, Elektrokhimiya 5 (1969) 608.
[33] F.Z. Sabirov, M.R. Tarasevich, R.Kh. Burshtein, Elektrokhimiya 6 (1970) 1130.
[34] S.M. Golabi, J.B. Raoof, J. Electroanal. Chem. 416 (1996) 75.
[35] A. Salimi, H. Esghi, H. Sharghi, S.M. Golabi, M. Shamsipur, Electroanalysis 11 (1999) 114.
[36] A. Sarapuu, K. Vaik, D.J. Schiffrin, K. Tammeveski, J. Electroanal. Chem. 541 (2003) 23.
[37] K. Vaik, D.J. Schiffrin, K. Tammeveski, Electrochem. Commun. 6 (2004) 1.
[38] J.-M. Seinberg, M. Kullapere, U. Mäeorg, F.C. Maschion, G. Maia, D.J. Schiffrin, K. Tammeveski, J. Electroanal. Chem. 624 (2008) 151.
[39] M. Kullapere, J.-M. Seinberg, U. Mäeorg, G. Maia, D.J. Schiffrin, K. Tammeveski, Electrochim. Acta 54 (2009) 1961.
[40] M. Mooste, E. Kibena, A. Sarapuu, L. Matisen, K. Tammeveski, J. Electroanal. Chem. 702 (2013) 8.
[41] T. Yano, D.A. Tryk, K. Hashimoto, A. Fujishima, J. Electrochem. Soc. 145 (1998) 1870.
[42] M.R. Tarasevich, F.Z. Sabirov, R.K. Burshtein, Elektrokhimiya 7 (1971) 404.
[43] R.J. Taylor, A.A. Humffray, J. Electroanal. Chem. 64 (1975) 95.
[44] J.R.T.J. Wass, E. Ahlberg, I. Panas, D.J. Schiffrin, Phys. Chem. Chem. Phys. 8 (2006) 4189.
[45] A. Sarapuu, PhD Thesis, Tartu University Press, Tartu, 2008.
[46] M. Kullapere, PhD Thesis, Tartu University Press, Tartu, 2010.
[47] G. Jürmann, D.J. Schiffrin, K. Tammeveski, Electrochim. Acta 53 (2007) 390.
[48] S. Sharma, B.G. Pollet, J. Power Sources 208 (2012) 96.
[49] A.L. Dicks, J. Power Sources 156 (2006) 128.
[50] T.C. Liu, Y.Y. Li, Carbon 44 (2006) 2045.
[51] R.C. Haddon, S.–Y. Chow, Pure. Appl. Chem. 71 (1999) 289.
[52] P.J. Britto, K.S.V. Santhanam, A. Rubio, A. Alonso, P.M. Ajayan, Adv. Mater. 11 (1999) 154.
[53] M.S. Dresselhaus, G. Dresselhaus, P.C. Eklund, Science of Fullerenes and Carbon Nanotubes, Academic Press, New York, 1996.
[54] T.W. Ebbesen, Carbon Nanotubes: Preparation and Properties, CRC Press, Boca Raton, FL, 1997, pp. 225–248.
[55] K. Matsubara, K. Waki, Electrochim. Acta 55 (2010) 9166.
[56] N. Alexeyeva, E. Shulga, V. Kisand, I. Kink, K. Tammeveski, J. Electroanal. Chem. 648 (2010) 169.
[57] P. Gajendran, R. Saraswathi, J. Phys. Chem. C. 111 (2007) 11320.
[58] G.-J. Sohn, H.-J. Choi, I.-Y. Jeon, D. W. Chang, L. Dai, J.-B. Baek, ACS Nano 6 (2012) 6345.
[59] F. Wang, S. Hu, Electrochim. Acta 51 (2006) 4228.
[60] S. Wang, D. Yu, L. Dai, J. Am. Chem. Soc. 133 (2011) 5182.
[61] F. Wang, S. Hu, J. Electroanal. Chem. 580 (2005) 68.
[62] Y.Q. Chu, C.A. Ma, F.M. Zhao, H. Huang, Chinese Chem. Lett. 7 (2004) 805.
[63] G. Jürmann, K. Tammeveski, J. Electroanal. Chem. 597 (2006) 119.

[64] M. Zhang, Y. Yan, K. Gong, L. Mao, Z. Guo, Y. Chen, Langmuir 20 (2004) 8781.
[65] S. Shanmugam, A. Gedanken, J. Phys. Chem. B 110 (2006) 2037.
[66] G. Che, B.B. Lakshmi, E.R. Fisher, C.R. Martin, Nature 393 (1998) 346.
[67] M. Carmo, V.A. Paganin, J.M. Rosolen, E.R. Gonzalez, J. Power Sources 142 (2005) 169.
[68] K. Matsubara, K. Waki, Electrochem. Solid-State Lett. 13 (2010) F7.
[69] J. Maruyama, I. Abe, J. Electroanal. Chem. 527 (2002) 65.
[70] V.V. Strelko, N.T. Kartel, I.N. Dukhno, V.S. Kuts, R.B. Clarkson, B.M. Odintsov, Surf. Sci. 548 (2004) 281.
[71] S. Park, R.S. Ruoff, Nat. Nanotechnol. 4 (2009) 217.
[72] C.E. Banks, A. Crossley, C. Salter, S.J. Wilkins, R.G. Compton, Angew. Chem. Int. Ed. 45 (2006) 2533.
[73] B. Šljukic, C.E. Banks, R.G. Compton, Nano Lett. 6 (2006) 1556 .
[74] A.F. Ismail, P.S. Goh, J.C. Tee, S.M. Sanip, Nano 3 (2008) 127.
[75] T.-J. Park, S. Banerjee, T. Hemeraj-Benny, S.S. Wong, J. Mater. Chem. 16 (2006) 141.
[76] K. MacKenzie, O. Dunens, A.T. Harris, Sep. Purif. Technol. 66 (2009) 209.
[77] M. Pumera, B. Šmid, K. Veltruska, J. Nanosci. Nanotechnol. 9 (2009) 2671.
[78] S.K. Pillai, S.S. Ray, M. Moodley, J. Nanosci. Nanotechnol. 8 (2008) 6187.
[79] J.L. Lyon, K.J. Stevenson, Langmuir 23 (2007) 11311.
[80] M.S. Saha, A. Kundu, J. Power Sources 195 (2010) 6255.
[81] S. Osswald, M. Havel, Y. Gogotsi, J. Raman Spectrosc. 38 (2007) 728.
[82] V. Datsyuk, M. Kalyva, K. Papagelis, J. Parthenios, D. Tasis, A. Siokou, I. Kallitsis, C. Galiotis, Carbon 46 (2008) 833.
[83] P. Hojati-Talemi, R. Cervini, G.P. Simon, J. Nanopart. Res. 12 (2010) 393
[84] C.H. Lau, R. Cervini, S.R. Clarke, M.G. Markovic, J.G. Matisons, S.C. Hawkins, C.P. Huynh, G.P. Simon, J. Nanopart. Res. 10 (2008) 77.
[85] I.W. Chiang, B.E. Briston, R.E. Smalley, J.L. Margrave, R.H. Hauge, J. Phys. Chem. B 105 (2001) 1157.
[86] P.-X. Hou, C. Liu, H.-M. Cheng, Carbon 46 (2008) 2003.
[87] E.J. Biddinger, U.S. Ozkan, J. Phys. Chem. C 114 (2010) 15306.
[88] C.E. Banks, X. Ji, A. Crossley, R.G. Compton, Electroanalysis 18 (2006) 2137.
[89] H. Hiura, T.W. Ebbesen, K. Tanigaki, Adv. Mater. 7 (1995) 275.
[90] M.S.P. Shaffer, X. Fax, A.H. Windle, Carbon 36 (1998) 1603.
[91] M. Musameh, N.S. Lawrence, J. Wang, Electrochem. Commun. 7 (2005) 14.
[92] Z.W. Zhang, D.A. Tryk, E.B. Yeager, in: S. Sarangapani, J.R. Akridge, B. Schumm (Eds.), Proc. Workshop on the Electrochemistry of Carbon, The Electrochemical Society, Pennington, New Jersey, 1984, pp. 158–78.
[93] M.J. Ledoux, R. Vieira, C. Pham-Huu, N. Keller, J. Catal. 216 (2003) 333.
[94] D. Pan, M. Ombaba, Z.-Y. Zhou, Y. Liu, S. Chen, J. Lu, ACS Nano 6 (2012) 10720.
[95] Y.A. Kim, T. Hayashi, M. Endo, M.S. Dresselhaus, in: R. Vajtai (Ed.), Carbon Nanofibers, Springer Handbook of Nanomaterials, Springer-Verlag Publishers, Heidelberg, 2013, pp. 1–27.
[96] T.G. Ros, D.E. Keller, A.J. van Dillen, J.W. Geus, D.C. Koningsberger, J. Catal. 211 (2002) 85.
[97] D. Sebastián, M.J. Lázaro, I. Suelves, R. Moliner, V. Baglio, A. Stassi, A.S. Aricò, Int. J. Hydrogen Energy 37 (2012) 6253.

[98] J.-S. Zheng, X.-S. Zhang, P. Li, X.-G. Zhou, W.-K. Yuan, Catal. Today 131 (2008) 270.
[99] M. Endo, Y.A. Kim, T. Fukai, T. Hayashi, K. Oshida, M. Terrones, T. Yanagisawa, S. Higaki, M.S. Dresselhaus, Appl. Phys. Lett. 80 (2002) 1267.
[100] N.M. Rodriguez, A. Chambers, R.T.K. Baker, Langmuir 11 (1995) 3862.
[101] J.-S. Zheng, X.-S. Zhang, P. Li, X.-G. Zhou, D. Chen, Y. Liu, W.-K. Yuan, Electrochim. Acta 53 (2008) 3587.
[102] Y.A. Kim, H. Takuya, F. Yasuo, M. Endo, Mol. Cryst. Liq. Cryst. 387 (2002) 157.
[103] K.P. de Jong, J.W. Geus, Catal. Rev. Sci. Eng. 42 (2000) 481.
[104] J.-S. Zheng, X.-S. Zhang, P. Li, J. Zhu, X.-G. Zhou, W.-K. Yuan, Electrochem. Commun. 9 (2007) 895.
[105] K. Gong, S. Chajrabarti, L. Dai, Angew. Chem. Int. Ed. 47 (2008) 5446.
[106] R.-S. Zhong, Y.-H. Qin, D.-F. Niu, J.-W. Tian, X.-S. Zhang, X.-G. Zhou, S.-G. Sun, W.-K. Yuan, J. Power Sources 225 (2013) 192.
[107] Y. Gogotsi, R.K. Dash, G. Yushin, T. Yildirim, G. Laudisio, J.E. Fischer, J. Am. Chem. Soc. 127 (2005) 16006.
[108] I. Tallo, T. Thomberg, K. Kontturi, A. Jänes, E. Lust, Carbon 49 (2011) 4427.
[109] G. Yushin, R.K. Dash, J. Jagiello, J.E. Fischer, Y. Gogotsi, Adv. Funct. Mater. 16 (2006) 2288.
[110] Y. Gogotsi, A. Nikitin, H. Ye, W. Zhou, J.E. Fischer, B. Yi, H.C. Foley, M.W. Barsoum, Nat. Mater. 2 (2003) 591.
[111] A.J. Appleby, J. Marie, Electrochim. Acta 24 (1979) 195.
[112] E. Härk, J. Nerut, K. Vaarmets, I. Tallo, H. Kurig, J. Eskusson, K. Kontturi, E. Lust, J. Electroanal. Chem. 689 (2013) 176.
[113] L. Borchardt, F. Hasche, M.R. Lohe, M. Oschatz, F. Schmidt, E. Kockrick, C. Ziegler, T. Lescouet, A. Bachmatiuk, B. Büchner, D. Farrusseng, P. Strasser, S. Kaskel, Carbon 50 (2012) 1861.
[114] C.R. Pérez, S.-H. Yeon, J. Ségalini, V. Presser , P.-L. Taberna P. Simon, Y. Gogotsi, Adv. Funct. Mater. 23 (2012) 1081.
[115] K. Vaarmets, S. Sepp, J. Nerut, E. Härk, I. Tallo, E. Lust, J. Solid State Electrochem. 17 (2013) 1729.
[116] K. Vaarmets, J. Nerut, E. Härk, E. Lust, Electrochim. Acta 104 (2013) 216.
[117] A. Schlange, A.R. Santos, B. Hasse, B.J.M. Etzold, U. Kunz, T. Turek, J. Power Sources 199 (2012) 22.
[118] M.J. Allen, V.C. Tung, R.B. Kaner, Chem. Rev. 110 (2010) 132.
[119] C.N.R. Rao, A.K. Sood, K.S. Subrahmanyam, K.S. Govindaraj, Angew. Chem. Int. Ed. 48 (2009) 7752.
[120] K.S. Novoselov, A.K. Geim, S.V. Morozov, D. Jiang, Y. Zhang, S.V. Dubonos, I.V. Grigorieva, A.A. Firsov, Science 306 (2004) 666.
[121] A.K. Geim, K.S. Novoselov, Nat. Mater. 6 (2007) 183.
[122] D.A.C. Brownson, D.K. Kampouris, C.E. Banks, Chem. Soc. Rev. 41 (2012) 6944.
[123] E. Antolini, Appl. Catal. B. Environ. 123 (2012) 52.
[124] M.D. Stoller, S. Park, Y. Zhu, J. An, R.S. Ruoff, Nano Lett. 8 (2008) 3498.
[125] C. Zhu, S. Dong, Nanoscale 5 (2013) 1753.
[126] F. Lima, G.V. Fortunato, G. Maia, RSC Adv. 3 (2013) 9550.
[127] S. Wang, D. Yu, L. Dai, D.W. Chang, J.-B. Baek, ACS Nano 5 (2011) 6202.

[128] D. Huang, B. Zhang, Y. Zhang, F. Zhan, X. Xu, Y. Shen, M. Wang, J. Mater. Chem. A 1 (2013) 1415.
[129] M.S. Ahmed, S. Jeon, J. Power Sources 218 (2012) 168.
[130] L. Tang, Y. Wang, Y. Li, H. Feng, J. Lu, J. Li, Adv. Funct. Mater. 19 (2009) 2782.
[131] S. Stankovich, D.A. Dikin, R.D. Piner, K.A. Kohlhaas, A. Kleinhammes, Y. Jia, Y. Wu, R.S. Ruoff, Carbon 45 (2007) 1558.
[132] X.L. Li, H.L. Wang, J.T. Robinson, H. Sanchez, G. Diankov, H.J. Dai, J. Am. Chem. Soc. 131 (2009) 15939.
[133] S. Zhang, S. Tang, J. Lei, H. Dong, H. Ju, J. Electroanal. Chem. 656 (2011) 285.
[134] Z.H. Sheng, L. Shao, J.J. Chen, W.J. Bao, F.B. Wang, X.H. Xia, ACS Nano 5 (2011) 4350.
[135] L. Qu, Y. Liu, J.-B. Baek, L.M. Dai, ACS Nano 4 (2010) 1321.
[136] C. Zhang, R. Hao, H. Yin, F. Liu, Y. Hou, Nanoscale 4 (2012) 7326.
[137] M. Jahan, Q. Bao, K.P Loh, J. Am. Chem. Soc. 134 (2012) 6707.
[138] E. Yoo, H. Zhou, J. Sources 2013 (Article in Press).
[139] R. Jasinski, Nature 201 (1964) 1212.
[140] J.H. Zagal, Coord. Chem. Rev. 119 (1992) 89.
[141] P. Vasudevan, S.N. Mann, S. Tyagi, Transition Met. Chem. 15 (1990) 81.
[142] J.H. Zagal, S. Griveau, J.F. Silva, T. Nyokong, F. Bedioui, Coord. Chem. Rev. 254 (2010) 2755.
[143] J.H. Zagal, S. Griveau, K.I. Ozoemena, T. Nyokong, F. Bedioui, J. Nanosci. Nanotechnol. 9 (2009) 2201.
[144] M.R. Tarasevich, G.V. Zhutaeva, M.V. Radina, Z.R. Karichev, E.A. Teishev, J.H. Miners, P. Goueres, E. Sanches-Corteron, Russ. J. Electrochem. 39 (2003) 1224.
[145] J. Guo, H. He, D. Chu, R. Chen, Electrocatalysis 3 (2012) 252.
[146] S. Baranton, C. Coutanceau, C. Roux, F. Hahn, J.-M. Léger. J. Electroanal. Chem. 577 (2005) 223.
[147] S.N.S. Goubert-Renaudin, X. Zhu, A. Wieckowski, Electrochem. Commun. 12 (2010) 1457.
[148] Q. He, T. Mugadza, G. Hwang, T. Nyokong, Int. J. Electrochem. Sci. 7 (2012) 7045.
[149] Y. Kiros, Int. J. Electrochem. Sci. 2 (2007) 285.
[150] X. Hu, D. Xia, L. Zhang, J. Zhang, J. Power Sources 231 (2013) 91.
[151] T. Schilling, A. Okunola, J. Masa, W. Schuhmann, M. Bron, Electrochim. Acta 55 (2010) 7597.
[152] E. Claude, T. Addou, J.-M. Latour, P. Aldebert, J. Appl. Electrochem. 28 (1998) 57.
[153] G. Lalande, G. Faubert, R. Côté, D. Guay, J.P. Dodelet, L.T. Weng, P. Bertrand, J. Power Sources 61 (1996) 227.
[154] X. Li, B.N. Popov, T. Kawahara, H. Yanagi, J. Power Sources 196 (2011) 1717.
[155] H. Kalvelage, A. Mecklenburg, U. Kunz, U. Hoffmann, Chem. Eng. Technol. 23 (2000) 803.
[156] V. Bambagioni, C. Bianchini, J. Filippi, A. Lavacchi, W. Oberhauser, A. Marchionni, S. Moneti, F. Vizza, R. Psaro, V. Dal Santo, A. Gallo, S. Recchia, L. Sordelli, J. Power Sources 196 (2011) 2519.
[157] Y. Yuan, J. Ahmed, S. Kim, J. Power Sources 196 (2011) 1103.
[158] R. Baker, D.P. Wilkinson, J. Zhang, Electrochim. Acta 53 (2008) 6906.

[159] J.H. Zagal, M.J. Aguirre, M.A. Paez, J. Electroanal. Chem. 437 (1997) 45.
[160] A. Morozan, S. Camidelli, A. Filoramo, B. Jousselme, S. Palacin, Carbon 49 (2011) 4839.
[161] R. Boulatov, in: J.H. Zagal, F. Bedioui, J.-P. Dodelet (eds), N4 – Macrocyclic metal complexes, Springer Science + Business Media, New York, 2006, pp. 1–40.
[162] J.H. Zagal, M.A. Paez, J.F. Silva, in: J.H. Zagal, F. Bedioui, J.-P. Dodelet (Eds), N4 – Macrocyclic metal complexes, Springer Science + Business Media, New York, 2006, pp. 41–82.
[163] S. Zecevic, B. Simic-Glavski, E. Yeager, A.B.P. Lever, P.C. Minor J. Electroanal. Chem. 196 (1985) 339.
[164] A. van der Putten, A. Elzing, W. Visscher, E. Barendrecht, J. Electroanal. Chem. 221 (1987) 95.
[165] J.H. Zagal, M. Paez, A.A. Tanaka, J.R. dos Santos, C. Linkous, J. Electroanal. Chem. 339 (1992) 13.
[166] E. Theodoridou, A.D. Jannakoudakis, P.D. Jannakoudakis, J.O. Besenhard, J. Appl. Electrochem. 22 (1992) 733.
[167] C. Shi, F.C. Anson, Inorg. Chem. 29 (1990) 4298.
[168] C.L. Ni, F.C. Anson, Inorg. Chem. 24 (1984) 4754.
[169] A.A. Tanaka, C. Fierro, D.A. Scherson, E. Yeager, Mat. Chem. Phys. 22 (1989) 431.
[170] Y. Nabe, S. Moriya, K. Matsubayashi, S.M. Lyth, M. Malon, L. Wu, N.M. Islam, Y. Koshigoe, S. Kuroki, M. Kakimoto, S. Miyata, J. Ozaki, Carbon 48 (2010) 2613.
[171] L. Ding, X. Dai, R. Lin, H. Wang, J. Qiao, J. Electrochem. Soc. 159 (2012) F577.
[172] A. Okunola, B. Kowalewska, M. Bron, P.J. Kulesza, W. Schuhmann, Electrochim. Acta 54 (2009) 1954.
[173] S.-I. Yamazaki, Y. Yamada, T. Ioroi, N. Fujiwara, Z. Siroma, K. Yasuda, Y. Miyazaki, J. Electroanal. Chem. 576 (2005) 253.
[174] C. Mocchi, S. Trasatti, J. Mol. Catal. A: Chem. 204–205 (2003) 713.
[175] W. Zhang, A.U. Shaikh, E.Y. Tsui, T.M. Swager, Chem. Mater. 21 (2009) 3234.
[176] C. Medard, M. Lefevre, J.P. Dodelet, F. Jaouen, G. Lindbergh, Electrochim. Acta 51 (2006) 3202.
[177] S.A. Mamuru, K.I. Ozoemena, Electroanalysis 22 (2010) 985.
[178] R.L. Arechederra, K. Artyushkova, P. Atanassov, S.D. Minteer, ACS Appl. Mater. Interfaces 2 (2010) 3295.
[179] N. Li, M. Zhu, M. Qu, X. Ago, X. Li, W. Zhang, J. Zhang, J. Ye, J. Electroanal. Chem. 651 (2011) 12.
[180] Z. Xu, H. Li, G. Cao, Q. Zhang, K. Li, X. Zhao, J. Mol. Catal. A: Chem. 335 (2011) 89.
[181] H. Li, Z. Xu, K. Li, X. Hou, G. Cao, Q. Zhang, Z. Cao, J. Mater. Chem. 21 (2011) 1181.
[182] G. Dong, M. Huang, L. Guan, Phys. Chem. Chem. Phys. 14 (2012) 2557.
[183] C.A. Fierro, M. Mohan, D.A. Scherson, Langmuir 6 (1990) 1338.
[184] J. Pavez, M. Paez, A. Ringuede, F. Bedioui, J.H. Zagal, J. Solid State Electrochem. 9 (2005) 21.
[185] K. Shigehara, F.C. Anson, J. Phys. Chem. 86 (1982) 2776.

[186] A.L. Bouwkamp-Wijnoltz, W. Visscher, J.A.R. van Veen, Electrochim. Acta 43 (1998) 3141.
[187] G. Lalande, R. Côté, D. Guay, J.-P. Dodelet, L.T. Weng, P. Bertrand, Electrochim. Acta 42 (1997) 1378.
[188] H. Jahnke, M. Schönborn, G. Zimmermann, Top. Cur. Chem. 61 (1976) 133.
[189] A.L. Zhu, H. Wang, W. Qu, X. Li, Z. Jong, H. Li, J. Power Sources 195 (2010) 5587.
[190] H. Meng, N. Larouche, M. Lefevre, F. Jaouen, B. Stansfield, J.-P. Dodelet, Electrochim. Acta 55 (2010) 6450.
[191] L.N. Ramavathu, K.K. Maniam, K. Gopalram, R. Chetty, J. Appl. Electrochem. 42 (2012) 945.
[192] T. Schilling, M. Bron, Electrochim. Acta 53 (2008) 5379.
[193] V.S. Bagotsky, M.R. Tarasevich, K.A. Radyushkina, O.E. Levina, S.I. Andrusyova, J. Power Sources 2 (1977) 233.
[194] K. Wiesener, Electrochim. Acta 31 (1986) 1073.
[195] J.-P. Dodelet, in: J.H. Zagal, F. Bedioui, J.-P. Dodelet (eds), N4 – Macrocyclic metal complexes, Springer Science + Business Media, New York, 2006, pp. 83–147.
[196] P. Bogdanoff, I. Herrmann, M. Hilgendorff, I. Dorbandt, S. Fiechter, H. Tributsch, J. New Mater. Electrochem. Syst. 7 (2004) 85.
[197] M. Ladouceur, G. Lalande, D. Guay, J. P. Dodelet, L. Dignard-Bailey, M. L. Trudeau, R. Schulz, J. Electrochem. Soc. 140 (1993) 1974.
[198] J.A.R. van Veen, H.A. Colijn, Ber. Bunsenges Phys. Chem. 85 (1981) 700.
[199] U.I. Kramm, I. Abs-Wurmbach, I. Herrmann-Geppert, J. Radnik, S. Fiechter, P. Bogdanoff, J. Electrochem. Soc. 158 (2011) B69.
[200] P.H. Matter, E.J. Biddinger, U.S. Ozkan, Catalysis 20 (2007) 338.
[201] J. Herranz, M. Lefevre, N. Larouche, B. Stansfield, J.-P. Dodelet, J. Phys. Chem. C 111 (2007) 19033.
[202] L. Elbaz, E. Korin, L. Soifer, A. Bettelheim, J. Phys. Chem. Lett. 1 (2010) 398.
[203] L. Carrette, K.A. Friedrich, U. Stimming, Fuel Cells 1 (2001) 5.
[204] Y.-J. Wang, J. Qiao, R. Baker, J. Zhang, Chem. Soc. Rev. 42 (2013) 5768.
[205] J.R. Varcoe, R.C.T. Slade, Fuel Cells 5 (2005) 187.
[206] E. Agel, J. Bouet, J.F. Fauvarque, J. Power Sources 101 (2001) 267.
[207] H. Hunger, Proc. Ann. Power Sources Conf. 14 (1960) 55.
[208] M. Mamlouk, K. Scott, J. Power Sources 211 (2012) 140.
[209] E.H. Yu, K. Scott, R.W. Reeve, J. Electroanal. Chem. 547 (2003) 17.
[210] M. Mamlouk, X. Wang, K. Scott, J.A. Horsfall, C. Williams, J. Power and Energy 225 (2011) 152.
[211] C. Coutanceau, L. Demarconnay, C. Lamy, J.M. Leger, J. Power Sources 156 (2006) 14.
[212] K. Matsuoka, Y. Iriyama, T. Abe, M. Matsuoka, Z. Ogumi, J. Power Sources 150 (2005) 27.
[213] J. Park, S. Park, S. Yim, Y. Yoon, W. Lee, C. Kim, J. Power Sources 178 (2008) 620.
[214] M. Piana, M. Boccia, A. Filipi, E. Flammia, H. Miller, M. Orsini, F. Salusti, S. Santiccioli, F. Ciardelli, A. Pucci, J. Power Sources 195 (2010) 5875.
[215] L. Sun, J. Guo, J. Zhou, Q. Xu, D. Chu, R. Chen, J. Power Sources 202 (2012) 70.
[216] Y.S. Li, T.S. Zhao, Int. J. Hydrogen Energy 37 (2012) 15334.

[217] A.M. Bartrom, J.L. Haan, J. Power Sources 214 (2012) 68.
[218] W.S. Hummers, R. Offeman, J. Am. Chem. Soc. 80 (1958) 1339.
[219] J.I. Paredes, S. Villar-Rodil, A. Martinez-Alonso, J.M.D. Tascon, Langmuir 24 (2008) 10560.
[220] A.A. Tanaka, C. Fierro, D. Scherson, E.B. Yeager, J. Phys. Chem. 91 (1987) 3799.
[221] J.P. Jones, K. Jurkschat, A. Crossley, R.G. Compton, B.L. Riehl, C.E. Banks, Langmuir 23 (2007) 9501.
[222] M. Pumera, Y. Miyahara, Nanoscale 1 (2009) 260.
[223] K. Strong, D.P. Anderson, K. Lafdi, J. N. Kuhn, Carbon 41 (2003) 1477.
[224] A.T. Masheter, L. Xiao, G.G. Wildgoose, A. Crossley, J.H. Jones, R.G. Compton, J. Mater. Chem. 17 (2007) 3515.
[225] G.G. Wildgoose, P. Abiman, R.G. Compton, J. Mater. Chem. 19 (2009) 4875.
[226] M.S. Dresselhaus, A. Jorio, M. Hofmann, G. Dresselhaus, R. Saito, Nano. Lett. 10 (2010) 751.
[227] J.H. Lehman, M. Terrones, E. Mansfield, K.E. Hurst, V. Meunier, Carbon 49 (2011) 2581.
[228] I. Dumitrescu, N.R. Wilson, J.V. Macpherson, J. Phys. Chem. C 111 (2007) 12944.
[229] J.J. Gooding, Electrochim. Acta 50 (2005) 3049.
[230] M. Pumera, H. Iwai, J. Phys. Chem. C 113 (2009) 4401.
[231] J.H. Zhou, Z.J. Sui, J. Zhu, P. Li, D. Chen, Y.C. Daí, W.K. Yuan, Carbon 45 (2007) 785.
[232] J.L. Figueiredo, M.F.R. Pereira, M.M.A. Freitas, J.J.M. Orfao, Carbon 37 (1999) 1379.
[233] N. Aleksejeva, PhD Thesis, Tartu University Press, Tartu, 2010.
[234] D.R. Lawson, L.D. Whiteley, C.R. Martin, M.N. Szentirmay, J.I. Song, J. Electrochem. Soc. 135 (1988) 2247.
[235] A.J. Bard, L.R. Faulkner, Electrochemical Methods, 2nd ed., John Wiley & Sons, New York, 2001.
[236] S. Gottesfeld, I.D. Raistrick, S. Srinivasan, J. Electrochem. Soc. 134 (1987) 1455.
[237] D. Yu, E. Nagelli, F. Du, L. Dai, J. Phys. Chem. Lett. 1 (2010) 2165.
[238] R.E. Davis, G.L. Horvath C.W. Tobias, Electrochim. Acta 12 (1967) 287.
[239] J. Schreurs, J. van den Berg, A. Wonders, E. Barendrecht, Recl. Trav. Chim. Pays-Bas 103 (1984) 251.
[240] J. Yu, N. Grossiord, C.E. Koning, J. Loos, Carbon 45 (2007) 618.
[241] K.H. An, W.S. Kim, Y.S. Park, Y.C. Choi, S.M. Lee, D.C. Chung, D.J. Bae, S.C.K. Lim, Y.H. Lee, Adv. Mater. 13 (2001) 497.
[242] S. Alvarez, M.C. Blanco-Lopez, A.C. Miranda-Ordieres, A.B. Fuertes, T.A. Centeno, Carbon 43 (2005) 866.
[243] L. Giorgi, E. Antolini, A. Pozio, E. Passalacqua, Electrochim. Acta 43 (1998) 3675.
[244] J. Perez, A.A. Tanaka, E.R. Gonzalez, E.A. Ticianelli, J. Electrochem. Soc. 141 (1994) 431.
[245] E. Lobyntseva, T. Kallio, N. Alexeyeva, K. Tammeveski, K. Kontturi, Electrochim. Acta 52 (2007) 7262.
[246] H.S. Wroblowa, Y.-C. Pan, G. Razumney, J. Electroanal. Chem. 69 (1976) 195.
[247] M. Appel, A.J. Appleby, Electrochim. Acta 23 (1978) 1243.

[248] U.A. Paulus, T.J. Schmidt, H.A. Gasteiger, R.J. Behm, J. Electroanal. Chem. 495 (2001) 134.
[249] A.A. Franco, M. Gerard, J. Electrochem Soc. 155 (2008) B367.
[250] T. Burchardt, J. Power Sources 135 (2004) 192.
[251] J.S. Campos-Martin, G. Blanco-Brieva, J.L.G. Fierro, Angew. Chem. Int. Ed. 45 (2006) 6962.
[252] A. Widelöv, R. Larson, Electrochim. Acta 37 (1992) 187.
[253] P. Gouerec, M. Savy, J. Riga, Electrochim. Acta 43 (1998) 743.
[254] M.C.M. Alves, J.P. Dodelet, D. Guay, M. Ladouceur, G. Tourillon, J. Phys. Chem. 96 (1992) 10898.
[255] S. Gupta, D. Tryk, I. Bae, W. Aldred, E. Yeager, J. Appl. Electrochem. 19 (1989) 19.
[256] Z. Mo, S. Liao, Y. Zheng, Z. Fu, Carbon 50 (2012) 2620.
[257] S.L. Gojković, S. Gupta, R.F. Savinell, J. Electrochem. Soc.145 (1998) 3493.
[258] E.E. Switzer, T.S. Olson, A.K. Datye, P. Atanassov, M.R. Hibbs, C. Fujimoto, C.J. Cornelius, Electrochim. Acta 55 (2010) 3404.
[259] M. Lefevre, E. Proietti, F. Jaouen, J.P. Dodelet, Science 324 (2009) 71.
[260] L. Cui, G. Lv, Z. Dou, X. He, Electrochim. Acta 106 (2013) 272.

9. KOKKUVÕTE

Hapniku elektroredutseerumine süsiniknanomaterjalidel põhinevatel katalüsaatoritel

Doktoritöös uuriti hapniku elektrokeemilist redutseerumist erinevatel süsiniknanomaterjalidel (I–V). Süsinikmaterjalide pinda modifitseeriti ka metalloftalotsüaniinide ning -porfüriinidega ja uuriti nende elektrokatalüütilisi omadusi (VI–IX).

Töö esimene osa keskendus süsiniknanotorude puhastamisele hapetes ning hapete segus (3 M HCl, 3 M HNO_3, kontsentreeritud H_2SO_4 ning HNO_3 ja H_2SO_4 segu) ning hapniku elektrokeemilise redutseerumise uurimisele happelises keskkonnas. Hapniku redutseerumise poollainepotensiaal nihkus, võrreldes töötlemata mitmeseinaliste süsiniknanotorudega, 0,2 V negatiivses suunas. Seega võib pöörleva ketaselektroodi abil saadud mõõtmistulemuste alusel väita, et süsiniknanotorude hapetes töötlemisel on materjali elektrokatalüütilistele omadustele märkimisväärne mõju ning süsiniknanotorude sünteesi käigus neisse jäävad metallide jäägid (peamiselt Fe, Co) määravad paljuski nende materjalide elektrokatalüütilise aktiivsuse O_2 redutseerumisel happelises keskkonnas [I].

Töö teises osas uuriti hapniku redutseerumist mitmeseinaliste süsiniknanotorudega modifitseeritud kõrgorienteeritud pürografiitelektroodidel ja kaheseinaliste süsiniknanotorudega modifitseeritud klaassüsinikelektroodidel leeliselises keskkonnas. Kõrgorienteeritud pürografiitelektroodi pinna modifitseerimine põhines nanotorude füüsikalisel seondumisel ketaselektroodi pinnale ja sellel eesmärgil kasutati hüdrodünaamilist meetodit. Modifitseeritud pinna morfoloogilised uuringud viidi läbi multifunktsionaalse teravikmikroskoobi abil. Mõõtmistulemused kinnitasid hüdrodünaamilise modifitseerimismeetodi efektiivsust. Pöörleva ketaselektroodi eksperimendid näitasid, et taolised elektroodi pinnal ühtlaselt jaotunud väikesed mitmeseinaliste nanotorude puntrad ja üksikud nanotorud on hapniku redutseerumise seisukohalt küllaltki efektiivsed [II]. Kaheseinaliste süsiniknanotorudega modifitseeritud klaassüsinikelektroodide elektrokeemiline käitumine hapniku elektrokeemilisel redutseerumisel sarnanes kõrgorienteeritud pürografiitelektroodidele seondatud mitmeseinaliste süsiniknanotorude käitumisega. Samas näitasid kaheseinalised süsiniknanotorud küllaltki madalat elektrokatalüütilist aktiivsust hapniku redutseerumisel happelises keskkonnas, viidates selle materjali võimalikule sobivusele teiste katalüsaatormaterjalide kandjana madalatel pH väärtustel [III].

Hapniku elektrokeemilise redutseerumise pH-sõltuvuse ja pindaktiivsete ainete efekti uurimiseks modifitseeriti klaassüsinikelektroode mitmeseinaliste süsiniknanotorude suspensiooniga naatriumdodetsüülsulfaadi, tsetüültrimetüülammooniumbromiidi, diheksadetsüülvesinikfosfaadi ja Triton X-100 vesilahustes. Süsiniknanotorudega modifitseeritud klaassüsinikelektroodil toimunud O_2 redutseerumise uurimisel leiti, et madalamatel pH väärtustel on üleminevate elektronide arv ligikaudu 2, mis näitab, et nendes lahustes redutseerub hapnik

vesinikperoksiidiks, kuid peroksiid edasi ei redutseeru. Kõrgemate pH väärtuste korral näitasid mitmeseinalised süsiniknanotorud aga suurepärast elektrokatalüütilist aktiivsust. Mitmeseinaliste süsiniknanotorudega modifitseeritud elektroodidel saadud hapniku redutseerumise pH-sõltuvus sarnaneb kvalitatiivselt poleeritud klaassüsinikelektroodiga saadud andmetele. Mõõtmistulemuste alusel võib väita ka seda, et pindaktiivsete ainete mõju hapniku elektrokeemilisele redutseerumisele on ilmne [IV].

Erinevate süsiniknanomaterjalide elektrokatalüütiliste omaduste võrdluse tarvis modifitseeriti klaassüsinikelektroode süsiniknanomaterjali ja polütetrafluoroetüleeni suspensiooniga. Elektrokeemilised mõõtmised viidi läbi nii pöörleva ketaselektroodi kui ka pöörleva rõngas-ketaselektroodi meetodil. Erinevate süsiniknanomaterjalidega modifitseeritud elektroodide hapniku elektrokeemilise redutseerumise uuringud näitasid, et kõigil kasutatud süsinikmaterjalidel oli leeliselistes lahustes suur katalüütiline aktiivsus. Süsinikmaterjalide kõrge elektrokatalüütilise aktiivsuse leeliselises keskkonnas põhjustasid nähtavasti süsinikmaterjali pinnale omased kinoonset tüüpi funktsionaalrühmad. Pinnal asetsevate funktsionaalsete rühmade kõrval mõjutas süsinikmaterjalide elektrokatalüütilisi omadusi kindlasti ka materjali struktuur ja poorsus [V].

Töö ühe osana valmistati süsiniknanotorude ja metalloftalotsüaniinide ning –porfüriinide abil edukalt madalatemperatuurilise kütuseelemendi katalüsaatormaterjale. Raud- ja koobaltporfüriini ning -ftalotsüaniinidega modifitseeritud katalüsaatorid valmistati vastavate MN_4 makrotsüklite ja mitmeseinaliste süsiniknanotorude suhtega 50/50 ning neid materjale testiti nii happelises [VI] kui ka aluselises [VII] keskkonnas. Katalüsaatormaterjali sünteesiks dispergeeriti süsiniknanotorud metalloftalotsüaniinide ning -porfüriinide isopropanooli lahuses. Nende elektrokatalüsaatorite puhul kasutati kahte pürolüüsi temperatuuri. Hapniku redutseerumist nendel materjalidel uuriti pöörleva ketaselektroodi meetodil ning leiti, et 800 °C juures näitab pürolüüsitud katalüsaator hapniku elektroredutseerumisel kõrgeimat aktiivsust. Röntgenfotoelektronspektroskoopiline analüüs kinnitas MN_4 makrotsüklite lagunemist pürolüüsi käigus ning elektrokatalüütiliselt aktiivsete lämmastiku- ning metallitsentrite teket süsiniknanotorude pinnale.

Lisaks viidi läbi ka katalüsaatormaterjalide uurimine leeliselises OH^- ioonvahetusmembraaniga kütuseelemendis. Kütuseelemendis kasutati anoodimaterjalina kommertsiaalset plaatinakatalüsaatorit (Pt/C) ning katoodimaterjalina süsiniknanotorudele kantud raudftalotsüaniin või koobaltftalotsüaniin katalüsaatoreid ning võrdluseks ka 20%-lise ja 46%-lise Pt sisaldusega kommertsiaalseid Pt/C katalüsaatoreid. Üherakulise leeliselise kütuseelemendi töötemperatuuriks oli 45 °C ning töögaasideks niisutatud H_2 ja O_2. Kõrgeimat võimsustihedust näitas võrdluseks kasutatud 46%-line Pt/C katalüsaator (~120 mW cm^{-2}). Koobaltftalotsüaniin/süsiniknanotorud katalüsaatori maksimaalne võimsustihedus oli sarnane 20%-lisele Pt/C katalüsaatorile (~100 mW cm^{-2}). Samas raudftalotüaniin/süsiniknanotorud katalüsaatori korral oli võimsustihedus vaid 60 mW cm^{-2} [VIII].

Töö viimases osas uuriti redutseeritud grafeenoksiidi pinda mitmete füüsikaliste meetoditega ning valmistati katalüsaatormaterjalid hapniku elektrokeemiliseks redutseerumiseks, kasutades selleks metalloftalotsüaniine ja -porfüriine. Need MN_4 makrotsüklid seondati redutseeritud grafeeni pinnale füüsikalise adsorptsiooni meetodil. Elektrokeemilised mõõtmised näitasid ülalmainitud grafeenil põhinevate katalüsaatorite suurepäraseid katalüütilisi omadusi hapniku redutseerumisel leeliselises keskkonnas [IX].

10. ACKNOWLEDGEMENTS

First of all I would like to thank my supervisor, Associate Professor Kaido Tammeveski for his continuous support, patience and investment of his time to supervise me in my academic life. These nine original papers presented in this thesis and dissertation itself would not been possible without his considerable help and contribution.

I would like to thank the staff at the Institute of Physics, especially Professor Väino Sammelselg and his co-workers Dr. Leonard Matisen for the XPS measurements, Jekaterina Kozlova for HR-SEM and EDS measurements, Dr. Margus Marandi for the AFM measurements and Jayanta Mondal for the preparation of graphene nanosheets.

I am truly grateful to Associate Professor Arunachalanadar Madakannan for a great experience and the knowledge acquired from the Arizona State University Fuel Cell Lab.

I thank Dr. Jaan Leis and Dr. Mati Arulepp for supporting me with different carbon materials for my research.

I also thank Professor Kyösti Kontturi and his colleagues at Aalto University for performing the TEM measurements.

I wish to thank Professor Juan M. Feliu and Dr. Jose Solla-Gullón from the University of Alicante for the TEM measurements and electrochemical characterisation of carbon nantube materials.

I would also like to thank my colleagues, former colleagues and friends from the Chair of Colloid and Environmental Chemistry. Special thanks to Dr. Nadezda Aleksejeva, Dr. Marko Kullapere, Dr. Ave Sarapuu, Elo Kibena, Heiki Erikson, Merilin Vikkisk and Kristel Jukk.

My research was financially supported by the Estonian Science Foundation (grants nos. 6651, 7546, 8666 and 9323), the Estonian Research Council (grants nos.IUT-02-24, TK-117), the project “Developement and Testing Materials and Single Cells for Solid Oxide Fuel Cells, Polymer Electrolyte Fuel Cells and Super Capacitors” (project no. 3.2.0501.10-0015), the US Civilian Research and Development Foundation (award # ESC2-2975-TR-09), Graduate School on Functional Materials and Technologies (ESF project 1.2.0401.09-0079), Archimedes Foundation and DoRa scholarships.

The author thanks the Tokuyama Corporation, Japan for providing A201 membranes and AS4 ionomer samples.

I thank my friends in Estonia and elsewhere for their support and encouragement throughout.

Most importantly, I am grateful for my parents and family who have given me their unequivocal support throughout.

11. PUBLICATIONS

CURRICULUM VITAE

Nimi: Ivar Kruusenberg
Date of birth: July 31, 1984
Citizenship: Estonian
Address: Ravila 14a, 50411 Tartu, Estonia
Phone: +372 737 5174; +372 50 36963
E-mail: ivar.kruusenberg@ut.ee

Education:

2009–2013	PhD student, Institute of Chemistry, University of Tartu, Estonia; doctoral advisor Kaido Tammeveski
2007–2009	graduate student, Institute of Chemistry, University of Tartu, Estonia, *M.Sc* (molecular technology) 2009
2003–2007	undergraduate student, Institute of Chemistry, University of Tartu, Estonia, *B.Sc* (chemistry) 2007

Professional employment:

2007– University of Tartu, Institute of Chemistry, chemist (0.5)
2006–2007 University of Tartu, Institute of Chemistry, technician (0.25)

Main scientific publications:

1. I. Kruusenberg, N. Alexeyeva, K. Tammeveski, J. Kozlova, L. Matisen, V. Sammelselg, J. Solla-Gullón, J.M. Feliu, Effect of purification of carbon nanotubes on their electrocatalytic properties for oxygen reduction in acid solution, Carbon 49 (2011) 4031–4039.
2. I. Kruusenberg, M. Marandi, V. Sammelselg, K. Tammeveski, Hydrodynamic deposition of carbon nanotubes onto HOPG: The reduction of oxygen on CNT/HOPG electrodes in alkaline solution, Electrochemical and Solid-State Letters 12 (2009) F31–F34.
3. I. Kruusenberg, L. Matisen, H. Jiang, M. Huuppola, K. Kontturi, K. Tammeveski, Electrochemical reduction of oxygen on double-walled carbon nanotube modified glassy carbon electrodes in acid and alkaline solutions, Electrochemistry Communications 12 (2010) 920–923.
4. I. Kruusenberg, N. Alexeyeva, K. Tammeveski, The pH-dependence of oxygen reduction on multi-walled carbon nanotube modified glassy carbon electrodes, Carbon 47 (2009) 651–658.
5. I. Kruusenberg, J. Leis, M. Arulepp, K. Tammeveski, Oxygen reduction on carbon nanomaterial modified glassy carbon electrodes in alkaline solution, Journal of Solid State Electrochemistry 14 (2010) 1269–1277.
6. I. Kruusenberg, L. Matisen, K. Tammeveski, Oxygen electroreduction on multi-walled carbon nanotube supported metal phthalocyanines and porphyrins in acid media, International Journal of Electrochemical Science 8 (2013) 1057–1066.

7. I. Kruusenberg, L. Matisen, K. Tammeveski, Oxygen electroreduction on multi-walled carbon nanotube supported metal phthalocyanines and porphyrins in alkaline media, Journal of Nanoscience and Nanotechnology 13 (2013) 621–627.
8. I. Kruusenberg, L. Matisen, Q. Shah, A.M. Kannan, K. Tammeveski, Non-platinum cathode catalysts for alkaline membrane fuel cells, International Journal of Hydrogen Energy 37 (2012) 4406–4412.
9. I. Kruusenberg, J. Mondal, L. Matisen, V. Sammelselg, K. Tammeveski, Oxygen reduction on graphene-supported MN_4 macrocycles in alkaline media, Electrochemistry Communications 33 (2013) 18–22.
10. M. Vikkisk, I. Kruusenberg, U. Joost, E. Shulga, K. Tammeveski, Electrocatalysis of oxygen reduction on nitrogen-containing multi-walled carbon nanotube modified glassy carbon electrodes, Electrochimica Acta 87 (2013) 709–716.

ELULOOKIRJELDUS

Nimi: Ivar Kruusenberg
Sünniaeg: 31. juuli 1984
Kodakondsus: Eesti
Aadress: Ravila 14a, 50411 Tartu, Eesti
Telefon: +372 737 5174; +372 50 36963
E-post: ivar.kruusenberg@ut.ee

Haridus:

2009–2013	Tartu Ülikool, Loodus- ja tehnoloogiateaduskond, Keemia instituudi doktoriõppe üliõpilane, juhendaja Kaido Tammeveski
2007–2009	Tartu Ülikool, Loodus- ja tehnoloogiateaduskond, *M.Sc* (molekulaartehnoloogia) 2009
2003–2007	Tartu Ülikool, Füüsika-keemiateaduskond, *B.Sc* (keemia) 2007

Teenistuskäik:

2007–	Tartu Ülikool, Keemia instituut, keemik (0,5)
2006–2007	Tartu Ülikool, Keemia instituut, tehnik (0,25)

Tähtsamad teaduspublikatsioonid:

1. I. Kruusenberg, N. Alexeyeva, K. Tammeveski, J. Kozlova, L. Matisen, V. Sammelselg, J. Solla-Gullón, J.M. Feliu, Effect of purification of carbon nanotubes on their electrocatalytic properties for oxygen reduction in acid solution, Carbon 49 (2011) 4031–4039.
2. I. Kruusenberg, M. Marandi, V. Sammelselg, K. Tammeveski, Hydrodynamic deposition of carbon nanotubes onto HOPG: The reduction of oxygen on CNT/HOPG electrodes in alkaline solution, Electrochemical and Solid-State Letters 12 (2009) F31–F34.
3. I. Kruusenberg, L. Matisen, H. Jiang, M. Huuppola, K. Kontturi, K. Tammeveski, Electrochemical reduction of oxygen on double-walled carbon nanotube modified glassy carbon electrodes in acid and alkaline solutions, Electrochemistry Communications 12 (2010) 920–923.
4. I. Kruusenberg, N. Alexeyeva, K. Tammeveski, The pH-dependence of oxygen reduction on multi-walled carbon nanotube modified glassy carbon electrodes, Carbon 47 (2009) 651–658.
5. I. Kruusenberg, J. Leis, M. Arulepp, K. Tammeveski, Oxygen reduction on carbon nanomaterial modified glassy carbon electrodes in alkaline solution, Journal of Solid State Electrochemistry 14 (2010) 1269–1277.
6. I. Kruusenberg, L. Matisen, K. Tammeveski, Oxygen electroreduction on multi-walled carbon nanotube supported metal phthalocyanines and porphyrins in acid media, International Journal of Electrochemical Science 8 (2013) 1057–1066.

7. I. Kruusenberg, L. Matisen, K. Tammeveski, Oxygen electroreduction on multi-walled carbon nanotube supported metal phthalocyanines and porphyrins in alkaline media, Journal of Nanoscience and Nanotechnology 13 (2013) 621–627.
8. I. Kruusenberg, L. Matisen, Q. Shah, A.M. Kannan, K. Tammeveski, Non-platinum cathode catalysts for alkaline membrane fuel cells, International Journal of Hydrogen Energy 37 (2012) 4406–4412.
9. I. Kruusenberg, J. Mondal, L. Matisen, V. Sammelselg, K. Tammeveski, Oxygen reduction on graphene-supported MN_4 macrocycles in alkaline media, Electrochemistry Communications 33 (2013) 18–22.
10. M. Vikkisk, I. Kruusenberg, U. Joost, E. Shulga, K. Tammeveski, Electrocatalysis of oxygen reduction on nitrogen-containing multi-walled carbon nanotube modified glassy carbon electrodes, Electrochimica Acta 87 (2013) 709–716.

DISSERTATIONES CHIMICAE UNIVERSITATIS TARTUENSIS

1. **Toomas Tamm.** Quantum-chemical simulation of solvent effects. Tartu, 1993, 110 p.
2. **Peeter Burk.** Theoretical study of gas-phase acid-base equilibria. Tartu, 1994, 96 p.
3. **Victor Lobanov.** Quantitative structure-property relationships in large descriptor spaces. Tartu, 1995, 135 p.
4. **Vahur Mäemets.** The ^{17}O and ^{1}H nuclear magnetic resonance study of H_2O in individual solvents and its charged clusters in aqueous solutions of electrolytes. Tartu, 1997, 140 p.
5. **Andrus Metsala.** Microcanonical rate constant in nonequilibrium distribution of vibrational energy and in restricted intramolecular vibrational energy redistribution on the basis of slater's theory of unimolecular reactions. Tartu, 1997, 150 p.
6. **Uko Maran.** Quantum-mechanical study of potential energy surfaces in different environments. Tartu, 1997, 137 p.
7. **Alar Jänes.** Adsorption of organic compounds on antimony, bismuth and cadmium electrodes. Tartu, 1998, 219 p.
8. **Kaido Tammeveski.** Oxygen electroreduction on thin platinum films and the electrochemical detection of superoxide anion. Tartu, 1998, 139 p.
9. **Ivo Leito.** Studies of Brønsted acid-base equilibria in water and non-aqueous media. Tartu, 1998, 101 p.
10. **Jaan Leis.** Conformational dynamics and equilibria in amides. Tartu, 1998, 131 p.
11. **Toonika Rinken.** The modelling of amperometric biosensors based on oxidoreductases. Tartu, 2000, 108 p.
12. **Dmitri Panov.** Partially solvated Grignard reagents. Tartu, 2000, 64 p.
13. **Kaja Orupõld.** Treatment and analysis of phenolic wastewater with microorganisms. Tartu, 2000, 123 p.
14. **Jüri Ivask.** Ion Chromatographic determination of major anions and cations in polar ice core. Tartu, 2000, 85 p.
15. **Lauri Vares.** Stereoselective Synthesis of Tetrahydrofuran and Tetrahydropyran Derivatives by Use of Asymmetric Horner-Wadsworth-Emmons and Ring Closure Reactions. Tartu, 2000, 184 p.
16. **Martin Lepiku.** Kinetic aspects of dopamine D_2 receptor interactions with specific ligands. Tartu, 2000, 81 p.
17. **Katrin Sak.** Some aspects of ligand specificity of P2Y receptors. Tartu, 2000, 106 p.
18. **Vello Pällin.** The role of solvation in the formation of iotsitch complexes. Tartu, 2001, 95 p.

19. **Katrin Kollist.** Interactions between polycyclic aromatic compounds and humic substances. Tartu, 2001, 93 p.
20. **Ivar Koppel.** Quantum chemical study of acidity of strong and superstrong Brønsted acids. Tartu, 2001, 104 p.
21. **Viljar Pihl.** The study of the substituent and solvent effects on the acidity of OH and CH acids. Tartu, 2001, 132 p.
22. **Natalia Palm.** Specification of the minimum, sufficient and significant set of descriptors for general description of solvent effects. Tartu, 2001, 134 p.
23. **Sulev Sild.** QSPR/QSAR approaches for complex molecular systems. Tartu, 2001, 134 p.
24. **Ruslan Petrukhin.** Industrial applications of the quantitative structure-property relationships. Tartu, 2001, 162 p.
25. **Boris V. Rogovoy.** Synthesis of (benzotriazolyl)carboximidamides and their application in relations with *N*- and *S*-nucleophyles. Tartu, 2002, 84 p.
26. **Koit Herodes.** Solvent effects on UV-vis absorption spectra of some solvatochromic substances in binary solvent mixtures: the preferential solvation model. Tartu, 2002, 102 p.
27. **Anti Perkson.** Synthesis and characterisation of nanostructured carbon. Tartu, 2002, 152 p.
28. **Ivari Kaljurand.** Self-consistent acidity scales of neutral and cationic Brønsted acids in acetonitrile and tetrahydrofuran. Tartu, 2003, 108 p.
29. **Karmen Lust.** Adsorption of anions on bismuth single crystal electrodes. Tartu, 2003, 128 p.
30. **Mare Piirsalu.** Substituent, temperature and solvent effects on the alkaline hydrolysis of substituted phenyl and alkyl esters of benzoic acid. Tartu, 2003, 156 p.
31. **Meeri Sassian.** Reactions of partially solvated Grignard reagents. Tartu, 2003, 78 p.
32. **Tarmo Tamm.** Quantum chemical modelling of polypyrrole. Tartu, 2003. 100 p.
33. **Erik Teinemaa.** The environmental fate of the particulate matter and organic pollutants from an oil shale power plant. Tartu, 2003. 102 p.
34. **Jaana Tammiku-Taul.** Quantum chemical study of the properties of Grignard reagents. Tartu, 2003. 120 p.
35. **Andre Lomaka.** Biomedical applications of predictive computational chemistry. Tartu, 2003. 132 p.
36. **Kostyantyn Kirichenko.** Benzotriazole – Mediated Carbon–Carbon Bond Formation. Tartu, 2003. 132 p.
37. **Gunnar Nurk.** Adsorption kinetics of some organic compounds on bismuth single crystal electrodes. Tartu, 2003, 170 p.
38. **Mati Arulepp.** Electrochemical characteristics of porous carbon materials and electrical double layer capacitors. Tartu, 2003, 196 p.

39. **Dan Cornel Fara.** QSPR modeling of complexation and distribution of organic compounds. Tartu, 2004, 126 p.
40. **Riina Mahlapuu.** Signalling of galanin and amyloid precursor protein through adenylate cyclase. Tartu, 2004, 124 p.
41. **Mihkel Kerikmäe.** Some luminescent materials for dosimetric applications and physical research. Tartu, 2004, 143 p.
42. **Jaanus Kruusma.** Determination of some important trace metal ions in human blood. Tartu, 2004, 115 p.
43. **Urmas Johanson.** Investigations of the electrochemical properties of polypyrrole modified electrodes. Tartu, 2004, 91 p.
44. **Kaido Sillar.** Computational study of the acid sites in zeolite ZSM-5. Tartu, 2004, 80 p.
45. **Aldo Oras.** Kinetic aspects of dATPαS interaction with $P2Y_1$ receptor. Tartu, 2004, 75 p.
46. **Erik Mölder.** Measurement of the oxygen mass transfer through the air-water interface. Tartu, 2005, 73 p.
47. **Thomas Thomberg.** The kinetics of electroreduction of peroxodisulfate anion on cadmium (0001) single crystal electrode. Tartu, 2005, 95 p.
48. **Olavi Loog.** Aspects of condensations of carbonyl compounds and their imine analogues. Tartu, 2005, 83 p.
49. **Siim Salmar.** Effect of ultrasound on ester hydrolysis in aqueous ethanol. Tartu, 2006, 73 p.
50. **Ain Uustare.** Modulation of signal transduction of heptahelical receptors by other receptors and G proteins. Tartu, 2006, 121 p.
51. **Sergei Yurchenko.** Determination of some carcinogenic contaminants in food. Tartu, 2006, 143 p.
52. **Kaido Tämm.** QSPR modeling of some properties of organic compounds. Tartu, 2006, 67 p.
53. **Olga Tšubrik.** New methods in the synthesis of multisubstituted hydrazines. Tartu. 2006, 183 p.
54. **Lilli Sooväli.** Spectrophotometric measurements and their uncertainty in chemical analysis and dissociation constant measurements. Tartu, 2006, 125 p.
55. **Eve Koort.** Uncertainty estimation of potentiometrically measured ph and pK_a values. Tartu, 2006, 139 p.
56. **Sergei Kopanchuk.** Regulation of ligand binding to melanocortin receptor subtypes. Tartu, 2006, 119 p.
57. **Silvar Kallip.** Surface structure of some bismuth and antimony single crystal electrodes. Tartu, 2006, 107 p.
58. **Kristjan Saal.** Surface silanization and its application in biomolecule coupling. Tartu, 2006, 77 p.
59. **Tanel Tätte.** High viscosity $Sn(OBu)_4$ oligomeric concentrates and their applications in technology. Tartu, 2006, 91 p.

60. **Dimitar Atanasov Dobchev**. Robust QSAR methods for the prediction of properties from molecular structure. Tartu, 2006, 118 p.
61. **Hannes Hagu**. Impact of ultrasound on hydrophobic interactions in solutions. Tartu, 2007, 81 p.
62. **Rutha Jäger.** Electroreduction of peroxodisulfate anion on bismuth electrodes. Tartu, 2007, 142 p.
63. **Kaido Viht.** Immobilizable bisubstrate-analogue inhibitors of basophilic protein kinases: development and application in biosensors. Tartu, 2007, 88 p.
64. **Eva-Ingrid Rõõm.** Acid-base equilibria in nonpolar media. Tartu, 2007, 156 p.
65. **Sven Tamp.** DFT study of the cesium cation containing complexes relevant to the cesium cation binding by the humic acids. Tartu, 2007, 102 p.
66. **Jaak Nerut.** Electroreduction of hexacyanoferrate(III) anion on Cadmium (0001) single crystal electrode. Tartu, 2007, 180 p.
67. **Lauri Jalukse.** Measurement uncertainty estimation in amperometric dissolved oxygen concentration measurement. Tartu, 2007, 112 p.
68. **Aime Lust.** Charge state of dopants and ordered clusters formation in CaF_2:Mn and CaF_2:Eu luminophors. Tartu, 2007, 100 p.
69. **Iiris Kahn**. Quantitative Structure-Activity Relationships of environmentally relevant properties. Tartu, 2007, 98 p.
70. **Mari Reinik.** Nitrates, nitrites, N-nitrosamines and polycyclic aromatic hydrocarbons in food: analytical methods, occurrence and dietary intake. Tartu, 2007, 172 p.
71. **Heili Kasuk.** Thermodynamic parameters and adsorption kinetics of organic compounds forming the compact adsorption layer at Bi single crystal electrodes. Tartu, 2007, 212 p.
72. **Erki Enkvist.** Synthesis of adenosine-peptide conjugates for biological applications. Tartu, 2007, 114 p.
73. **Svetoslav Hristov Slavov**. Biomedical applications of the QSAR approach. Tartu, 2007, 146 p.
74. **Eneli Härk.** Electroreduction of complex cations on electrochemically polished Bi(*hkl*) single crystal electrodes. Tartu, 2008, 158 p.
75. **Priit Möller.** Electrochemical characteristics of some cathodes for medium temperature solid oxide fuel cells, synthesized by solid state reaction technique. Tartu, 2008, 90 p.
76. **Signe Viggor.** Impact of biochemical parameters of genetically different pseudomonads at the degradation of phenolic compounds. Tartu, 2008, 122 p.
77. **Ave Sarapuu.** Electrochemical reduction of oxygen on quinone-modified carbon electrodes and on thin films of platinum and gold. Tartu, 2008, 134 p.
78. **Agnes Kütt.** Studies of acid-base equilibria in non-aqueous media. Tartu, 2008, 198 p.

79. **Rouvim Kadis.** Evaluation of measurement uncertainty in analytical chemistry: related concepts and some points of misinterpretation. Tartu, 2008, 118 p.
80. **Valter Reedo.** Elaboration of IVB group metal oxide structures and their possible applications. Tartu, 2008, 98 p.
81. **Aleksei Kuznetsov.** Allosteric effects in reactions catalyzed by the cAMP-dependent protein kinase catalytic subunit. Tartu, 2009, 133 p.
82. **Aleksei Bredihhin.** Use of mono- and polyanions in the synthesis of multisubstituted hydrazine derivatives. Tartu, 2009, 105 p.
83. **Anu Ploom.** Quantitative structure-reactivity analysis in organosilicon chemistry. Tartu, 2009, 99 p.
84. **Argo Vonk.** Determination of adenosine A_{2A}- and dopamine D_1 receptor-specific modulation of adenylate cyclase activity in rat striatum. Tartu, 2009, 129 p.
85. **Indrek Kivi.** Synthesis and electrochemical characterization of porous cathode materials for intermediate temperature solid oxide fuel cells. Tartu, 2009, 177 p.
86. **Jaanus Eskusson.** Synthesis and characterisation of diamond-like carbon thin films prepared by pulsed laser deposition method. Tartu, 2009, 117 p.
87. **Marko Lätt.** Carbide derived microporous carbon and electrical double layer capacitors. Tartu, 2009, 107 p.
88. **Vladimir Stepanov.** Slow conformational changes in dopamine transporter interaction with its ligands. Tartu, 2009, 103 p.
89. **Aleksander Trummal.** Computational Study of Structural and Solvent Effects on Acidities of Some Brønsted Acids. Tartu, 2009, 103 p.
90. **Eerold Vellemäe.** Applications of mischmetal in organic synthesis. Tartu, 2009, 93 p.
91. **Sven Parkel.** Ligand binding to 5-HT_{1A} receptors and its regulation by Mg^{2+} and Mn^{2+}. Tartu, 2010, 99 p.
92. **Signe Vahur.** Expanding the possibilities of ATR-FT-IR spectroscopy in determination of inorganic pigments. Tartu, 2010, 184 p.
93. **Tavo Romann**. Preparation and surface modification of bismuth thin film, porous, and microelectrodes. Tartu, 2010, 155 p.
94. **Nadežda Aleksejeva.** Electrocatalytic reduction of oxygen on carbon nanotube-based nanocomposite materials. Tartu, 2010, 147 p.
95. **Marko Kullapere.** Electrochemical properties of glassy carbon, nickel and gold electrodes modified with aryl groups. Tartu, 2010, 233 p.
96. **Liis Siinor.** Adsorption kinetics of ions at Bi single crystal planes from aqueous electrolyte solutions and room-temperature ionic liquids. Tartu, 2010, 101 p.
97. **Angela Vaasa.** Development of fluorescence-based kinetic and binding assays for characterization of protein kinases and their inhibitors. Tartu 2010, 101 p.

98. **Indrek Tulp.** Multivariate analysis of chemical and biological properties. Tartu 2010, 105 p.
99. **Aare Selberg.** Evaluation of environmental quality in Northern Estonia by the analysis of leachate. Tartu 2010, 117 p.
100. **Darja Lavõgina.** Development of protein kinase inhibitors based on adenosine analogue-oligoarginine conjugates. Tartu 2010, 248 p.
101. **Laura Herm.** Biochemistry of dopamine D_2 receptors and its association with motivated behaviour. Tartu 2010, 156 p.
102. **Terje Raudsepp.** Influence of dopant anions on the electrochemical properties of polypyrrole films. Tartu 2010, 112 p.
103. **Margus Marandi.** Electroformation of Polypyrrole Films: *In-situ* AFM and STM Study. Tartu 2011, 116 p.
104. **Kairi Kivirand.** Diamine oxidase-based biosensors: construction and working principles. Tartu, 2011, 140 p.
105. **Anneli Kruve.** Matrix effects in liquid-chromatography electrospray mass-spectrometry. Tartu, 2011, 156 p.
106. **Gary Urb.** Assessment of environmental impact of oil shale fly ash from PF and CFB combustion. Tartu, 2011, 108 p.
107. **Nikita Oskolkov.** A novel strategy for peptide-mediated cellular delivery and induction of endosomal escape. Tartu, 2011, 106 p.
108. **Dana Martin.** The QSPR/QSAR approach for the prediction of properties of fullerene derivatives. Tartu, 2011, 98 p.
109. **Säde Viirlaid.** Novel glutathione analogues and their antioxidant activity. Tartu, 2011, 106 p.
110. **Ülis Sõukand.** Simultaneous adsorption of Cd^{2+}, Ni^{2+}, and Pb^{2+} on peat. Tartu, 2011, 124 p.
111. **Lauri Lipping.** The acidity of strong and superstrong Brønsted acids, an outreach for the "limits of growth": a quantum chemical study. Tartu, 2011, 124 p.
112. **Heisi Kurig.** Electrical double-layer capacitors based on ionic liquids as electrolytes. Tartu, 2011, 146 p.
113. **Marje Kasari.** Bisubstrate luminescent probes, optical sensors and affinity adsorbents for measurement of active protein kinases in biological samples. Tartu, 2012, 126 p.
114. **Kalev Takkis.** Virtual screening of chemical databases for bioactive molecules. Tartu, 2012, 122 p.
115. **Ksenija Kisseljova**. Synthesis of aza-β^3-amino acid containing peptides and kinetic study of their phosphorylation by protein kinase A. Tartu, 2012, 104 p.
116. **Riin Rebane.** Advanced method development strategy for derivatization LC/ESI/MS. Tartu, 2012, 184 p.

117. **Vladislav Ivaništšev.** Double layer structure and adsorption kinetics of ions at metal electrodes in room temperature ionic liquids. Tartu, 2012, 128 p.
118. **Irja Helm.** High accuracy gravimetric Winkler method for determination of dissolved oxygen. Tartu, 2012, 139 p.
119. **Karin Kipper.** Fluoroalcohols as Components of LC-ESI-MS Eluents: Usage and Applications. Tartu, 2012, 164 p.
120. **Arno Ratas.** Energy storage and transfer in dosimetric luminescent materials. Tartu, 2012, 163 p.
121. **Reet Reinart-Okugbeni**. Assay systems for characterisation of subtype-selective binding and functional activity of ligands on dopamine receptors. Tartu, 2012, 159 p.
122. **Lauri Sikk.** Computational study of the Sonogashira cross-coupling reaction. Tartu, 2012, 81 p.
123. **Karita Raudkivi.** Neurochemical studies on inter-individual differences in affect-related behaviour of the laboratory rat. Tartu, 2012, 161 p.
124. **Indrek Saar.** Design of GalR2 subtype specific ligands: their role in depression-like behavior and feeding regulation. Tartu, 2013, 126 p.
125. **Ann Laheäär.** Electrochemical characterization of alkali metal salt based non-aqueous electrolytes for supercapacitors. Tartu, 2013, 127 p.
126. **Kerli Tõnurist.** Influence of electrospun separator materials properties on electrochemical performance of electrical double-layer capacitors. Tartu, 2013, 147 p.
127. **Kaija Põhako-Esko.** Novel organic and inorganic ionogels: preparation and characterization. Tartu, 2013, 124 p.